WINTER PRECIPITATION DEPTHS ACROSS THE NORTH SLOPE OF ALASKA SIMULATED FROM THE WEATHER RESEARCH AND FORECASTING MODEL AND SNOWTRAN-3D

A

THESIS

Presented to the Faculty

of the University of Alaska Fairbanks

in Partial Fulfillment of the Requirements

for the Degree of

MASTER OF SCIENCE

By

Sarah Jean Byam, B.S.

Fairbanks, Alaska

December 2012

WINTER PRECIPITATION DEPTHS ACROSS THE NORTH SLOPE OF ALASKA SIMULATED FROM THE WEATHER RESEARCH AND FORECASTING MODEL AND SNOWTRAN-3D

By

Sarah Jean Byam

RECOMMENDED:

Dr. Douglas Kane, Advisory Committee Member

Dr. Jessica Cherry, Advisory Committee Co-Chair

Dr. Horacio Toniolo, Advisory Committee Co-Chair

Dr. Robert Perkins, Chair, Department of Civil and Environmental Engineering

APPROVED:

Dr. Doug Goering, Dean, College of Engineering and Mines

Dr. John C. Eichelberger, Dean, Graduate School

12/17/12

Date

Abstract

Accurately predicting snow distribution and blowing snow conditions in the Arctic is critical to the design of ice road construction and maintenance as well as for predicting water supplies and runoff during snowmelt, estimating the cost of snow removal, and forecasting tundra travel conditions. A current atmospheric model used by both the operational weather prediction and research communities is the Weather Research and Forecasting model. However, the built-in snow schemes in the model neglect redistribution of snow via wind, one of the key processes in snow pack evolution. This study will involve three parts: (1) diagnostic of the differences in the current snow schemes of the model, (2) evaluation of the model's snow schemes as compared to observational data, and (3) asynchronous coupling of the SnowTran-3D to model predictions using a simple algorithm. The approach provides a simple method for the prediction of snow distribution, improving the realism of current snow distribution models, and will be easily employable for both operational and research applications.

Table of Contents

Page

List of Figures

Page

List of Tables

Page

Chapter 1 General Overview and Methodology

1 Introduction

Off-road travel across the Alaskan North Slope tundra is required by the oil and gas industry for exploration, building ice roads, construction, and maintenance of facilities (Bader and Guimond 2004; National Research Council 2003). The understanding and prediction of snow transport and distribution characteristics are critical for basic research as well as for transportation safety, engineering design, and ecosystem preservation. For example, poor nutrient soils, permafrost, short growing season, and extreme cold winters create two predominant tundra types on the North Slope: tussock and sedge (Walker 1999; Jorgenson and Heiner 2003; Jorgenson et al. 2009). Sedge-shrub tundra is a plant type with grass-like appearance and solid stems that are triangular in cross-section. Tussock tundra is a tufted plant type with many stems arising as a large dense cluster from the crown (Wielgolaski 1972). The fragile vegetation is easily scarred by physical disturbance of heavy equipment tracks and cat trains during seismic oil exploration. Furthermore, Arctic operations are high risk to both personnel safety and project cost/schedule impacts related to adverse driving conditions. The remoteness of tundra operations increases the impact of even minor incidents. Under strong wind conditions, roads can quickly become covered in snowdrifts several feet deep. Finally, because industrial operations on the tundra are so remote, adverse driving conditions caused by blowing snow in subzero temperatures can quickly become deadly due to reduced visibility. A prediction tool that could better explain snow distribution would reduce the number of incidents and provide a higher degree of confidence to planners and designers for road and site design. Such a tool could also help with environmental approvals, reducing impacts of poorly designed roads, and possibly reduce "over designing" to cover unknowns.

Design and construction of arctic ice roads and site development must consider the impacts to a variety of environmental variables. Examples would be short- and long-term impacts to vegetation, changes to permafrost and the soil active layer, groundwater and surface water impacts, etc. (a few of these factors are discussed in detail in the following paragraphs).

Snow plays a critical role in the climate, energy balance, and biology of the Arctic. The Alaskan North Slope is typically blanketed with snow for nine months of the year (Shulski and Wendler 2007). Snow's high albedo and low thermal conductivity affect the energy cycle while, as a source of meltwater, snow contributes to the hydrological cycle. An important influence on permafrost and active layer dynamics, the spatial and temporal patterns of snow vary considerably in the annual total snow depth, amount of moisture content, topography, vegetation, and the timing of seasonal snowfall events. This variation makes understanding snow's influence difficult (Arctic Research Commission 2003). Snow depth maxima at the end of the snow year are estimated at 35 cm and 70 cm, on average, for the coastal plain and foothills, respectively (Romanovsky et al. 2003). At the peak of the seasonal cycle, usually in May, the Arctic Ocean average snow depth is 34 cm (Warren et al. 1999). End of winter snow depth and snow water equivalent average from 2006 to 2011 for mountain, foothills, and coastal plain varied from site to site in the eastern portion of the North Slope primarily due to wind events and had small differences among regions (Kane et al. 2012). Snow depth accumulation is influenced by the seasonal sea ice cycle of the Arctic Ocean and storms from the Arctic Ocean contributed nearly half of this (Benson 1969). The annual accumulation of snowfall occurs in greatest amounts at the beginning and end of the season with warmer, wetter air, relatively to the dry core of winter (Bader and Guimond 2004). During 1966 to 2005 satellite observations for the Northern Hemisphere show that the snow covered area has decreased in extent for every month except November and December (Lemke et al. 2007). During the mid-

1960s to early 2000s, snowmelt in northern Alaska advanced by eight days (Stone et al. 2002).

In the continental interiors of the North Slope near the Brooks Range, cold temperatures create relatively dry and light snow. For most of the season, snow on the ground has low water content and is wind packed into a firm crust (Colbeck et al. 1990). At the soil-snow interface, moisture and heat transfer from the active layer into and through the snow, create a depth hoar (Woo 1982). Variations in the relative percentages of depth hoar and wind slab alter the bulk density of shallow seasonal snow considerably.

In the Arctic coastal region, the snow tends to have a higher bulk density than the more protected foothills (Bilello 1957, 1984; Sturm and Benson 2004). The density of snow depends on the wind's speed and duration (Gray and Male 1981). Initiated by wind action, densification of snow through time is influenced by condensation and melting. Increases in snow densities of twenty percent can result in decreases in the maximum temperature in the soil by 3.0°C, impacting snow surface temperature, active layer depth, and sensible and latent heat fluxes (Ling and Zhang 2006).

A combination of wind redistribution, precipitation, and heat fluxes generate layering. The type, solid or liquid, and timing of precipitation during the winter season also contribute to layer generation. Varying in density, age, and thickness, three types of snow layers dominate: hoar layers, ice layers, and wind crust or slab. Hoar tends to be uniform over horizontal distances hundreds of times the height of the snow depth while ice layers tend to be discontinuous over distances ten times the height of the snow depth and occur in vertical columns (Colbeck 1990). Layering varies in horizontal distance and thickness due to vegetation, topography, and redistribution by wind. Layering also impacts the flow of water vapor and meltwater from the surface to the ground. For example, upward flow of water vapor can be perturbed by a thin crust formed by freezing rain. In another example, downward flow of meltwater can be interrupted by a thick layer of depth hoar,

which may contribute to the mass of the snow pack. Snow properties such as permeability, thermal conductivity, and structural strength modify density and grain sizes (Colbeck 1987). Water flows through snow routes over and around ice layers, changing the effective porosity and permeability of the snow (Yosida 1955). Layers with poor layer-to-layer connection or low density restrict the flow of heat conduction, vapor diffusion, and air convection, while layers with good layer-to-layer connection or high density have better flow. Formation of the layers influences the structural integrity of the snowpack. For example, a large, thick wind slab over a weak layer on a slope potentially will creep, transmitting stress over distances many times the thickness of the slab and causing failure and, potentially, an avalanche (Colbeck 1990). In addition, layers form through wind action.

Factors associated with the influence of snow on the ground thermal regime are timing of snowfall, surface albedo, emissivity and absorptivity, thermal conductivity, and latent heat of fusion. Early snowfall generates a warmer thermal regime in the top layer of soil, which could cause later freeze up and create a thermal impediment throughout the rest of the season (Stieglitz et al. 2003; Romanovsky and Osterkamp 2000). Zhang et al. (1997) found the temperature of the ground surface increased by 2 to 7°C with snow cover insulation. New snow with high albedo of greater than 0.95 (Wendler and Kelley 1988; Zhang et al. 1996) reduces surface temperature and absorption of solar energy. Low emissivity of snow increases outgoing longwave radiation, creating lower surface temperatures compared to exposed bare soil by 3.6 to 4.4°C. A function of snow density, snow thermal conductivity ranges from 0.10 W $m^{-1}K^{-1}$ for fresh snow to 0.5 W $m^{-1}K^{-1}$ for wet snow, which is five to twenty times lower than mineral soils. Having a low thermal conductivity, and depending on thickness, timing, and duration of cover, snow can cause the soil surface temperature to be either higher or lower than air temperature through the prevention of thermal interaction between the air and the soil. For example, during the melt period, fusion of snow causes a large energy sink and decreases air temperatures,

creating the potential for higher temperatures in soil than air (Zhang 2005). The fluxes of latent and sensible heat between the soil and snow depend upon on duration of melting, timing, accumulation, and physical properties of snow and surrounding vegetation, topography, and soil properties.

For the northern third of Alaska, the active layer lies above more than 600 meters of permafrost (Ferrians 1994). Proportional to summer air temperatures and a degree-day thawing index, active layer thickness increases from the Arctic coast to the foothills (Hinzman et al. 1991; Zhang et al. 1997). Annual permafrost temperatures at 20 m below ground surface (bgs) are generally higher in the foothills, which range from -4 to -5°C, because the cold season atmospheric temperature inversion is less strong than along the coast, which experience temperatures less than -7°C (Zhang et al. 1997; Weller and Holmgren 1974; Wendler et al. 1974). Permafrost temperatures at 20 m bgs over the last nine years have been relatively stable on the North Slope (Smith et al. 2010). In addition to presence or absence of permafrost, ground hardness, or cementation of soil when frozen, is also influenced by soil moisture, which contributes to the structural strength of ice and bonding within a soil matrix (Paolo et al. 2007). Unfrozen water in the soil provides a latent heat source, allowing for higher temperatures in the soil than would be without water. For example, bonding through soil moisture lasts until mid-winter for shallow lakes and throughout the winter for deeper lakes (Liston and Sturm 2003; Sturm et al. 1995, Jeffries et al. 1999).

Covering more than twenty-five percent of the Arctic Coastal Plain and underlying the snowpack are shallow lakes (Sellman et al. 1975). Snow properties and conditions are altered over the lakes, relative to tundra. Less depth hoar, potentially lower water equivalent, and stronger thermal gradients than the surrounding tundra, the snow on frozen lakes has fewer layers and is easily affected by wind. Snow on lakes, which has lower snow water equivalent and is thinner, has less than half the thermal insulation of tundra snow (Sturm et al. 1997). Impacted by snow, the lakes hydrologic balance depends

on the timing of the snowfall and location of the redistributed snow. Frozen for eight months of the year, lakes' ice thickness growth depends on the timing of the snowfall (Jeffries et al. 1996). For example, thinner, denser, wind-blown snow is a poor insulator, allowing for thicker ice to form. Precipitation early in the season over unfrozen or partially frozen lakes melts into the lake water and leads to reduction in snow availability for redistribution and sublimation. Drifting on lakes creates bare sections of ice, thickening the opposite bank of the prevailing wind and making the snow cover of lakes bumpy and rough (Liston and Sturm 2003).

Wind action also affects snow cover over tundra. The tundra plain, with its short vegetation, creates an open wind fetch capable of scouring ridges and windward slopes, and depositing onto the leeward slopes, causing non-uniform distribution of snow cover (Doesken and Judson 1996). Higher snow levels are collected in bushes than grasses and sedges, creating strong dependability between vegetation and terrain in determining snow retention. Redistributed snow accumulates predominately in valley bottoms and along depressions, or water tracks, on hill slopes (Kane et al. 1991). Accumulation is most pronounced where sustained strong winds from one direction act on loose snow and less pronounced for winds low in speed and constantly changing direction (Steppuhn 1976). Wind direction on the Arctic coastal plain is primarily in two directions with prevailing winds from the east and storm winds from the west (Conover 1960; Benson 1969; Wendler 1978). For the eastern portion of the North Slope, wind directions prevail in the northeast and southwest, varying in alternating terrain due to topographic channeling (Kane et al. 2012). During light wind events, loose, dry snow is readily transported (Liston and Sturm 1998). Condensation, melt, and vegetation may inhibit snow transport; however, in strong wind events even large slabs can be moved. Erosion dominates at ridge crests. The potential of wind to transport snow can cause snow depth variation across the North Slope over short distances by factors of ten or more (Benson and Sturm 1993). Benson and Sturm (1993), through over thirty years of observations on northern

Alaskan tundra snow, found roughly fifty percent of all snowfall is eventually redistributed via wind. Pomeroy et al. (1993) on the Canadian prairies found 38-85 percent of annual snowfall is redistributed by wind transport with the percentage increasing with wind speed. The relationship between wind and topography is a key contributor to the direction, speed, and amount of snow transport with vegetation depth and canopy being other important factors.

Wind transport of snow occurs by three mechanisms: creep, saltation, and suspension (Table 1). Saltation transport determines the lower boundary conditions and degree of suspension transport. If turbulent motions in the atmospheric boundary layer (ABL) are sufficiently strong, some of the particles from the saltation layer may then be entrained into the suspension mode. In this situation, a balance between downward gravitational settling and upward turbulent diffusion leads to the suspension of blowing snow. Transport of snow near the surface is usually referred to as drifting snow while 'blowing snow' is snow lifted high (2 m or more) and blown about by wind. The wind speed sufficient to transport snow is determined by the threshold friction velocity or the velocity required to move a grain of snow from its stationary position. Movement of the snow particles occurs when the drag force exerted on the surface by the wind exceeds the surface shear strength (Liston and Sturm 1998).

Table 1: Wind driven snow transport mechanisms.

Type	Motion	Height	Windspeed
Creep	Roll	<1 cm	<< 5 m/s
Saltation	Bounce	1 cm - 10 cm	5 - 10 m/s
Saltation	Bounce	10 cm - 100 cm	> 10 m/s
Suspension	Suspended	1 m - 100 m	> 10 m/s

Sublimation is also a snow re-distributor and moisture sink in the Arctic, either during saltation and suspension transport or exchanges of moisture with the atmosphere, though the moisture exchange occurs at a much slower rate than mass loss of transport (Liston

and Sturm 1998). Estimating sublimation is essential for predicting moisture balance in the Arctic, and yet it is very difficult to measure accurately. The amount of sublimation is a primarily estimated value from physical models ranging from 10 to 50 percent with extreme cases of complete removal through katabatic winds (Liston and Sturm 2002, 2004). Savelyev et al. (2006) described a Canadian Arctic Shelf study that showed high relative humidity with respect to ice creates low latent heat fluxes, indicating low levels of sublimation of blowing snow. Hirashima et al. (2004) conducted a study in eastern Siberia of simulation versus observations, which approximated sublimation at 40 percent. Though the degree of sublimation differs by location and season, studies agree that sublimation is a function of air temperature, wind speed, humidity, solar radiation, and particle size (Lee 1975; Male 1980; Thorpe and Mason 1966).

Meteorological observations of the elements of the North Slope are few and lacking in longevity. Snow depth measurements are determined through manual probing, observations from a fixed marker, or automated recording such as through ultrasonic sensors (Lundberg and Halldin 2001). Snowfall measurements are achieved through precipitation gauges and snow trays and are often plagued with systematic errors from wind field distortion (Sevurk et al. 1989), drifting snow (World Meteorological Organization "WMO" 1994), and inaccurate daily totals (Goodison and Metcalfe 1988; Bakkehøi et al. 1985). Calibration against the errors of trace precipitation, wetting loss, evaporation loss, and blowing snow were assessed in the WMO Solid Precipitation Measurement Inter-comparison (1985). The calibration was further refined for the Arctic (Yang et al. 1998; Yang and Ohata 2001; Bogdanova et al. 2002; Sugiura et al. 2003, 2009) with thresholds for winds greater than 6 ms^{-1} (Sugiura et al. 2006) and efficiency under strong winds (Goodison et al. 1998).

Determined by the snow depth and soil temperature, the length of the winter tundra travel season (Figure 1) imposes a limitation on the annual industrial activity and has declined considerably over the last thirty years from 200 to 100 days. By compacting snow on the

surface and changing snow thickness, tundra travel treatment can influence the soil moisture content, active layer depth (Bader and Guimond 2004), and plant distribution (Evans et al. 1989). Additionally, the original regulations governing tundra travel set minimums of six inches (15.24 cm) of snow and one foot (30.48 cm) of frozen ground. Tundra travel regulations were further refined starting in 2002 to six inches (15.24 cm) of snow and -5°C soil temperature at one foot (30.48 cm) for the coastal plain and nine inches bgs (22.86 cm) snow depth and -5°C soil temperature at one foot bgs (30.48 cm) for the foothills (Schultz 2010).

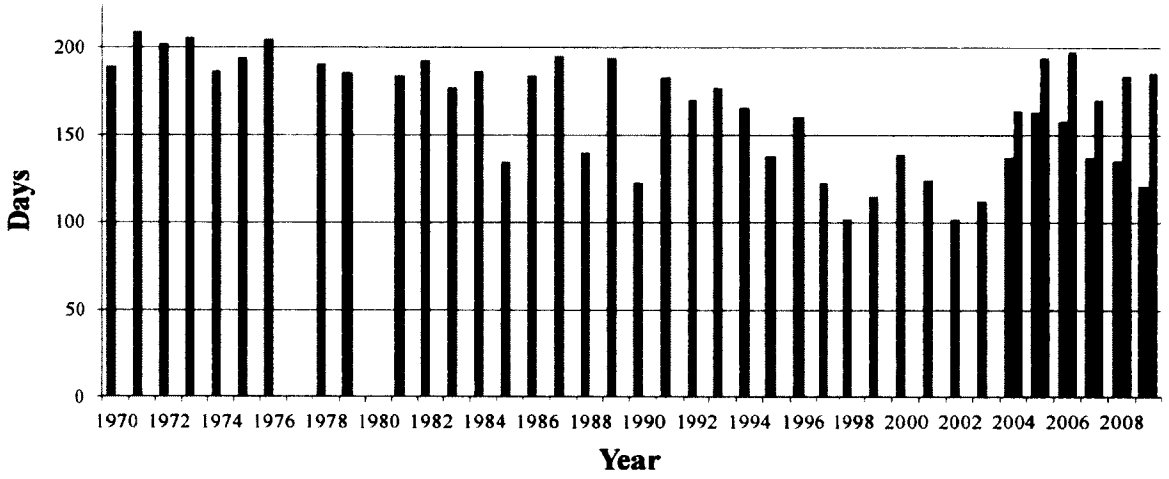

Figure 1: Alaskan North Slope winter exploration season length (blue) from 1985 to 2006 with ice road season length (red) (Schultz 2010).

Predictions and information of snow conditions, such as a visibility or changing conditions report, would aid tundra travel and thereby improve industrial activities. However, the general short and sparse amount of historical observational data for temperature, snow depth, and precipitation and the complexity of snow redistribution make prediction difficult. Using weather forecasts produced through a numerical model with a snow transport model, the snow depth and redistribution conditions potentially could be a tool to assist in the decision-making processes of industry and land-managers.

This study will involve three parts: (1) analysis of the differences in the current land surface model (LSM) snow schemes of the WRF model, (2) evaluation of the WRF's LSM snow schemes to observational data, and (3) asynchronous coupling of the SnowTran-3D to WRF predictions using a simple algorithm.

2 Models

2.1 Weather Research Forecasting Model

The Weather Research and Forecasting (WRF; Skamarock et al. 2008) modeling system, a multi-agency effort, is a mesoscale model and data assimilation system. This system contains several land surface models, which update the state variables of snow cover, soil temperature, and moisture, etc, and is suitable for a broad spectrum of applications across scales ranging from meters to thousands of kilometers. This next-generation numerical weather prediction system consists of multiple dynamical cores, a three-dimensional variational data assimilation system, and a software architecture allowing for computational parallelism and system extensibility. Within WRF, there are four land surface models (Table 2). Two of the four land surface models (LSM) considered in this project are the community of National Centers for Environmental Prediction, Oregon State University, Air Force, and Hydrologic Research Lab (NOAH, or commonly Noah) LSM (Chen and Dudhia 2001; Koren et al. 1999) and the Rapid Up-date Cycle (RUC) LSM (Smirnova et al. 2000).

Table 2: Land Surface Scheme Options in WRF (Skamarock *et. al.* 2008)

Scheme	Vegetation Processes	Soil Variables (Layers)	Snow Scheme
5-layer	N	Temperature (5)	none
Noah	Y	Temperature, Water+Ice, Water (4)	1-layer, fractional
RUC	Y	Temperature, Ice, Water+Ice (6)	multi-layer
Pliem-Xiu	Y	Temperature, Moisture (2)	input only

2.1.1 Land Surface Models

The Noah LSM consists of one-layer of vegetation, fractional snow cover, and the soil variables of temperature, water plus ice, and water in four layers. In the case of snow, the uppermost layer of the soil is treated as a blend of snow and soil impacts. Noah LSM also considers sensible and latent heat fluxes to the boundary layer. Noah also includes a variable heat capacity, liquid density and liquid storage.

The RUC scheme consists of a one-layer vegetation scheme, a multilayer snow scheme, and a soil model that considers soil variables of temperature, ice, and water plus ice with a default of six layers and the possibility of up to nine. The RUC LSM snow properties offer varying snow density, liquid water in snow pack, snow depth, temperature-dependent albedo, melting schemes for the interfaces between the snow-atmosphere and snow-soil, and fractional snow cover with latent and sensible heat variables (Skamarock et al. 2008). Thus, both models include vegetation effects, frozen soil physics, canopy water effects, and fractional snow cover. Beyond the number of layers of soil, the models differ by the number of layers of snow with RUC having a multiple layer snow with differing snow density and temperatures from internal values and Noah having a single layer with snow values from standard properties and tables (Baker and Kalnay 2008).

The Snow Model Intercomparison Project (SnowMIP 2001; Essery and Etchevers 2004; Etchevers et al. 2004) tabulated the snow processes of Noah and RUC, pointing out modeling parameters and characteristics. Differing in the number of snow layers, RUC also has the snow properties of heat capacity and surface roughness varying in time. The snow albedo depends on snow depth and snow-free albedo in RUC and snow temperature and the amount of snow in Noah. However, in the WRF version used for this study, a fixed value is used for albedo in Noah. The snow cover fraction depends on snow depth in RUC and vegetation and snow amount in Noah. RUC has the capacity to freeze water within the snow pack, while Noah does not.

2.2 SnowTran-3D

WRF's two snow schemes neglect the redistribution of snow via wind. However, through the use of a blowing snow model such as the three-dimensional model SnowTran-3D (Liston and Sturm 1998; Liston et al. 2007), simulation of the evolution of the snow depth over topographically varying terrain is possible. The processes of wind-induced surface shear stress, wind flow forcing field, transport of snow by turbulent suspension, transport of snow by saltation, accumulation and erosion of snow at the snow surface, and sublimation of transported snow are the primary components of the SnowTran-3D model. The model's initial conditions are determined by inputting spatially and temporally varying atmospheric variables of wind speed and direction, air temperature, humidity, and precipitation, as well as static information about topography and vegetation type. Each grid has a single, predefined type of vegetation with assigned canopy height and snow-holding depth (Table 3). The assigned canopy height and snow holding depth determine snow available for snow transport.

Table 3: Predefined vegetation types and associated snow-holding depths.

	Class	Description	Example	Snow-holding depth (m)	LAI max/min
1	Forest	Coniferous forest	Spruce-fir/taiga/lodgepole	15.00	2.5/2.5
2	Forest	Deciduous forest	Aspen forest	12.00	2.5/0.5
3	Forest	Mixed forest	Aspen/spruce-fir/low taiga	14.00	2.5/1.5
4	Forest	Scattered short-conifer	Pinyon-juniper	8.00	1.5/1.5
5	Forest	Clearcut forest	Stumps and regenerating	4.00	1.0/1.0
6	Shrub	Mesic upland shrub	Deeper soils, less rocky	0.50	-
7	Shrub	Xeric upland shrub	Rocky, windblown soils	0.25	-
8	Shrub	Playa shrubland	Greasewood, saltbush	1.00	-
9	Shrub	Shrib wetland/riparian	Willow along streams	1.75	-
10	Shrub	Erect shrub tundra	Arctic shrubland	0.65	-
11	Shrub	Low shrub tundra	Low to medium arctic shrubs	0.30	-
12	Grass	Grassland rangeland	Graminoids and forbs	0.15	-
13	Grass	Subalpine meadow	Meadows below treeline	0.25	-
14	Grass	Tundra (nontussock)	Alpine, high arctic	0.15	-
15	Grass	Tundra (tussock)	Graminoids and swarf shrubs	0.20	-
16	Grass	Prostrate shrub tundra	Graminoid dominated	0.10	-
17	Grass	Arctic gram, wetland	Grassy wetlands, wet tundra	0.20	-
18	Bare	Bare	-	0.01	-
19	Water	Water/possibly frozen	-	0.01	-
20	Water	Permanent snow/glacier	-	0.01	-
21	Human	Residential/urban	-	0.01	-
22	Human	Tall crops	Corn stubble	0.40	-
23	Human	Short crops	Wheat stubble	0.25	-

A mass balance equation, the foundation of the SnowTran-3D, is used to depict the temporal variation of snow depth at each point within the simulation domain. Changes in snow depth are controlled by the following parameters, assuming transport by creeping and rolling is small:

1) Changes in horizontal mass-transport rates of saltation, Q_{salt} (kg $m^{-1}s^{-1}$)
2) Changes in horizontal mass-transport rates of turbulent-suspended snow, Q_{turb} (kg $m^{-2}s^{-1}$)
3) Sublimation of transported snow particles, Q_v (kg $m^{-2}s^{-1}$)
4) Water equivalent precipitation rate, P (m s^{-1})

The equation for determining the temporal rate of change of snow depth is shown below (Eqn. 1). For each time-step and individual grid cell, the temporal rate of change of snow depth, ζ (m), is determined by a combination of summing the change of the rates of mass-transport and constants ρ_s (kg m^{-3}) as snow density, ρ_w (kg m^{-3}) as water density, t (s) is time, and x (m) and y (m) are horizontal coordinates in the west-east and north-south directions.

$$\frac{d\zeta}{dt} = \frac{1}{\rho_s}\left[\rho_w P - \left(\frac{dQ_{salt}}{dx} + \frac{dQ_{turb}}{dx} + \frac{dQ_{salt}}{dy} + \frac{dQ_{turb}}{dy}\right) + Q_v\right] \tag{1}$$

In an equation formulated by Pomeroy and Gray (1990), Q_{salt} is shown where the u^* (ms^{-1}) is the friction velocity, u_t^* (ms^{-1}) is the threshold friction velocity, u_n^* (ms^{-1}) is the non-erodible friction velocity, ρ (kgm^{-3}) is the fluid density, and g (ms^{-2}) is gravity (Eqn. 2).

$$Q_{salt} = \frac{0.68\rho}{u^* g}\left[u_t^* u^{*2} - u_t^* u_n^{*2} - u_t^{*3}\right] \tag{2}$$

For complete snow cover without exposed vegetation over plains, the non-erodible friction velocity is zero. Liston and Sturm (1998) added a factor to account for the overestimation of the saltation transport, Q_{salt_max}, where x* is the horizontal coordinate (Eqn. 3, 4).

$$Q_{salt\_max} = \frac{0.68\rho_a u_t^*}{u^* g}\left(u^{*2} - u_t^{*2}\right) \tag{3}$$

$$Q_{salt}(x^*) = Q_{salt\_max}\left[1 - \exp\left(-\mu\frac{x^*}{f}\right)\right] \tag{4}$$

Q_{turb} was formulated by Kind (1992), where φ is the volumetric concentration of suspended particles, z is the height of concentration, s is the settling velocity of particles (assumed to be 0.3 ms^{-1}), and the subscript r is a reference point (Eqn. 5).

$$\phi_t(x^*,z)=\phi_r\left[\left(\frac{\phi^* u^*}{\phi_r s}+1\right)\left(\frac{z}{z_{tr}}\right)^{-s/ku^*}-\frac{\phi^* u^*}{\phi_r s}\right] \tag{5}$$

Doorschot and Lehning (2002) showed saltation mass fluxes are much greater than those given by Pomeroy and Gray (1990). Liston and Sturm (1998) showed that the suspension transport for wind shear velocities greater than 0.4 ms^{-1} dominated similar to the Doorschot and Lehning (2002); therefore, the combination of saltation and suspension transport allowed for comparable transportation output to that of Doorschot and Lehning (2002) (Eqn. 6).

$$Q_{turb}(x^*)=\int_{h*}^{z_t}\phi_t(x^*,z)u^*(x^*,z)dz \tag{6}$$

3 Methodology

3.1 Meteorological Data

Observational data across the North Slope were collected from National Weather Service (NWS) stations, University of Alaska Fairbanks Water Environmental Research Center (WERC) Bullen Hydrology Project Stations, WERC Umiat Corridor Project Stations, National Resource Conservation Service's (NRCS) Snotel stations, the Remote automatic weather stations (RAWS) archived at the Western Regional Climate Center, and the United States Geological Survey (USGS) Water Resources Division and Hydrometeorological automated stations for a total of 17 sites (Table 4). The Alaskan

North Slope domain was determined as north of Atigun pass (latitude 68°7.8') and south of the Arctic Ocean (Figure 2).

Table 4: Locations of the seventeen weather stations with observational data.

Station	OPS	Latitude	Longitude	Elevation (m)
Accomplishment Creek	WERC	68°24.696'	148°8.190'	1473
Barrow (Wiley Post)	NWS	71°17'	156°46'	9
Bullen Point	WERC	70°4.792'	146°49.166'	26
Colville Village (Nuiqsut)	USGS	70°25'	150°24'	5
Imnaviat Creek	NRCS/WERC	68°37'	149°18'	930
Juniper	WERC	69°4.57'	146°30.294'	1318
Lower Kadleroshilik River	WERC	70°4.406'	147°39'	24
Kavik	WERC	69°40.402'	146°54.034'	198
Northwest Kuparuk	WERC	69°56.851'	149°55.014'	124
North White Hills	WERC	69°42.892'	149°28.227'	84
Ribdon	WERC	68°38.548'	147°21.107'	1416
Sag-Ivishak	WERC	69°12.933'	148°33.116'	431
South White Hills	WERC	69°12.043'	149°33.508'	293
Upper Kadlershilik	WERC	69°32.968'	147°56.505'	209
Upper Kuparuk	WERC	68°38.408'	149°24.39'	774
Umiat Airfield	RAWS	69°22.2'	152°8.166'	88
White Hills	WERC	69°29.187'	149°49.284'	293

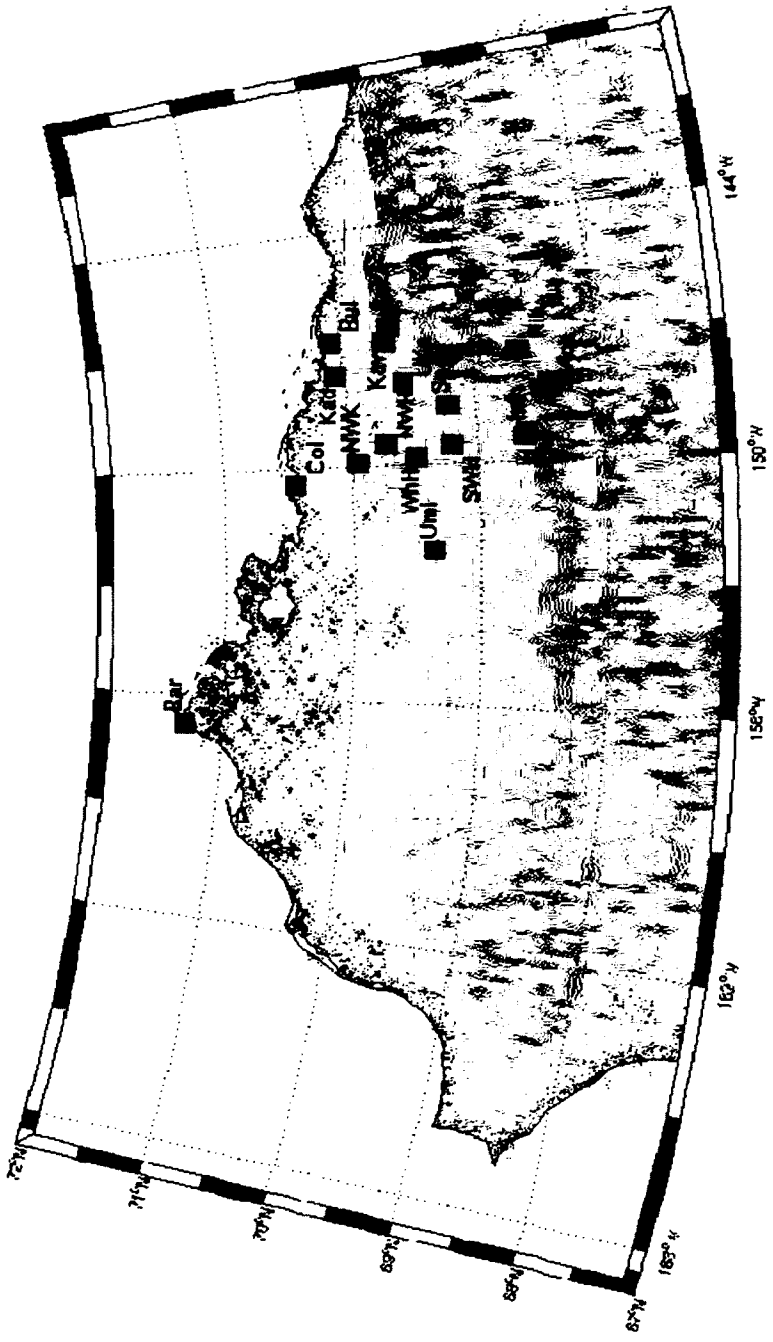

Figure 2: Alaskan North Slope domain and stations.

For a majority of the observational data, the SR-50a ultrasonic snow depth sensors were used, which allowed continuous time monitoring without having to submit to manual collection in the extreme weather conditions. This technique measures the time it takes a pulse of sound to reflect off the snow surface and return back to the sensor and derives the distance from the sensor to the ground. The sensor field of view is a 22 degree cone from the sensor head. The return time of the pulse to the sensor is adjusted based on the measured ambient air temperature. The return pulse time decreases with the accumulation of snow.

A comparison test was conducted between the sensor and manual measurements of total depth of snow at eighteen sites, including two in Alaska. Brazenec (2005) outfitted each site with three SR-50a sensors, providing redundancy, supporting quality assurance and quality control, and capturing spatial variance. Each site had a fabricated, flattened surface under the sensor to prevent biases created by uneven ground and/or irregular vegetation. Data analysis found typical results to be within one centimeter of accuracy under the sensor and two centimeters of accuracy for an average of several nearby ground measurements (Brazenec 2005; Ryan et al. 2008). Discrepancies in data points were noted to be associated with intense snowfall, low-density snow crystals, presence of blowing or drifting snow, high wind speeds, and uneven snow surface. For example, due to the high wind conditions creating scouring and drifts, spatial variability of the snow cover causes underestimation of total snow depth on the ground by two centimeters (Ryan et al. 2008).

For the WERC remote sensors quality assurance and quality control, fieldwork and data processing are conducted on each site to ensure the sensor's accuracy. The fieldwork includes measuring five distances under the sensor (four at 22 degrees and one directly underneath), the distance from the sensor to the snow surface, the temperature to ensure proper adjustment of the speed of sound, and noting any changes in angles or height of the sensor. The raw data is further processed by validating the field acquired data with the

sensor output, establishing baseline values to represent no snow, smoothing data when differences in adjacent data points are greater than 1.5 centimeters, and manually reviewing data for any erroneous values. Baseline values without adequate field data are difficult to establish when ground sensor height and angle alter due to freeze and thaw cycles and ground pulse time is reduced due to tussock, low shrub, and grass growth under the sensor. Differences of 1.5 centimeters or greater between points are replaced with the average of the following or previous five hours. In the case of blowing snow events and extreme cold periods, a ten-hour average replaces the anomaly in the series. During abrupt ablation, accumulation, or combinations of the two events, data is adjusted over a period of days. Other considerations to the sensor's output include wildlife chewing the wires, poor calibration, and time between maintenance (Berezovskaya et al. 2010).

3.2 Model Setup

3.2.1 WRF Domain and Parameterization

The WRF model domain encompasses the atmosphere above the North Slope with 200x150 grid-points, using a horizontal grid increment of 4 km and 28 vertical atmospheric layers reaching to 50 hectopascal. The 1.0^{o}x1.0^{o} and 6 hour resolution National Centers for Environmental Protection Global Forecast System final (GFS) analysis datasets serve as initial and boundary conditions. Initial snow cover, snow depth, precipitation, wind speed and direction, and temperatures are interpolated from GFS analyses. The domain is centered at 70^{o}N, 155^{o}W, roughly the center of the North Slope.

The WRF model configuration, based on the work of Chigullapalli and Molders (2008), determine cloud physics, long wave radiation physics, short wave radiation physics, surface layer physics, boundary layer physics, surface-atmosphere interaction, and

cumulus convection (Table 5). The Mellor-Yamada-Janjić (Janjić 1996, 2002) scheme runs in conjunction with the Eta Ferrier surface layer scheme to simulating near surface variables such as wind and mixing ratio (Baker et al. 2010). The Goddard scheme, with eleven spectral bands, represents diffuse and direct shortwave radiation (Chou and Suarez 1994).

The following WRF configuration was used for simulating five-day weather forecast: four five-day series in November 2007 and four five-day series in January-February 2008. These sets of four five-day series simulate weather at the beginning and the middle of the winter season. The dates are placed around precipitation events during a five-day period: without snowfall, snowfall occurring in the middle, snowfall occurring at the end, and snowfall occurring at the beginning (Table 6).

Table 5: Physics options and schemes used

Parameterization	Model
Microphysics	Eta Ferrier
Longwave Radiation	RRTM
Shortwave Radiation	Goddard shortwave
Surface Layer	Monin-Obukhov (Janjic)
Land Surface Model	Unified Noah LSM RUC LSM
Planetary Boundary Layer	Mellor-Yamada-Janjic
Cumulus Parameterization	Modified Grell-Devenyi ensemble

Table 6: Five-day weather simulation periods

Precipitation Event	November 2007.		January-February 2008	
	Start	End	Start	End
Without	11/24/2007	11/28/2007	1/7/2008	1/11/2008
At end	11/19/2007	11/23/2007	1/15/2008	1/19/2008
At beginning	11/23/2007	11/27/2007	1/22/2008	1/26/2008
Middle	11/21/2007	11/25/2007	2/19/2008	2/23/2008

3.2.2 SnowTran-3D Boundary Conditions and Parameterization

The wind speed sufficient to transport snow is largely determined by the wind shear velocity on the surface, u_* (ms^{-1}) which is determined by Eqn. 7.

$$u_* = u_r \frac{\kappa}{\ln(z_r / z_0)} \tag{7}$$

where u_r (ms^{-1}) is the wind speed at reference height, z_r (m), κ is the von Kármán's constant (maximum 0.41 in light winds over open water and smooth land surfaces and minimum near 0.37 in stronger winds over forests and cities) (Frenzen and Vogel 1995), and z_0 is the surface roughness length, which is defined by Eqn. 8 and 9.

$$z_0 = F_s z_{0\_snow} + (1 - F_s) z_{0\_veg} \tag{8}$$

$$F_s = \frac{\zeta}{C_v} \tag{9}$$

The depth-fraction of vegetation covered by snow, F_s, is determined through the depth of snow, ζ (m), and the vegetation snow holding capacity, C_v. The snow and vegetation roughness length are user-defined constants established during model simulations (Liston and Sturm 1998).

In arctic, low-temperature conditions, the snow density, ρ_s, and threshold, or friction, shear velocity are determined in the model to be constant temporally and spatially (Liston and Sturm 1998). Low temperatures, unlike temperatures near or at freezing, do not prevent surface snow drifting. Therefore, SnowTran-3D incorporates a snow density and threshold shear velocity that are dependent on temperature, T_{wb}, and wind speed, W_t. The model SnowTran-3D depicts the snow density as two layers: a "soft" layer that stores mobile snow, ρ_{ns}, and a "hard" immobile underlying layer, ρ_w. The hard layer accounts for the previously wind-transported snow that is generally harder to transport (Liston et

al. 2007). The threshold friction velocity, u_{*t}, is determined through the following (Eqn. 10-14):

$$u_{*t} = 0.005\exp(0.013\rho_s) \qquad 300 < \rho_s \leq 450 \qquad (10)$$

$$u_{*t} = 0.10\exp(0.003\rho_s) \qquad 50 < \rho_s \leq 300 \qquad (11)$$

where

$$\rho_s = \rho_{ns} + \rho_w \qquad (12)$$

$$\rho_{ns} = 50 + 1.7(T_{wb} - 25816)^{1.5} \qquad T_{wb} \geq 25816 \qquad (13)$$

$$\rho_{sw} = 25.0 kgm^{-3} + 2500 kgm^{-3}\{1.0 - \exp[-0.2 ms^{-1}(W_t - 5.0)]\} \qquad (14)$$

The air temperature-dependent new snow density, ρ_{ns} (kg m^{-3}), is calculated utilizing Anderson (1976) and LaChapelle (1969). For wind speeds greater or equal to 5 ms^{-1}, a wind-related density offset, ρ_{sw} (kg m^{-3}), is added to the temperature-dependent density. The terrain-modified wind speed, W_t (ms^{-1}), is calculated by the product of the station wind speed and a terrain-weighing factor. For comparison, snow density will also be defined as 280 kg m^{-3} as in Liston and Strum (1998) for Arctic conditions.

Saltation is calculated using equations described in Section 2.2 of this chapter. For complete snow cover without exposed vegetation over plains of the North Slope, the non-erodible friction velocity is zero. $Q_{salt}(x^*)$, Eqn. 3 of section 2.2, was applied where a boundary condition is set such that $f = x^* = 500$ and $\mu = 3.0$; therefore, the saltation flux is equal to 95% of Q_{salt_max} (Liston and Sturm 1998). In Eqn. 5 and 6 of Section 2.2, the particle settling velocity, s, is assumed to be 0.3 ms^{-1} (Schmidt 1982). In Eqn. 5 of Section 2.2, the ratio of the suspended volume to the reference mass concentration is as follows (Kind 1992) (Eqn. 15):

$$\frac{\phi^*}{\phi_r} = 0.5\frac{u_*}{u_r} \qquad (15)$$

The saltation layer height, h_* (m), is estimated according to Greeley and Iversen (1985) (Eqn. 16).

$$h_* = 1.6\frac{u_*^2}{2g} \tag{16}$$

The horizontal particle velocity within the saltation layer, u_p (ms^{-1}), was suggested as a constant with height by Pomeroy and Gray (1990) (Eqn. 17).

$$u_p = 2.8u_{*_t} \tag{17}$$

The saltation layer reference level mass concentration, ϕ_r (kg m^{-3}), is defined by Eqn. 18.

$$\phi_r = \frac{Q_s}{h_* u_p} \tag{18}$$

To focus on the redistribution of snow via wind, only the saltation and turbulent transfer will be considered for the rate of change of snow depth equation from SnowTran-3D (Liston and Strum 1998). Sublimation is a key factor in transfer rates for snow on the North Slope. The sublimation removal will potentially cause a negative bias for simulations to observations. The purpose of this study is to determine snow redistribution via wind; therefore, the sublimation transfer rate will be assumed to be zero to allow for the separation of wind transferred snow versus sublimated snow.

Chapter 2 Evaluation of Modeling Output

1 Results

1.1 Observation to Simulation Evaluation

In order to compare the observations to the simulations of the Noah LSM and RUC LSM snow schemes, the difference (a), absolute difference (b), and absolute percentage difference (c) were taken at each time step. The means of the time step differences for each five day period are shown in the following equations where x_i are the individual predictions and $x_{i,obs}$ are the observations (Eqn. 19-21).

$$a = x_i - x_{i,obs} \tag{19}$$

$$b = \left| x_i - x_{i,obs} \right| \tag{20}$$

$$c = \frac{\left| x_i - x_{i,obs} \right|}{x_{i,obs}} * 100 \tag{21}$$

Comparison of the observation to simulation snow height showed a discrepancy between initial values (Figure 3). The majority of the snow depths generated by the simulations showed an initial bias where these snow depths were greater than the observations. For example, there are extreme biases such as Accomplishment Creek with a simulation and observation difference of 60 cm; whereas, most of the biases were roughly between 10 and 20 cm. To achieve an understanding of the changing of the snow depth without this initial bias---which comes from the forcing data (GFS) rather than WRF itself--the initial values of the snow depths of the observations and simulations were subtracted from the rest of the time series observations and simulations, respectively. Therefore, the snow depth with the initial bias is removed and, hereafter, simply referred to as the snow depth bias.

The time series mean differences, absolute differences, and absolute percentage differences of the snow depth bias for each five-day period are shown in (Figure 4 - 51). For a point and pattern quantitative evaluation, average, difference, and the root mean square error (RMSE) were calculated hourly for temperature and wind speed and daily wind direction and snow depth bias (Table 7). Numbers shown in the table are the averages of the statistics calculated individually for each site from Table 4 for the five-day periods, utilizing Noah and RUC snow schemes. The range of the means is shown in the minimum and maximum values.

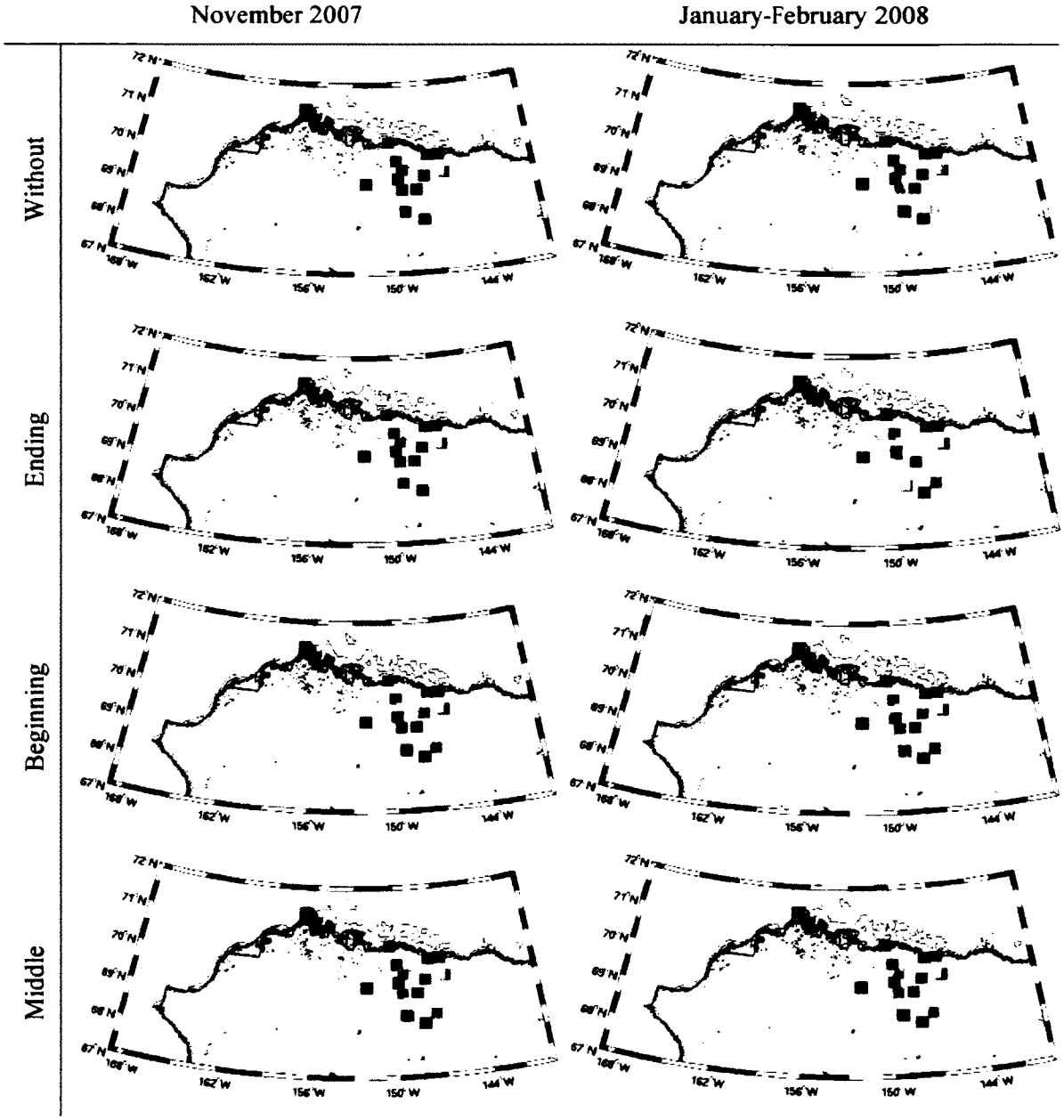

Figure 3: Snow depth bias (cm) between the initial values in the simulations and the observation for precipitation events during the five-day periods.

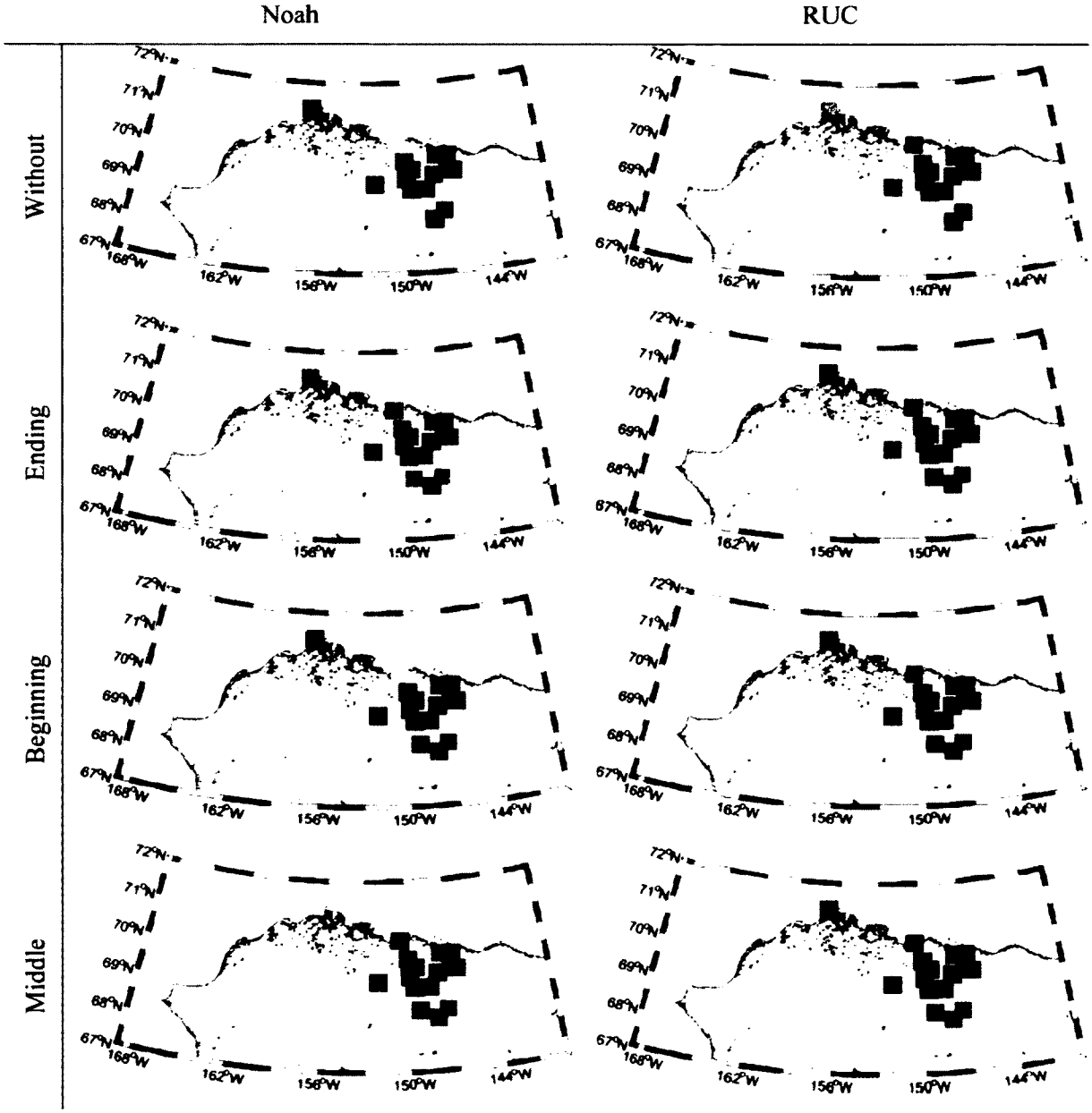

Figure 4: January-February temperature at 2m hourly means of the observation from simulation (sim-obs) differences for the events of precipitation.

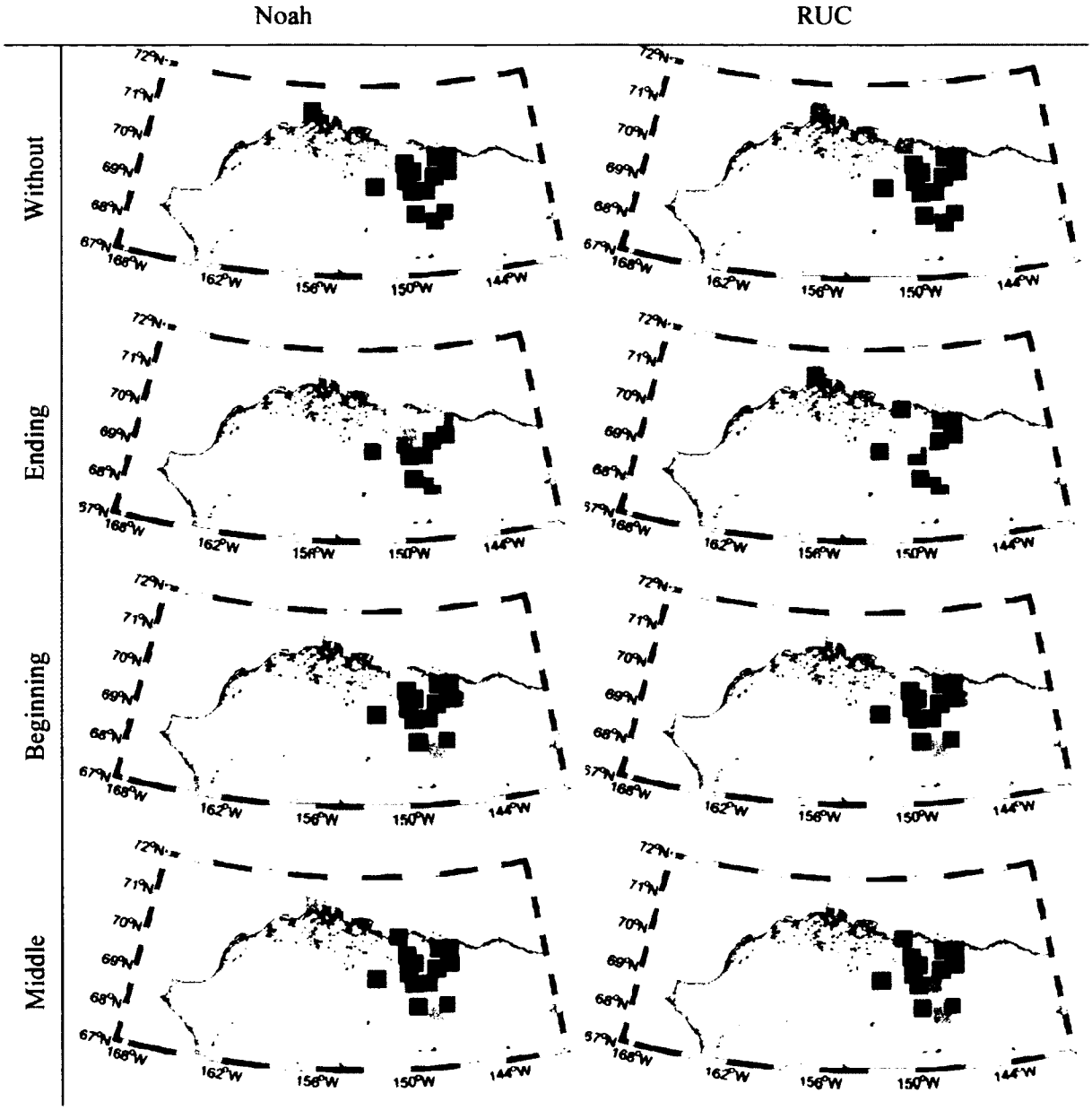

Figure 5: November temperature at 2m hourly means of the observation from simulation (sim-obs) differences for the events of precipitation.

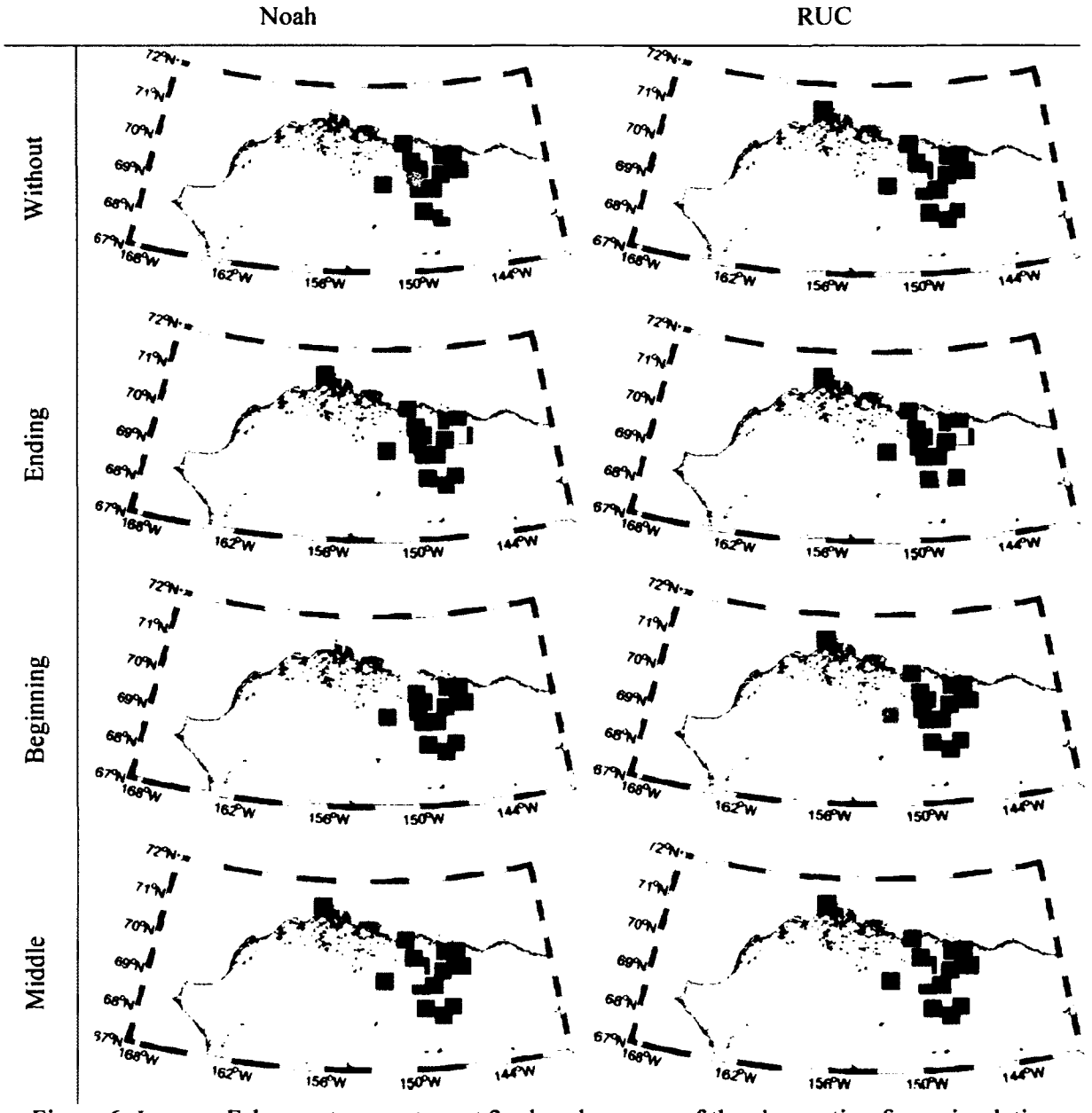

Figure 6: January-February temperature at 2m hourly means of the observation from simulation (sim-obs) absolute difference for the events of precipitation.

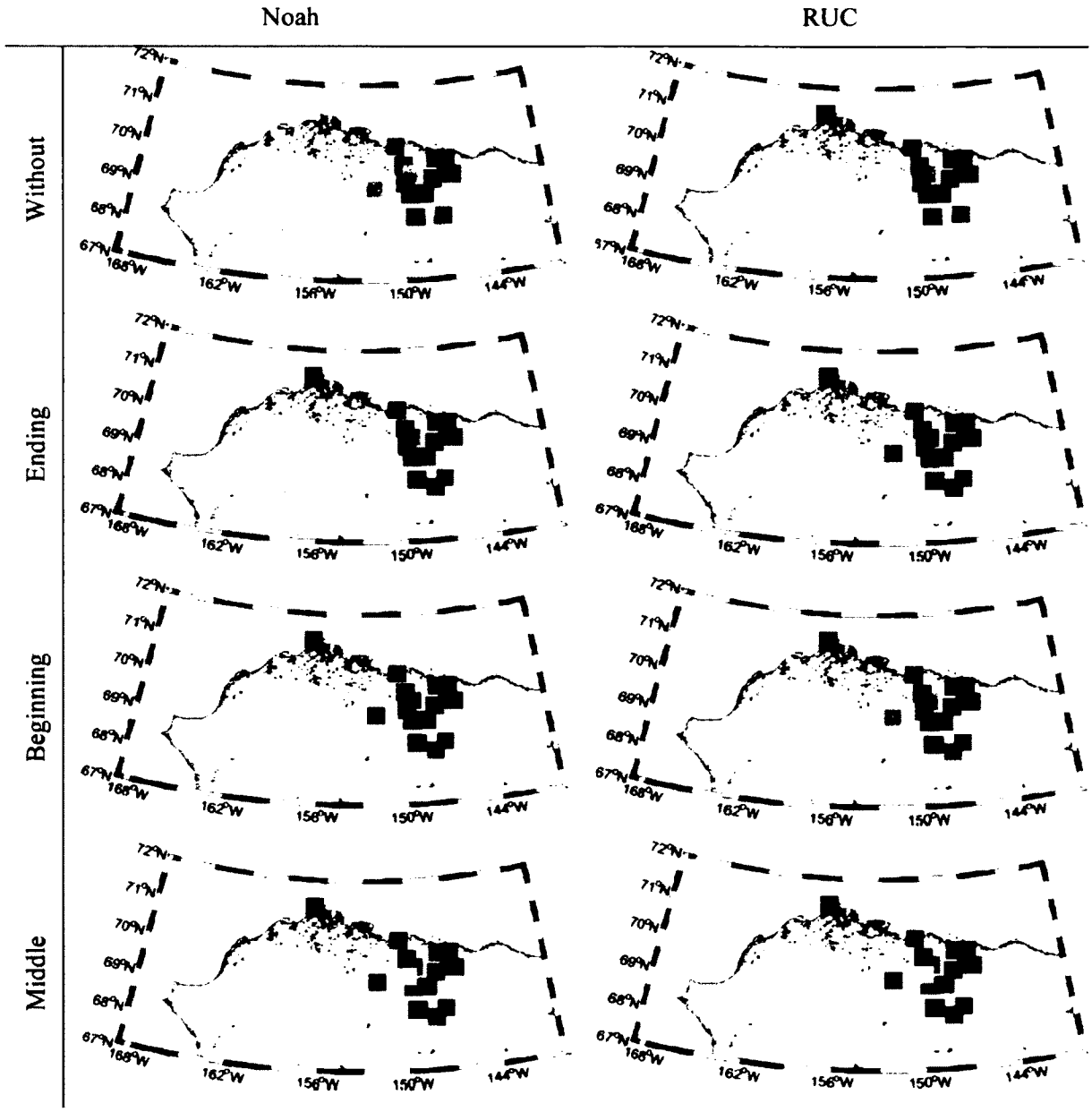

Figure 7: November temperature at 2m hourly means of the observation from simulation (sim-obs) absolute difference for the events of precipitation.

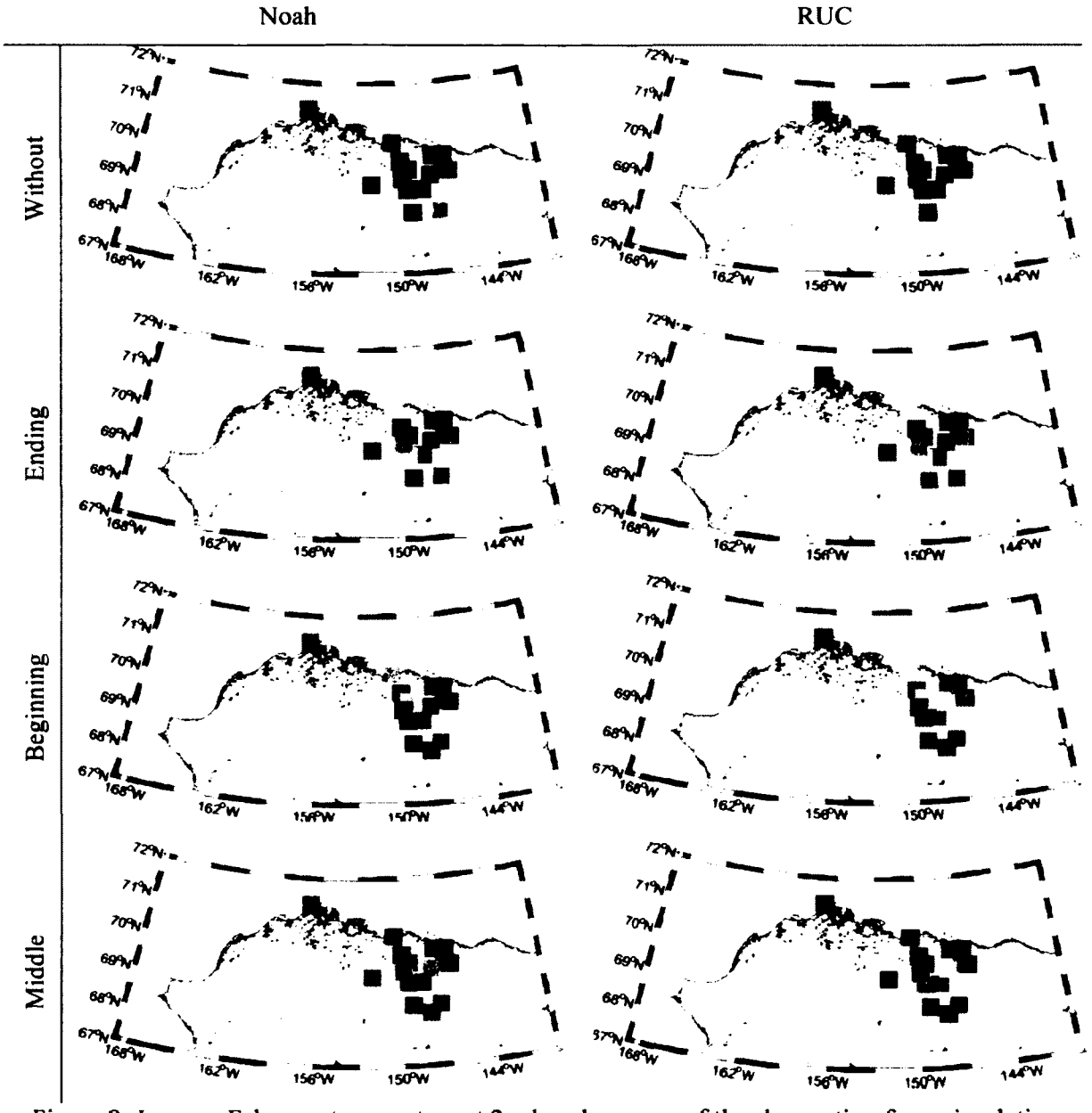

Figure 8: January-February temperature at 2m hourly means of the observation from simulation (sim-obs) absolute percentage difference for the events of precipitation.

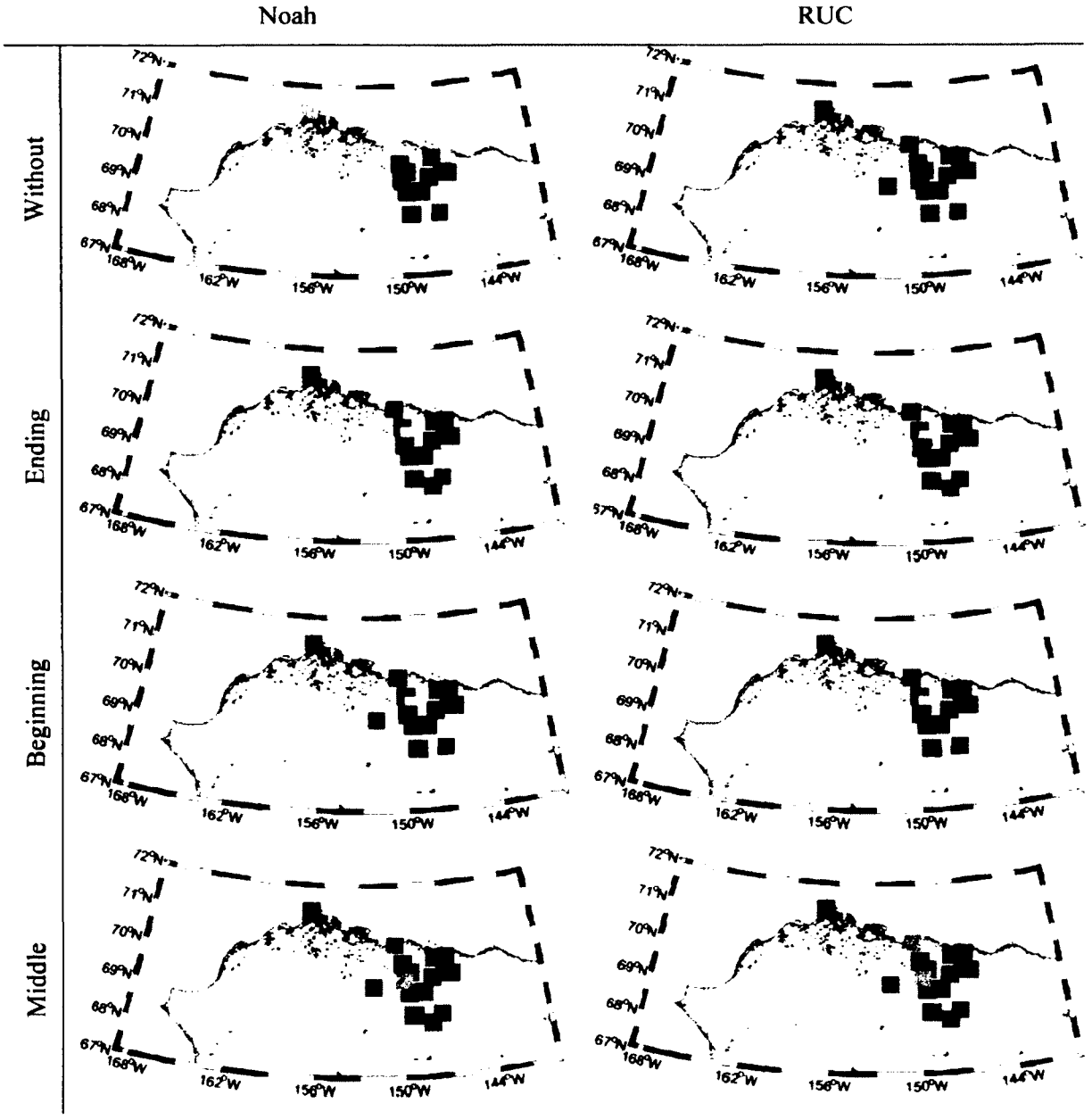

Figure 9: November temperature at 2m hourly means of the observation from simulation (sim-obs) absolute percentage difference for the events of precipitation.

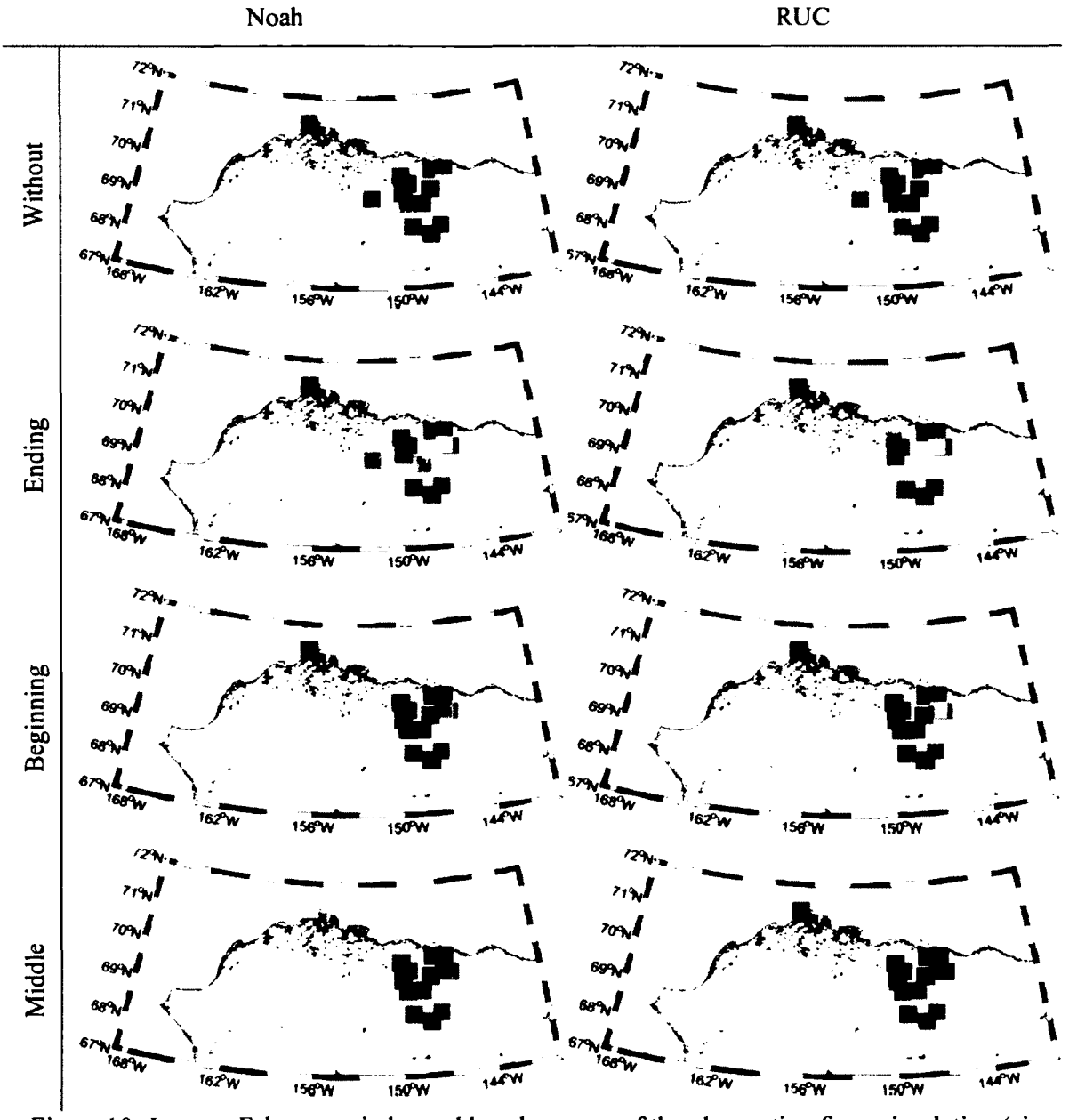

Figure 10: January-February wind speed hourly means of the observation from simulation (sim-obs) difference for the events of precipitation.

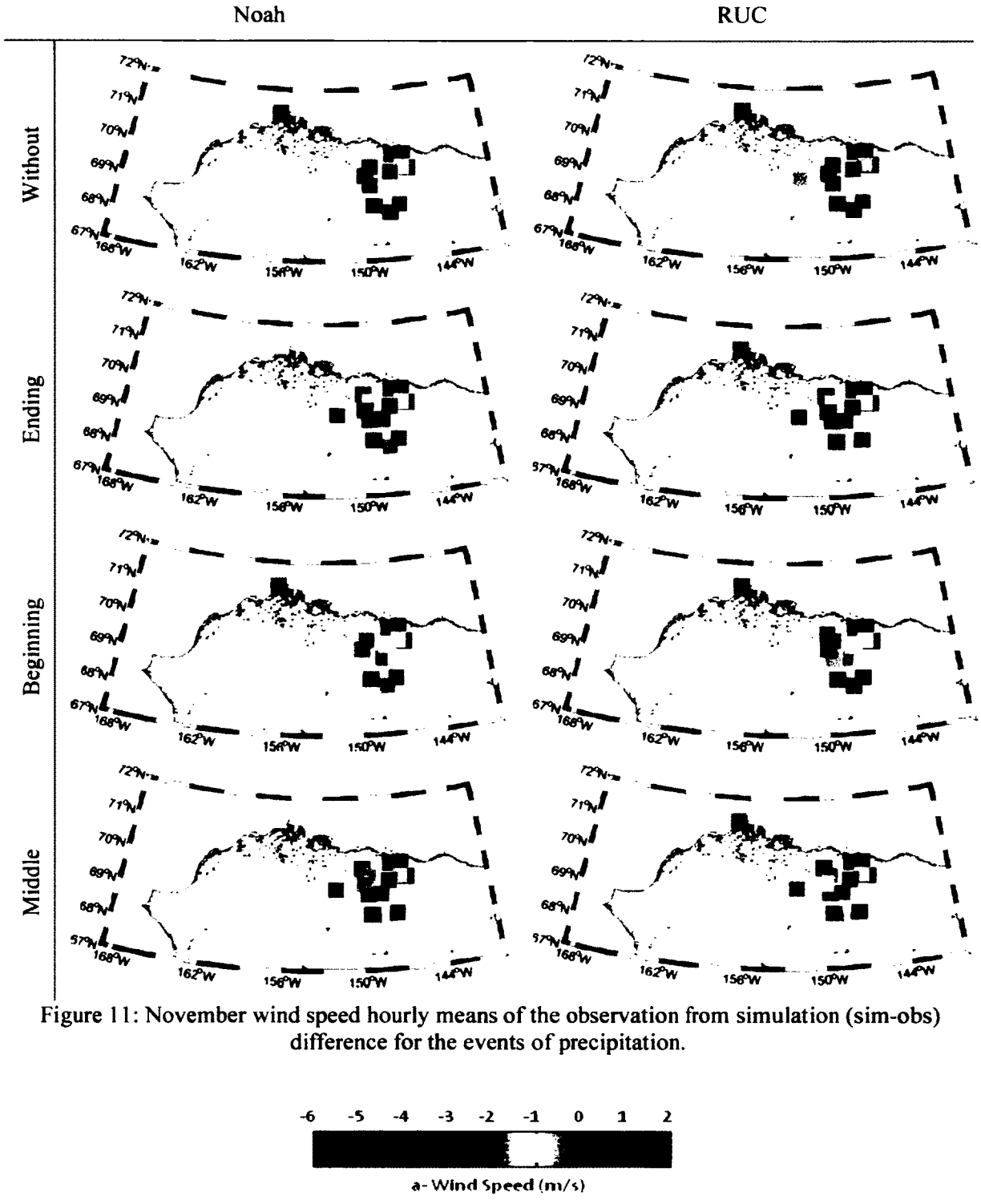

Figure 11: November wind speed hourly means of the observation from simulation (sim-obs) difference for the events of precipitation.

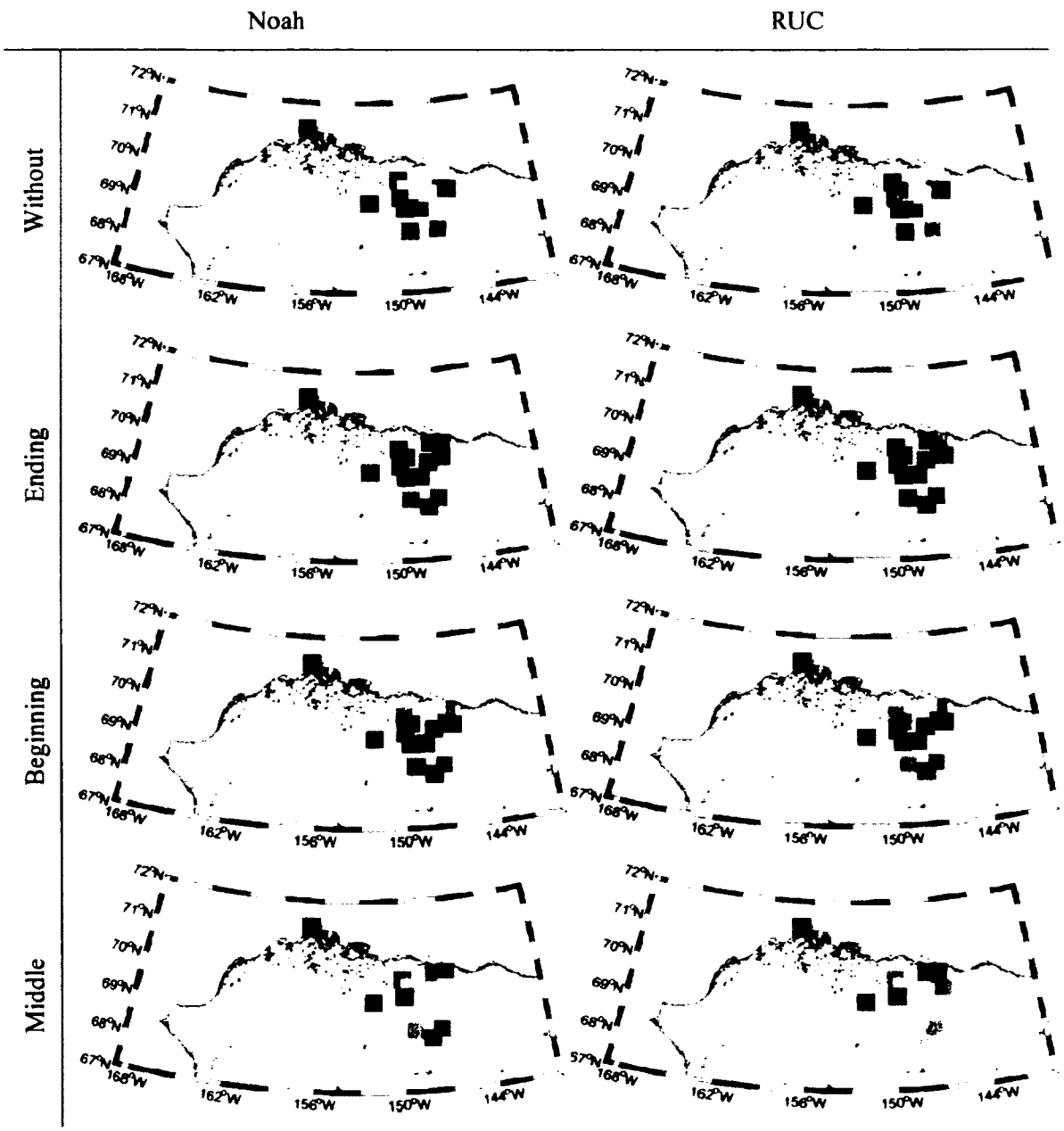

Figure 12: January-February wind speed hourly means of the observation from simulation (sim-obs) absolute difference for the events of precipitation.

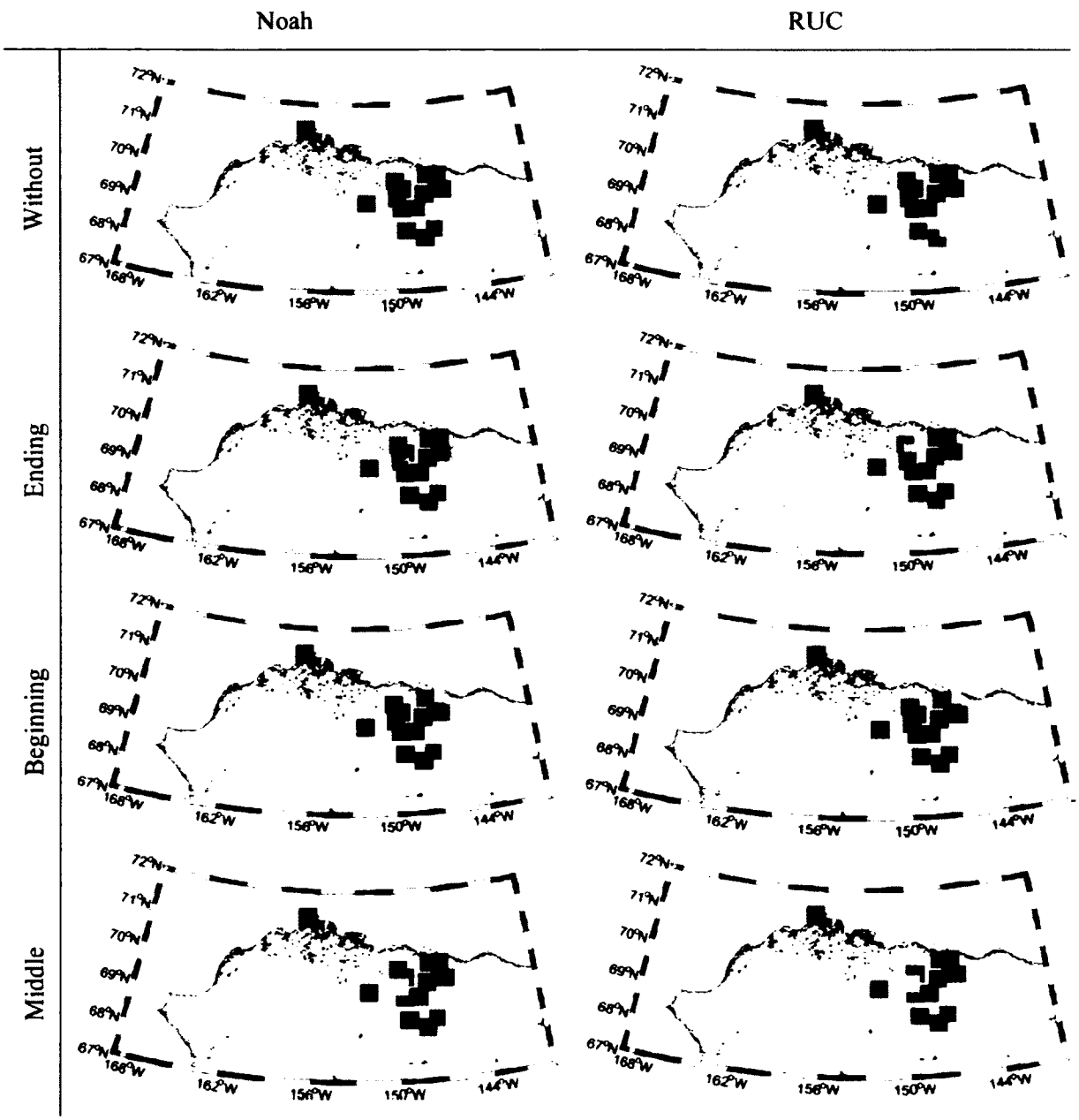

Figure 13: November wind speed hourly means of the observation from simulation (sim-obs) absolute difference for the events of precipitation.

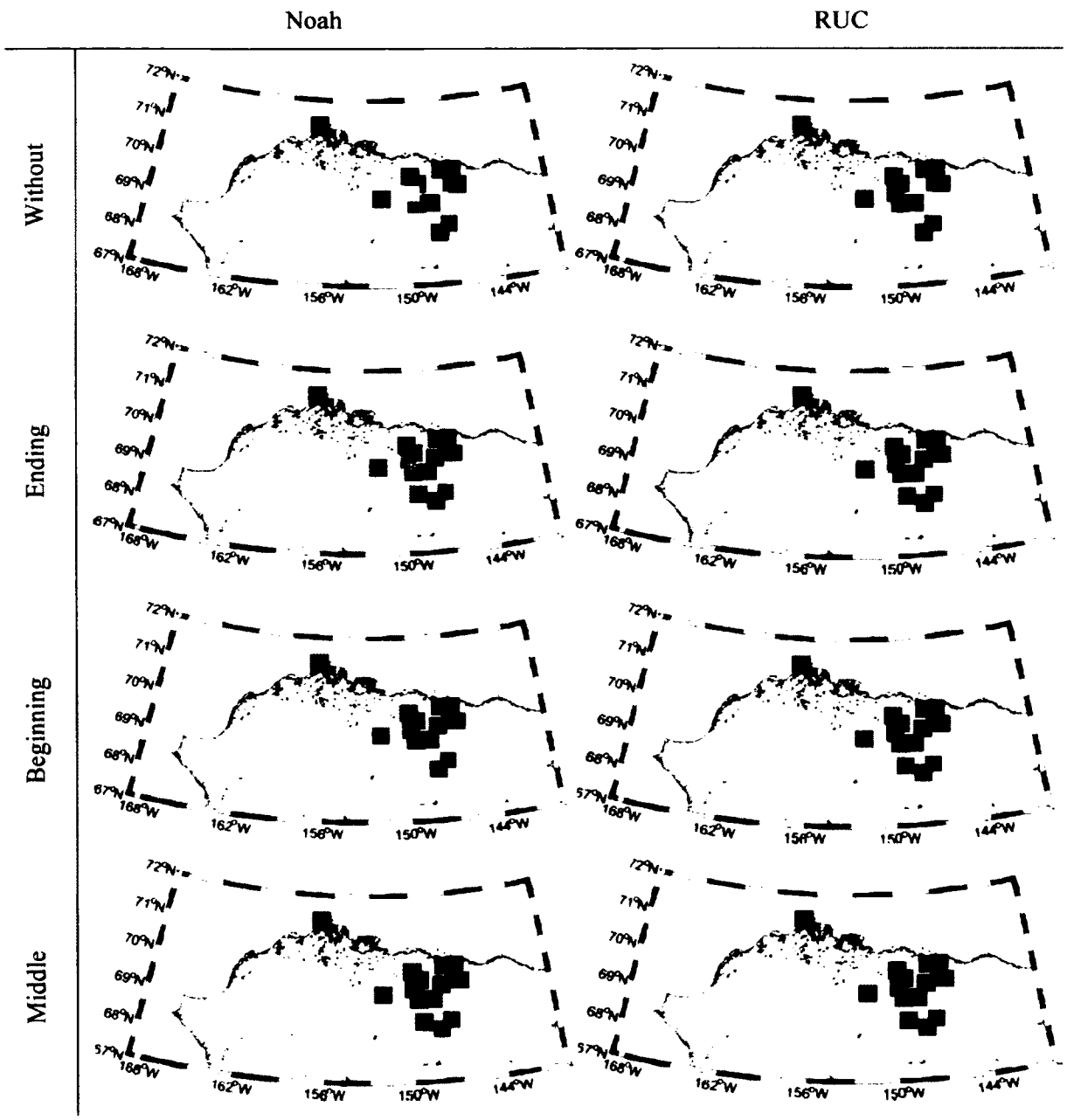

Figure 14: January-February wind speed hourly means of the observation from simulation (sim-obs) absolute percentage difference for the events of precipitation.

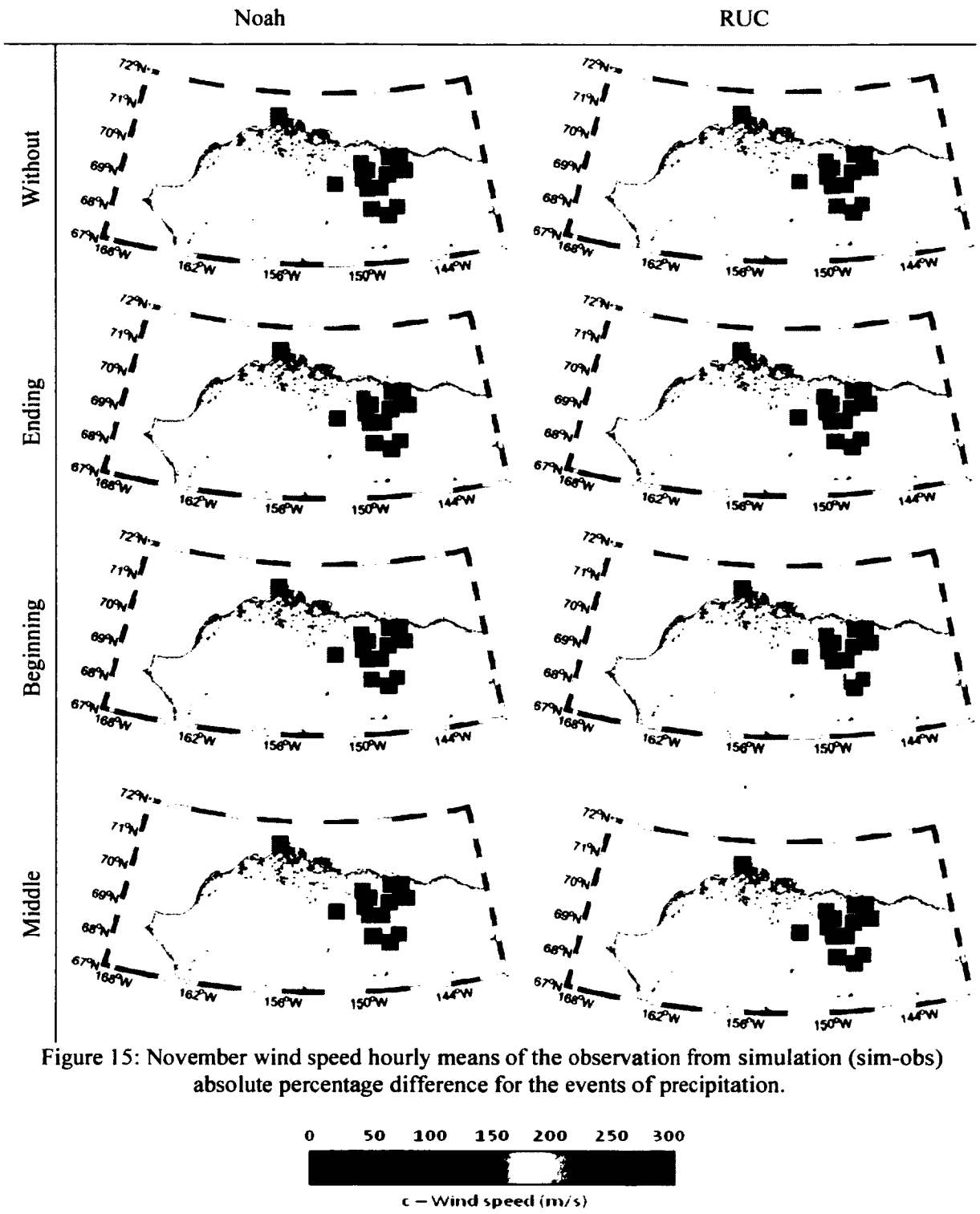

Figure 15: November wind speed hourly means of the observation from simulation (sim-obs) absolute percentage difference for the events of precipitation.

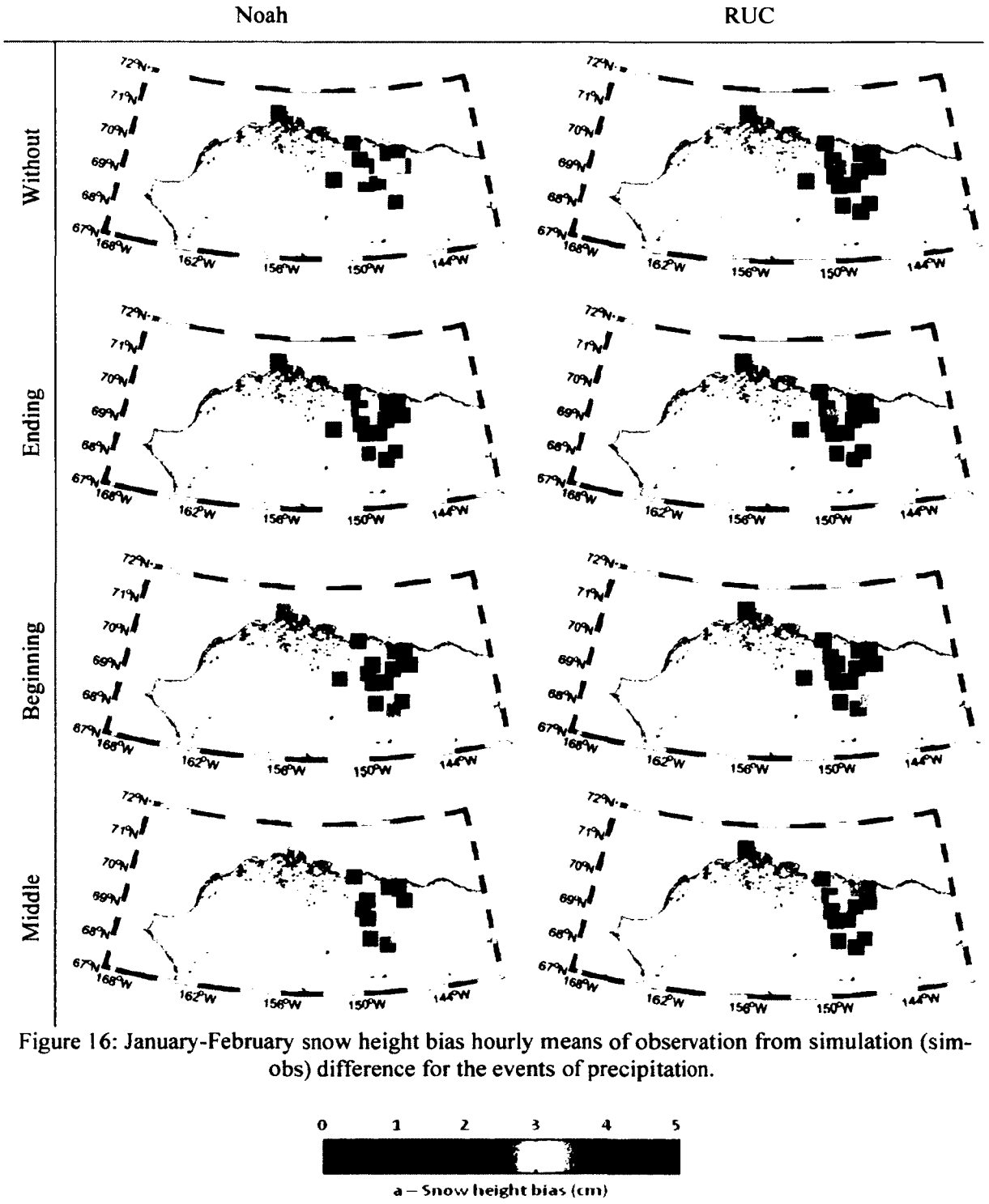

Figure 16: January-February snow height bias hourly means of observation from simulation (sim-obs) difference for the events of precipitation.

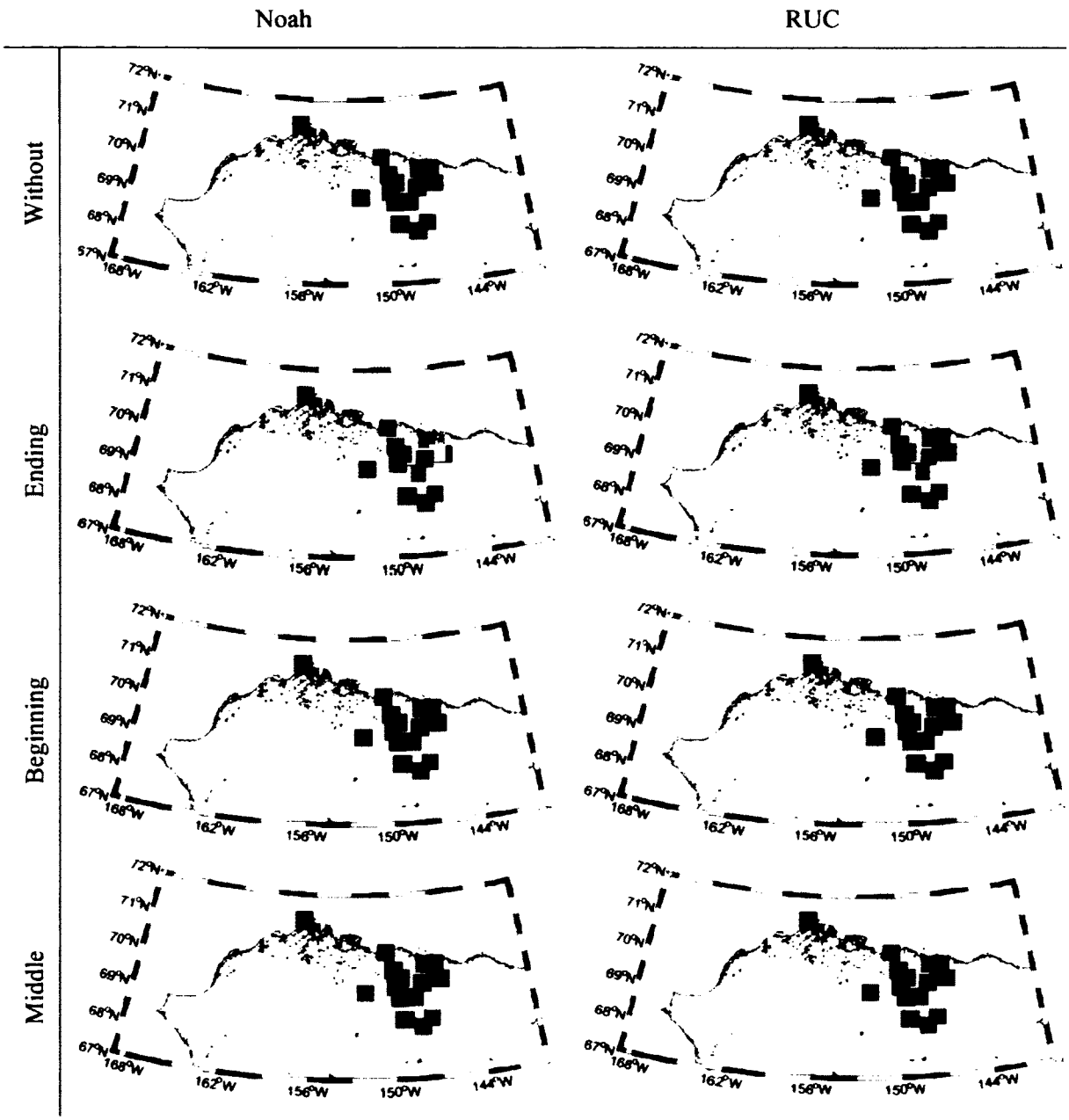

Figure 17: November snow height bias hourly means of observation from simulation (sim-obs) difference for the events of precipitation.

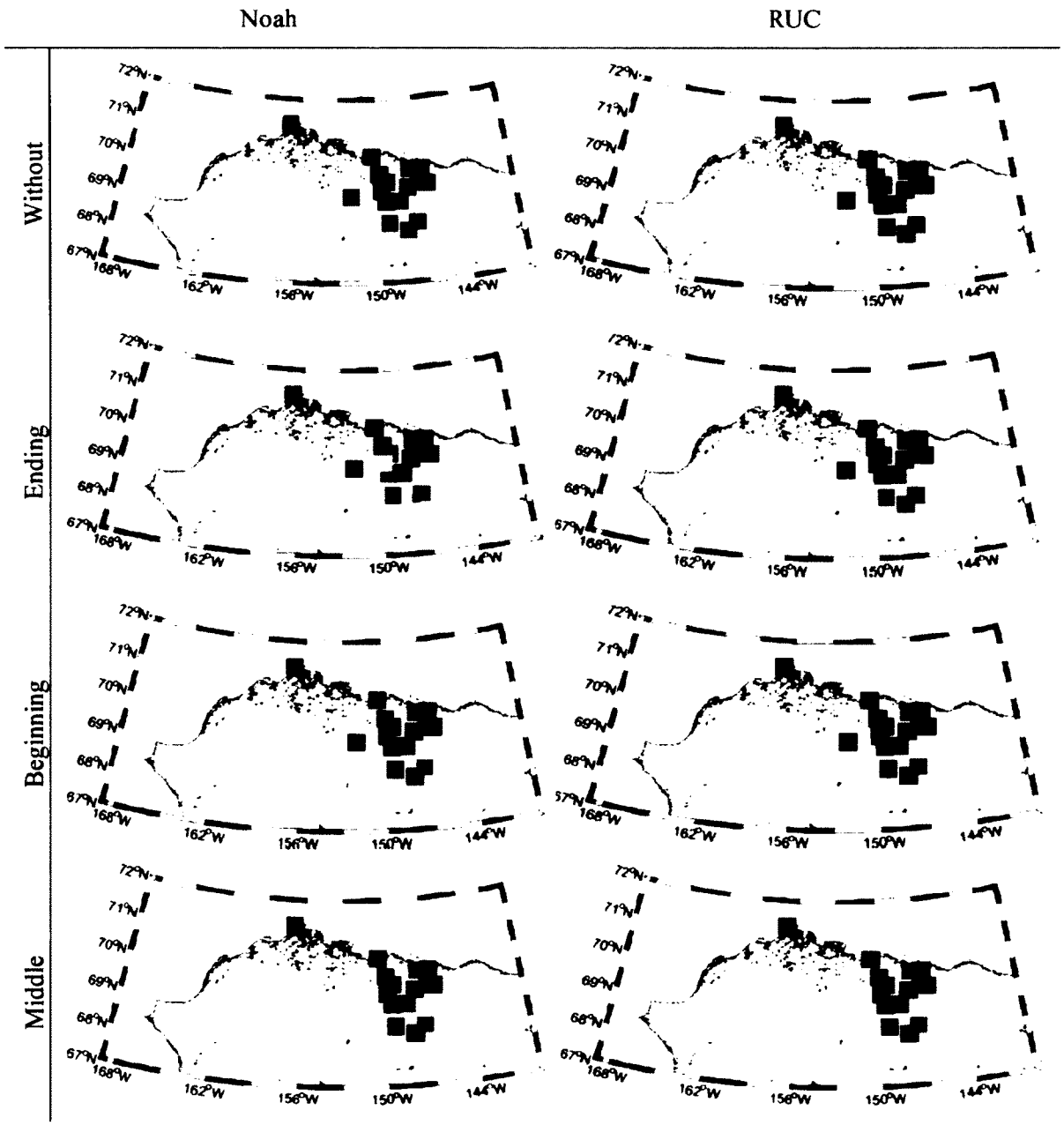

Figure 18: January-February snow depth bias hourly means of the observation from simulation (sim-obs) absolute difference for the events of precipitation.

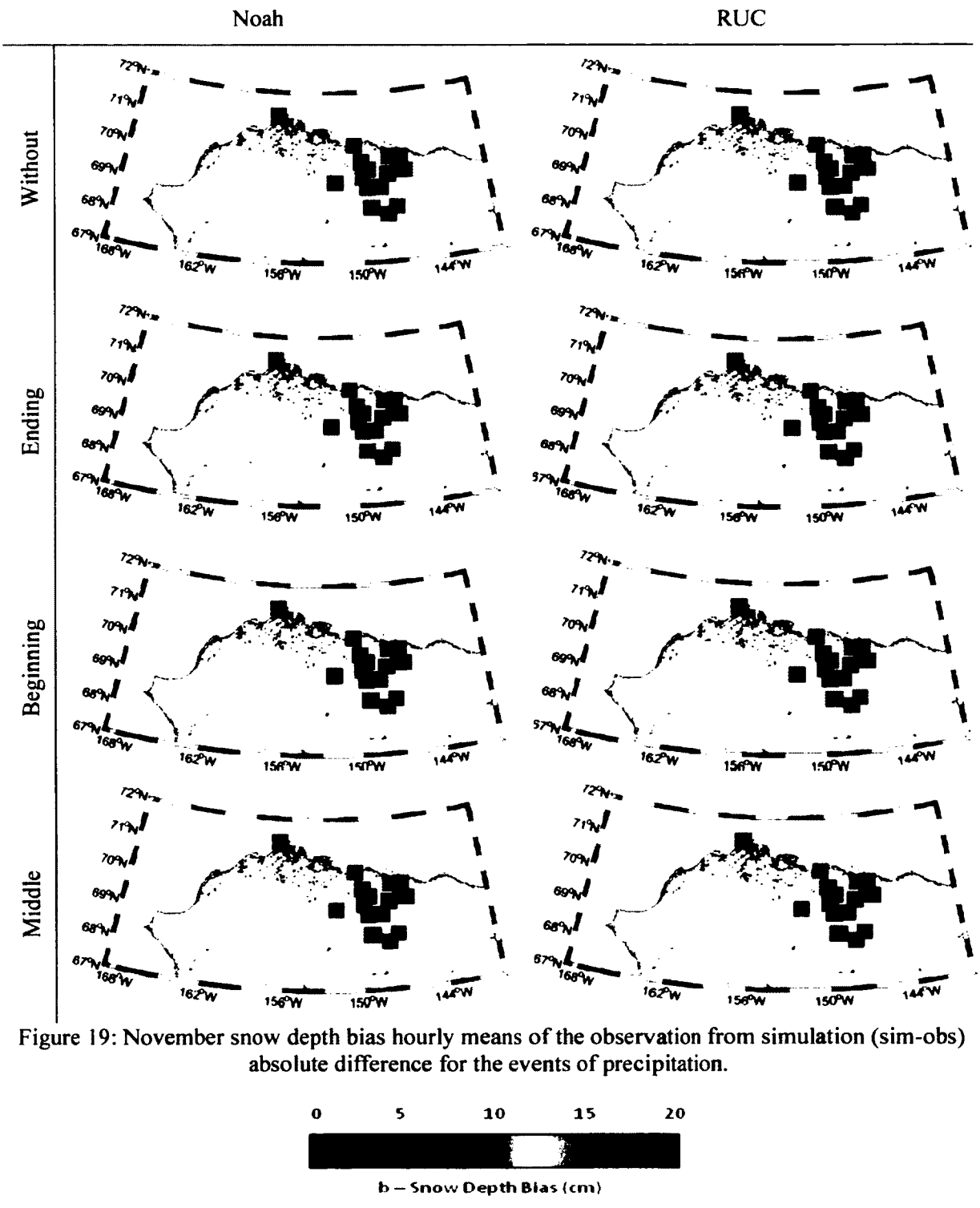

Figure 19: November snow depth bias hourly means of the observation from simulation (sim-obs) absolute difference for the events of precipitation.

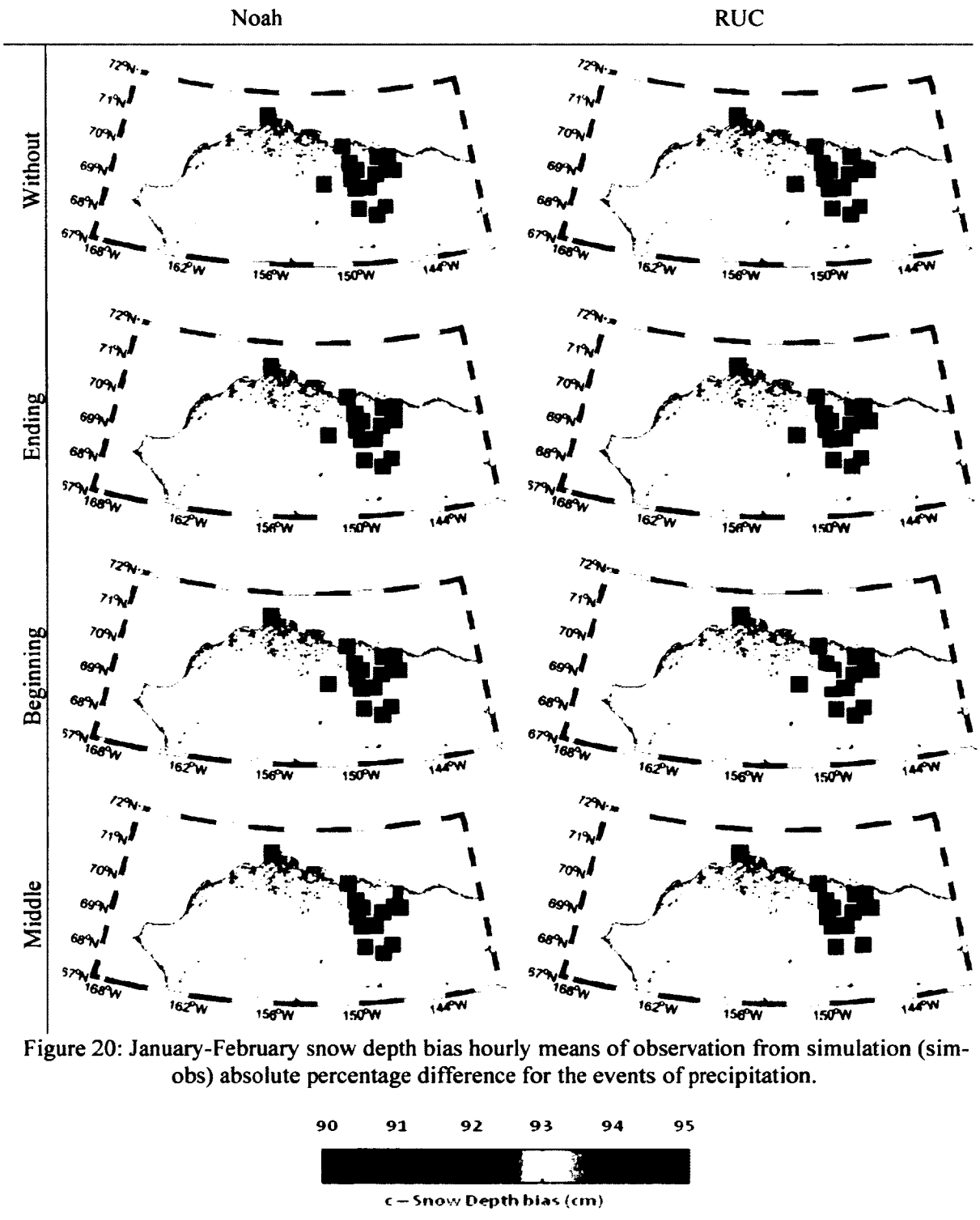

Figure 20: January-February snow depth bias hourly means of observation from simulation (sim-obs) absolute percentage difference for the events of precipitation.

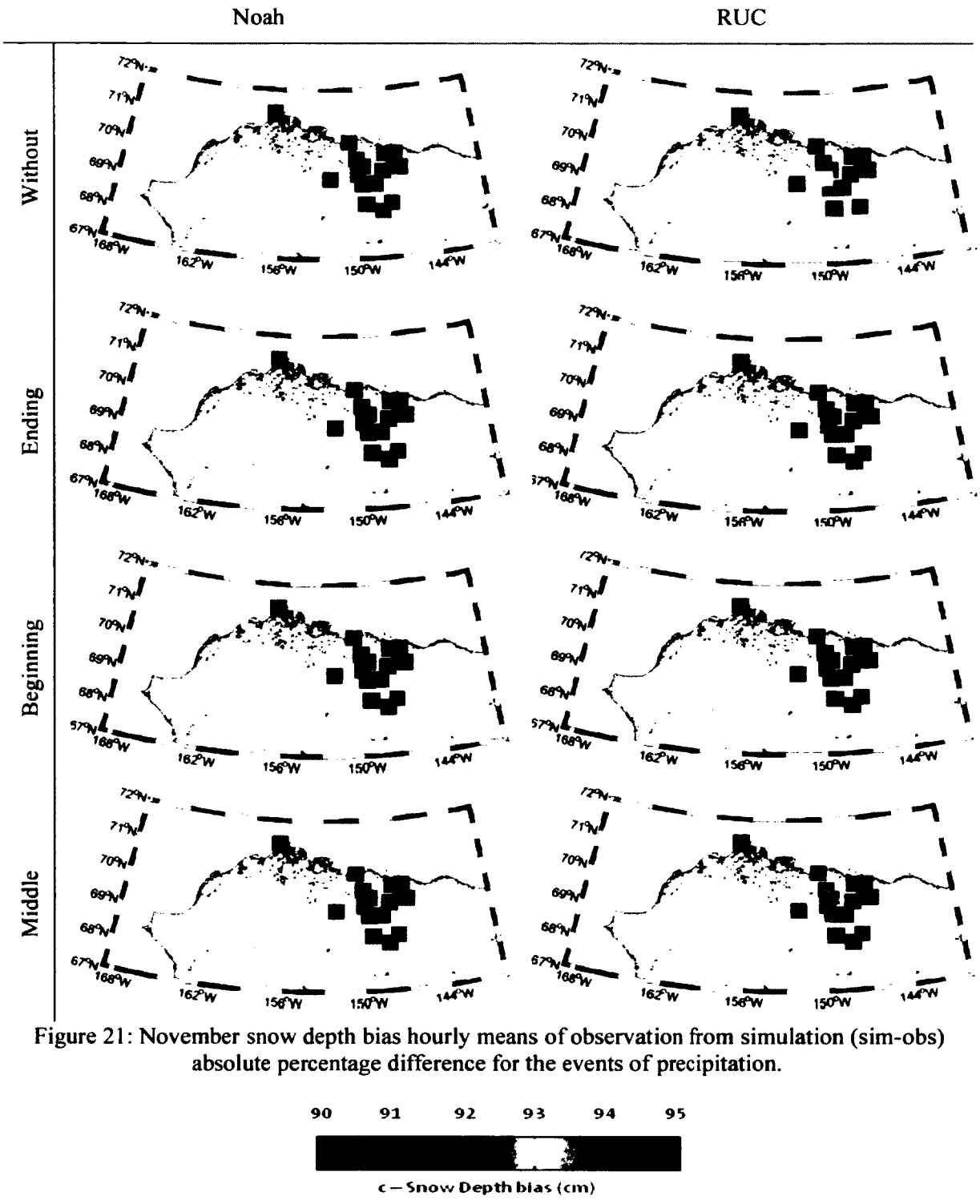

Figure 21: November snow depth bias hourly means of observation from simulation (sim-obs) absolute percentage difference for the events of precipitation.

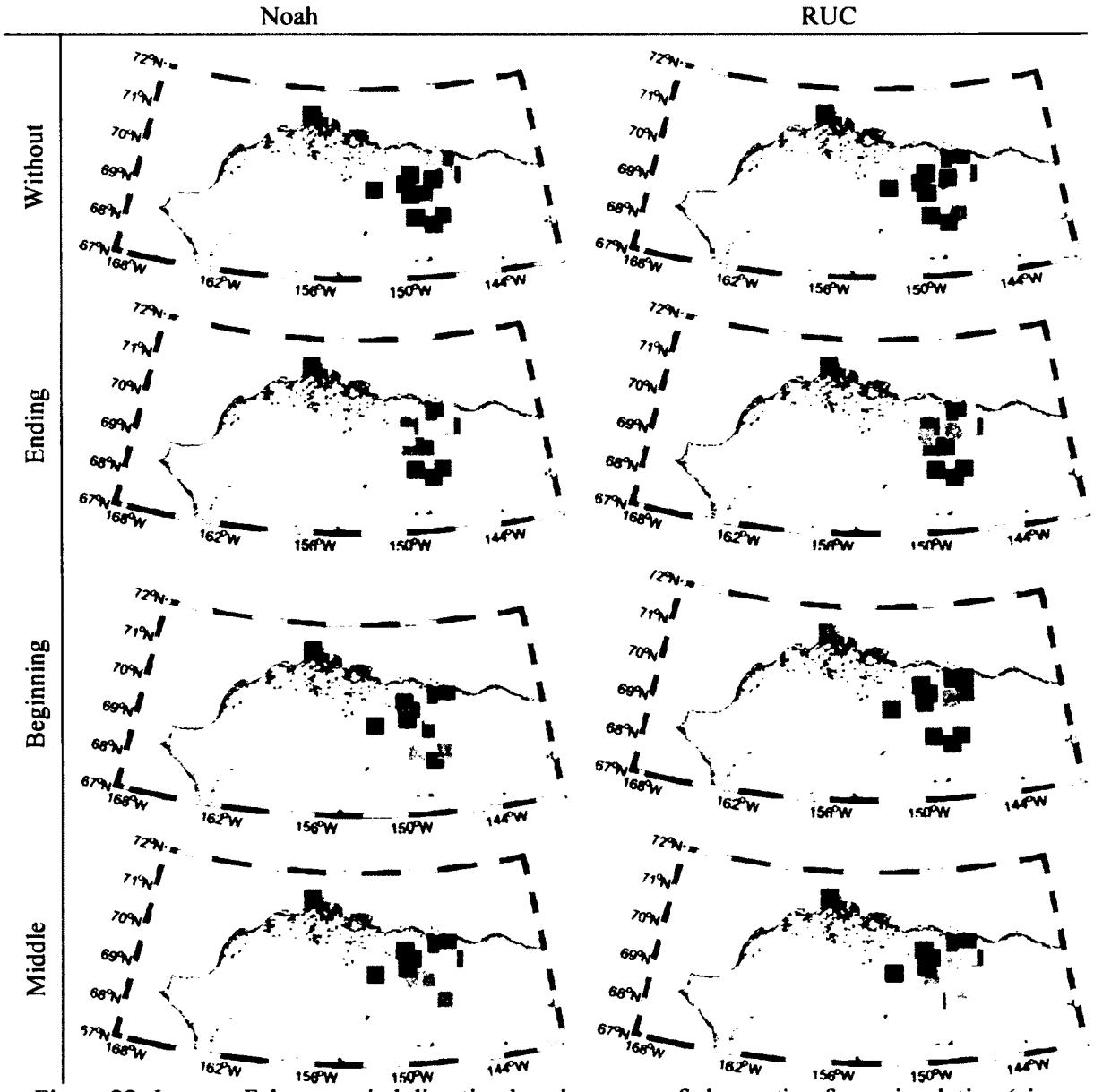

Figure 22: January-February wind direction hourly means of observation from simulation (sim-obs) difference for the events of precipitation.

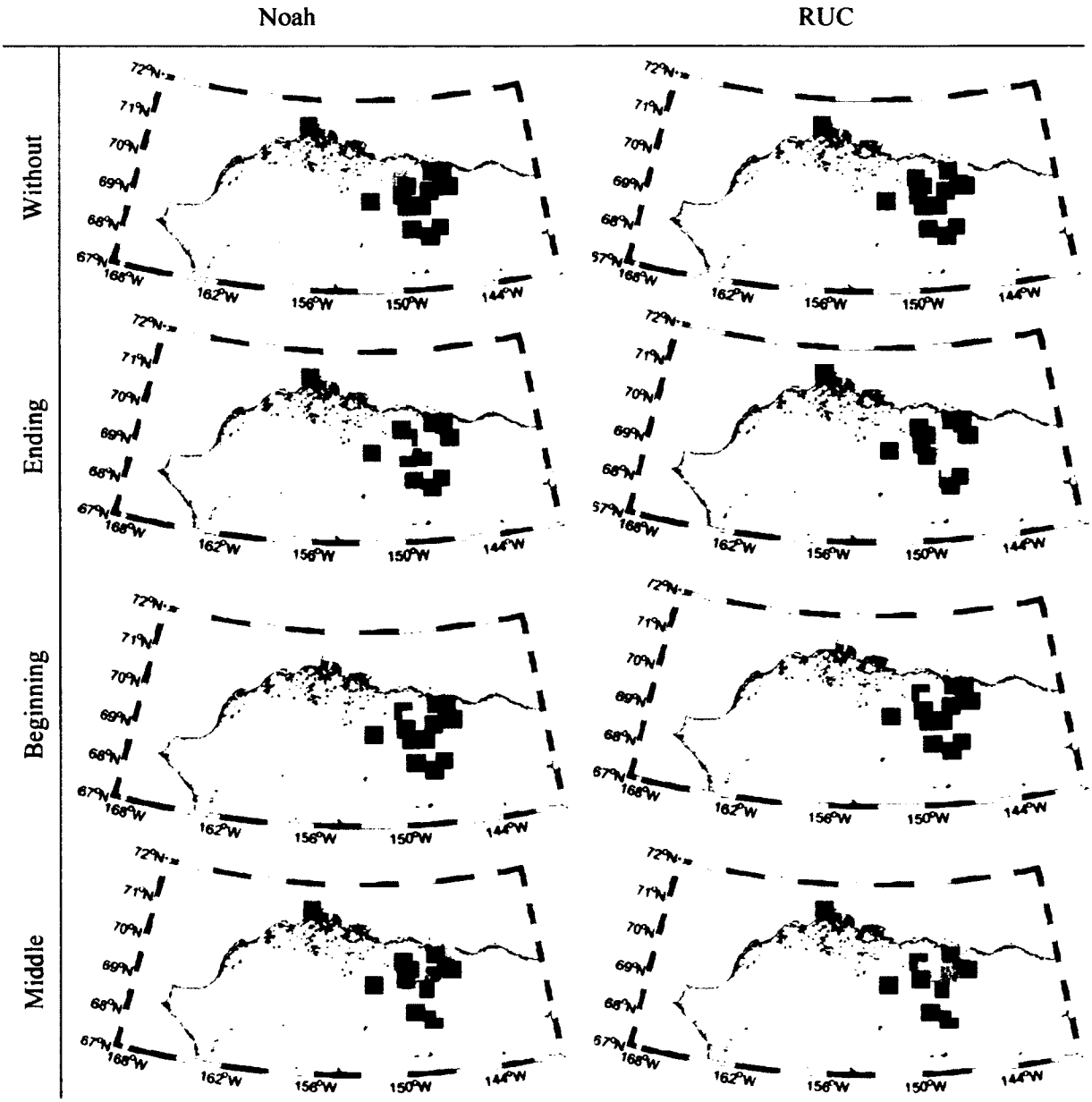

Figure 23: November wind direction hourly means of observation from simulation (sim-obs) difference for the events of precipitation.

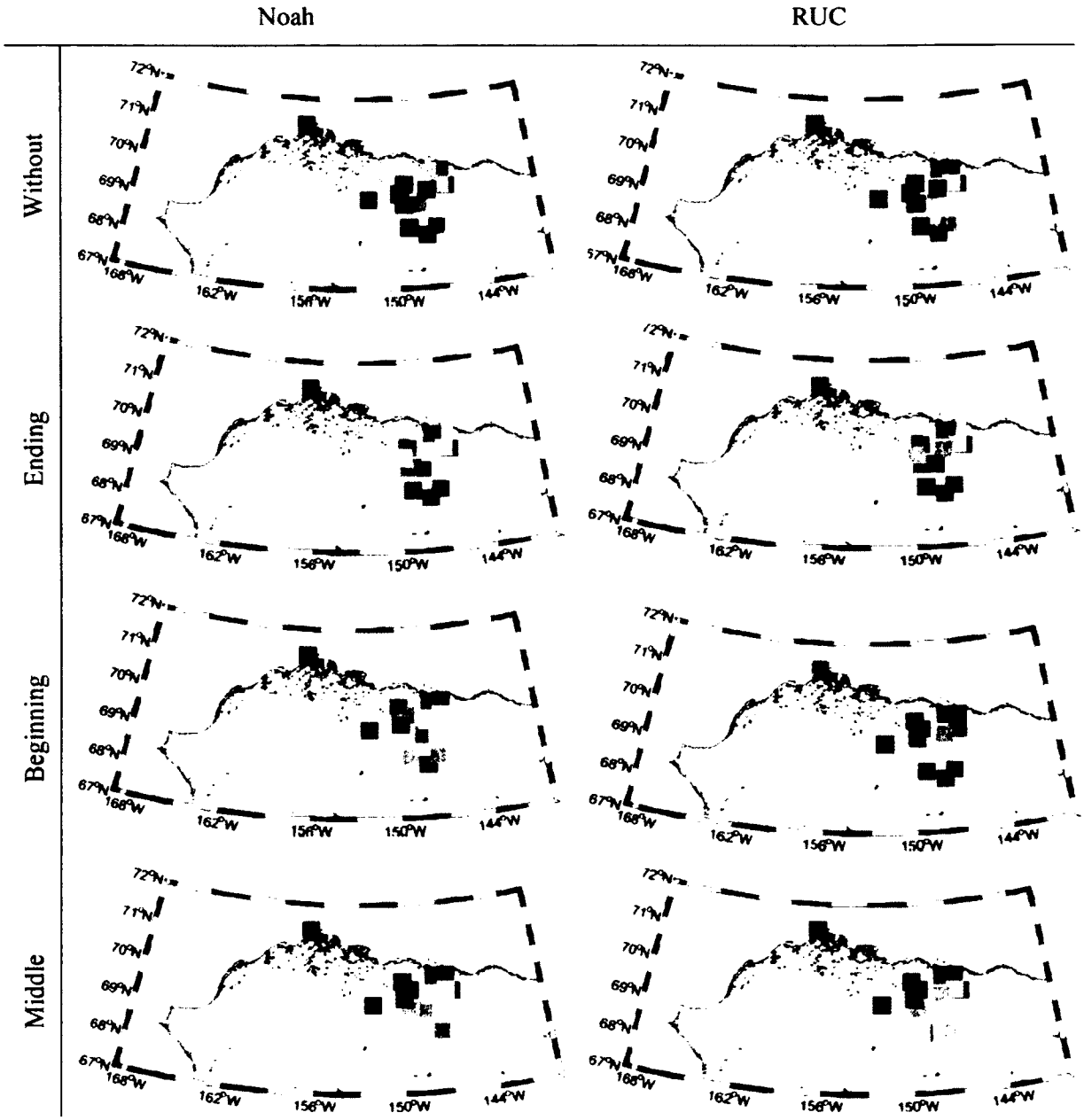

Figure 24: January-February wind direction hourly means of the observation from simulation (sim-obs) absolute difference for the events precipitation.

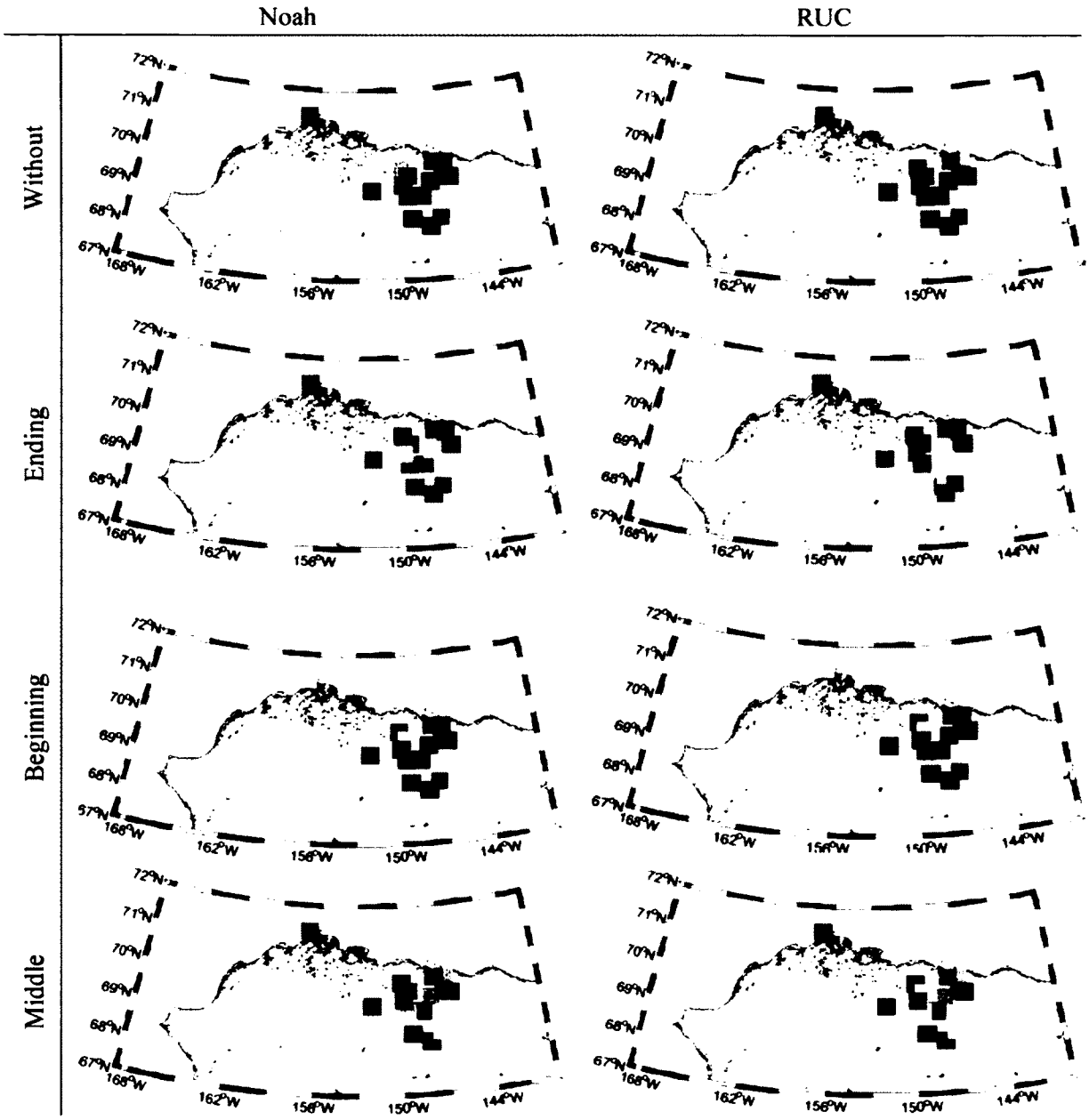

Figure 25: November wind direction hourly means of the observation from simulation (sim-obs) absolute difference for the events of precipitation.

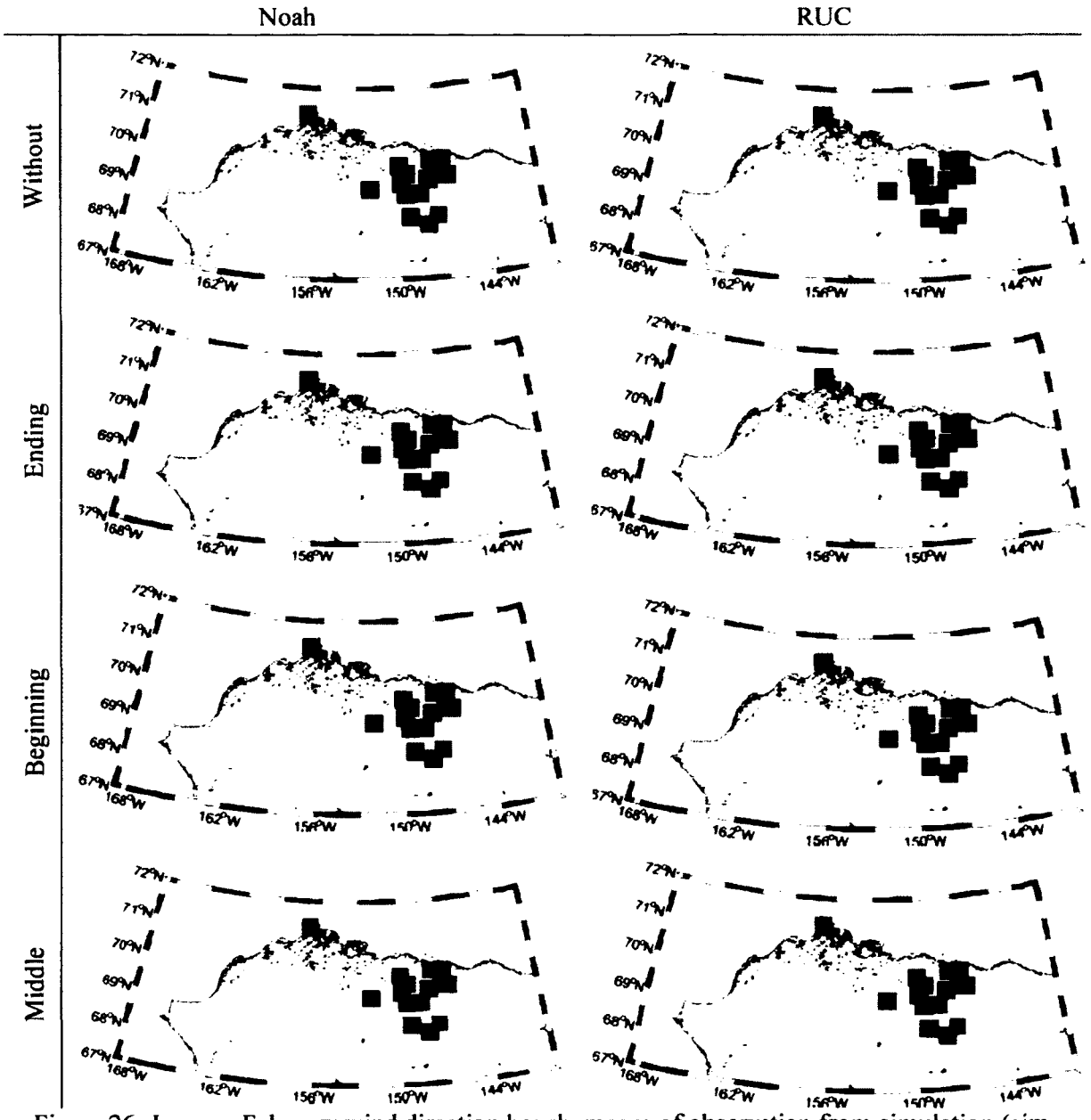

Figure 26: January-February wind direction hourly means of observation from simulation (sim-obs) absolute percentage difference for the events of precipitation.

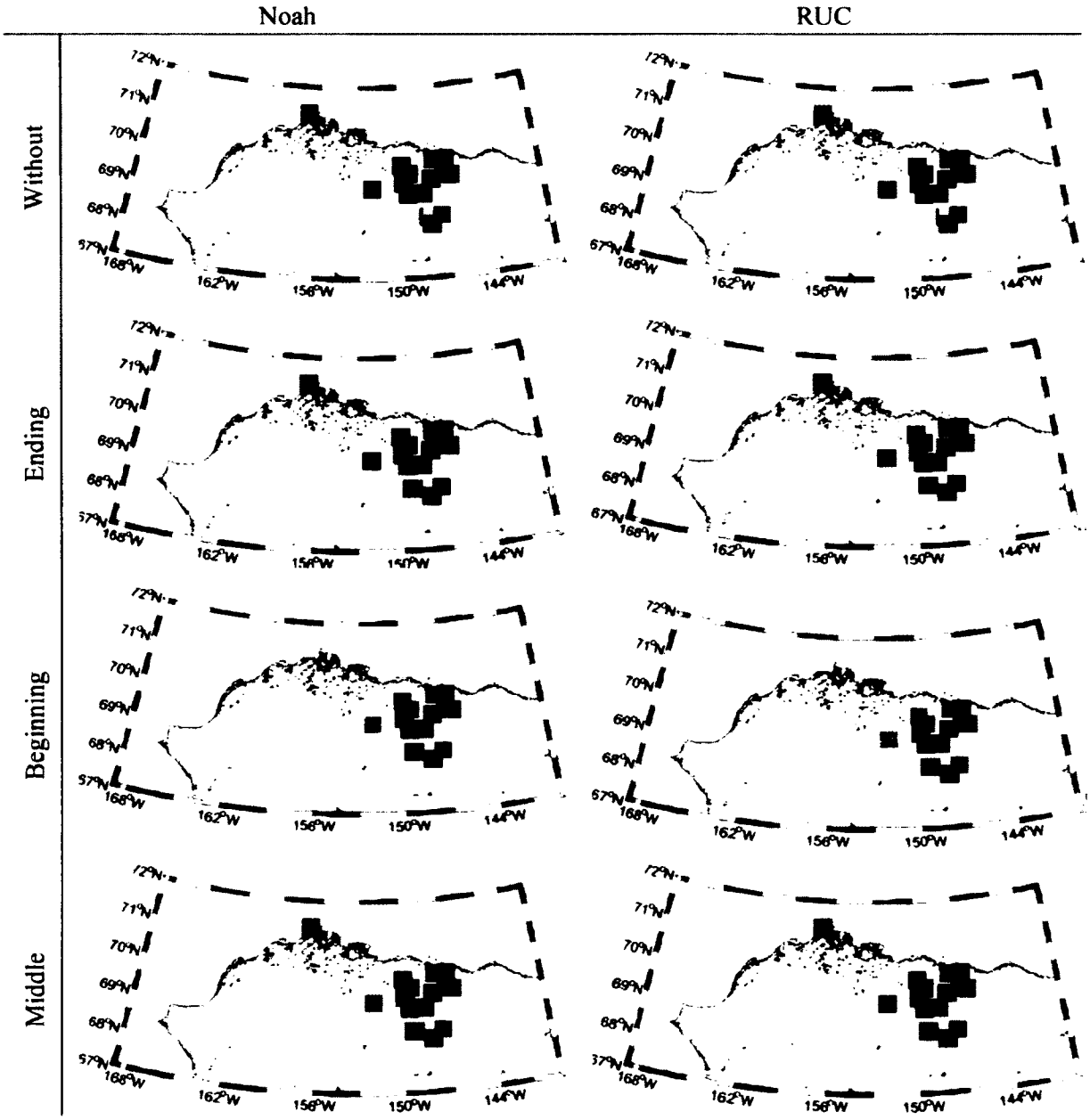

Figure 27: November wind direction hourly means of observation from simulation (sim-obs) absolute percentage difference for the events of precipitation.

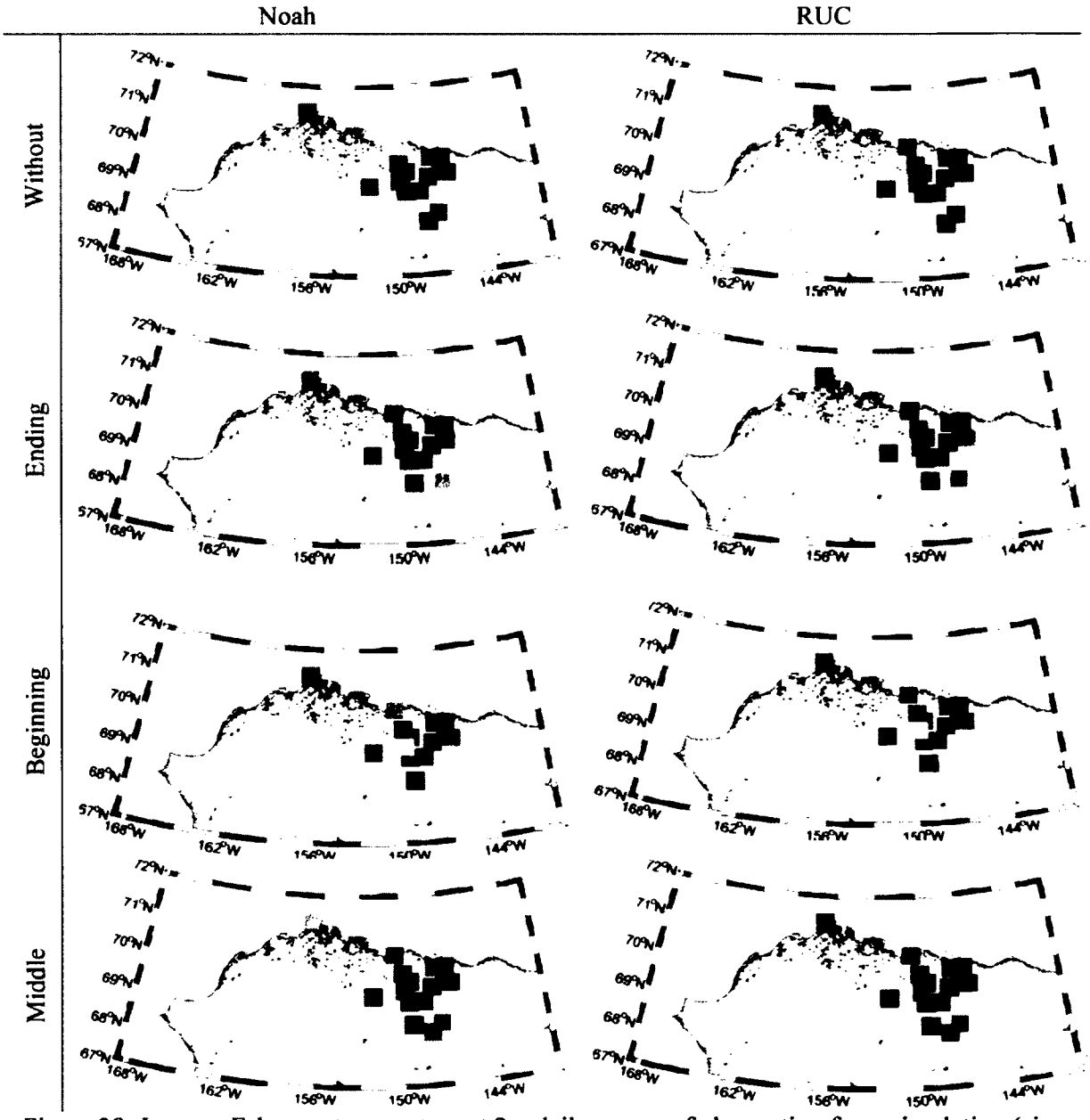

Figure 28: January-February temperature at 2m daily means of observation from simulation (sim-obs) difference for the events of precipitation.

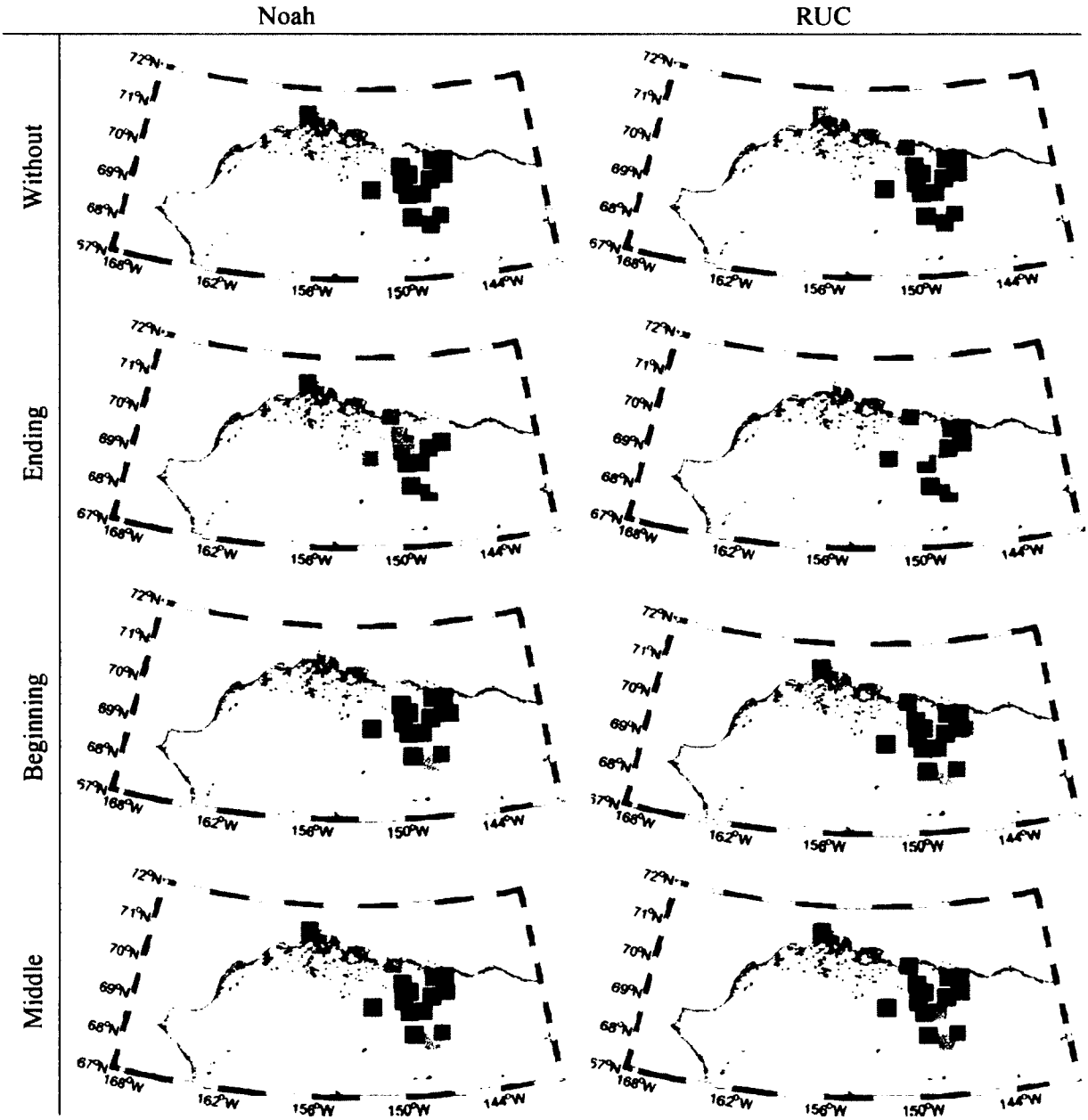

Figure 29: November temperature at 2m daily means of observation from simulation (sim-obs) difference for the events of precipitation.

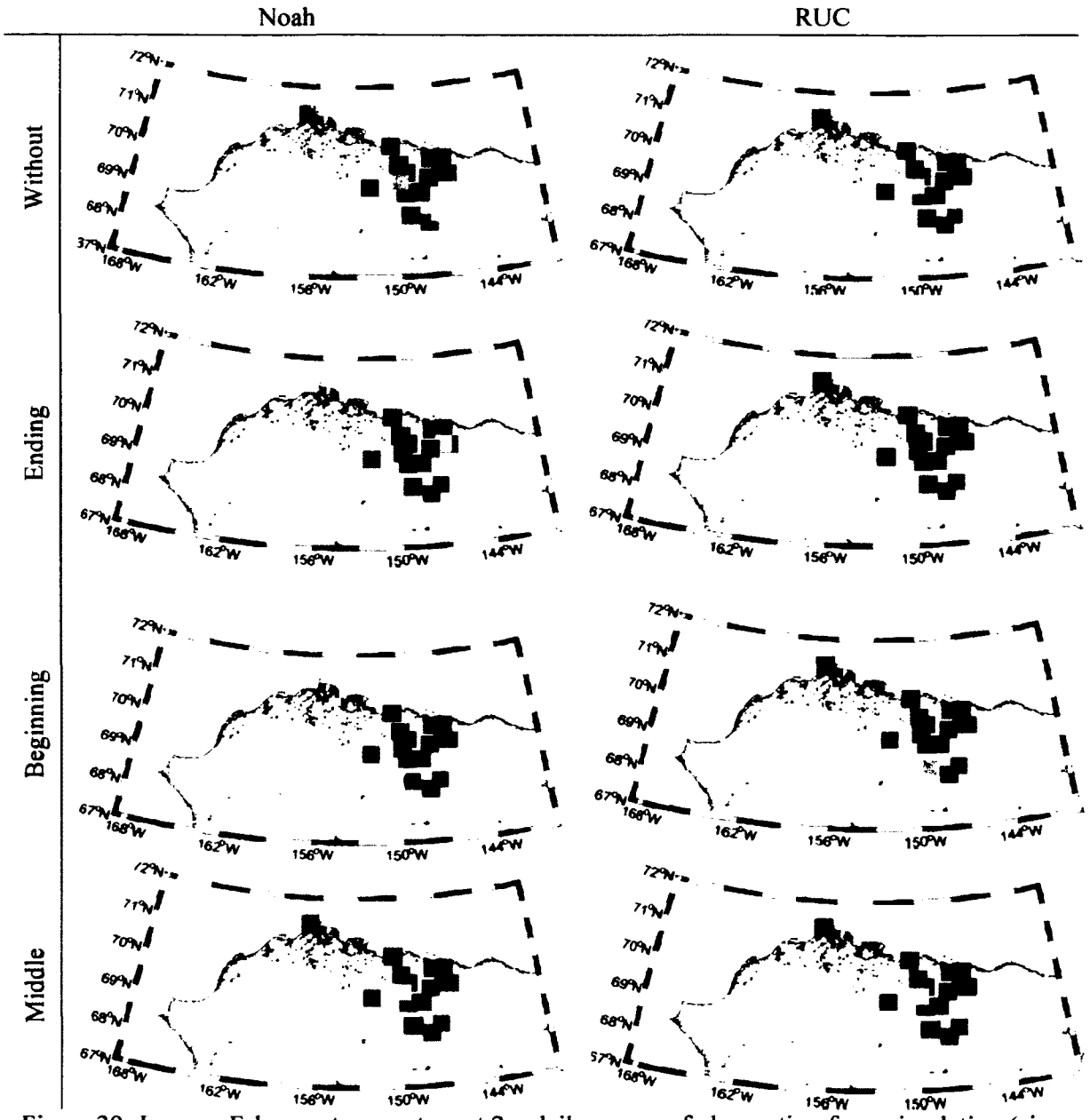

Figure 30: January-February temperature at 2m daily means of observation from simulation (sim-obs) absolute difference for the events of precipitation.

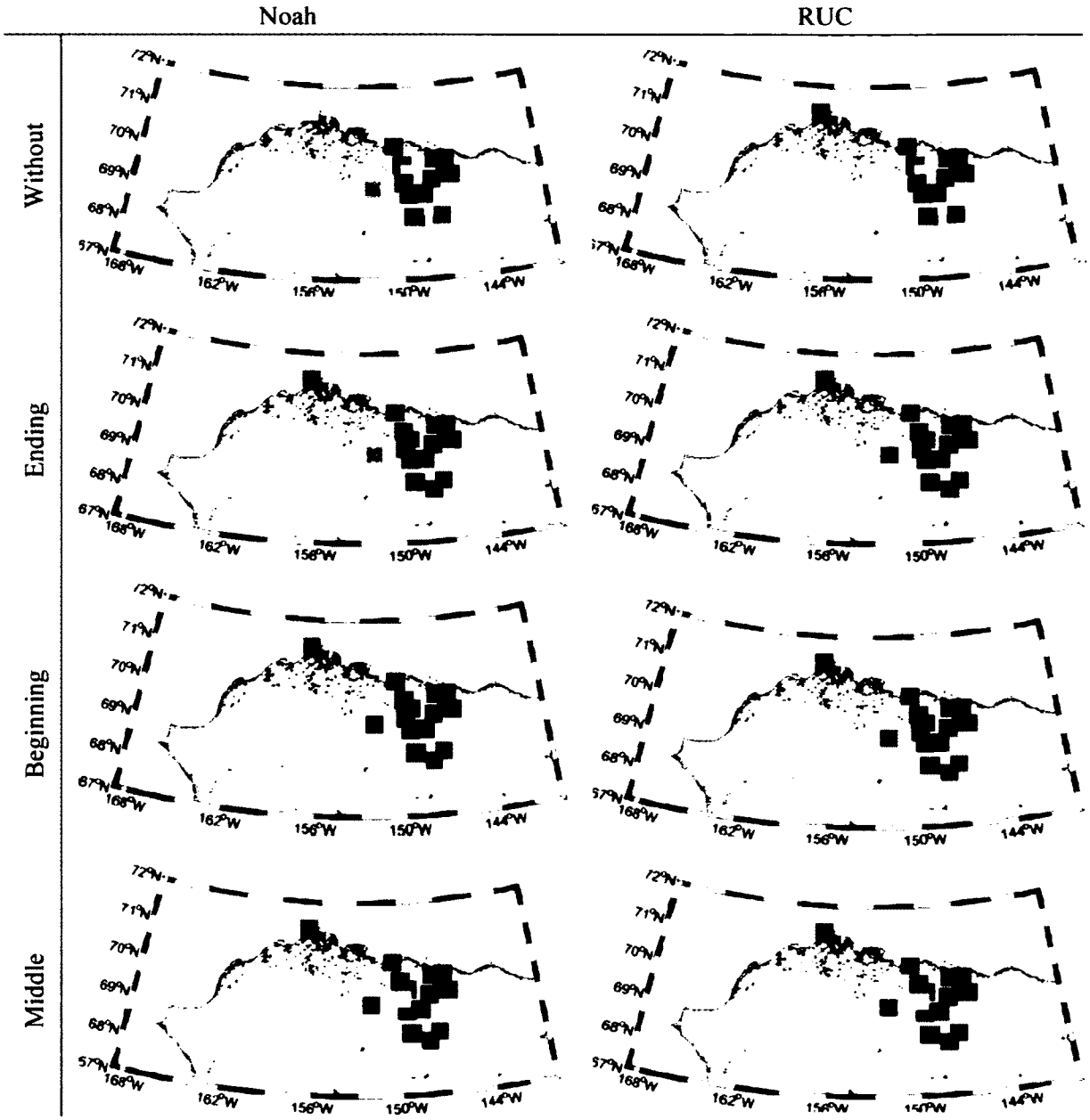

Figure 31: November temperature at 2m daily means of observation from simulation (sim-obs) absolute difference for the events of precipitation.

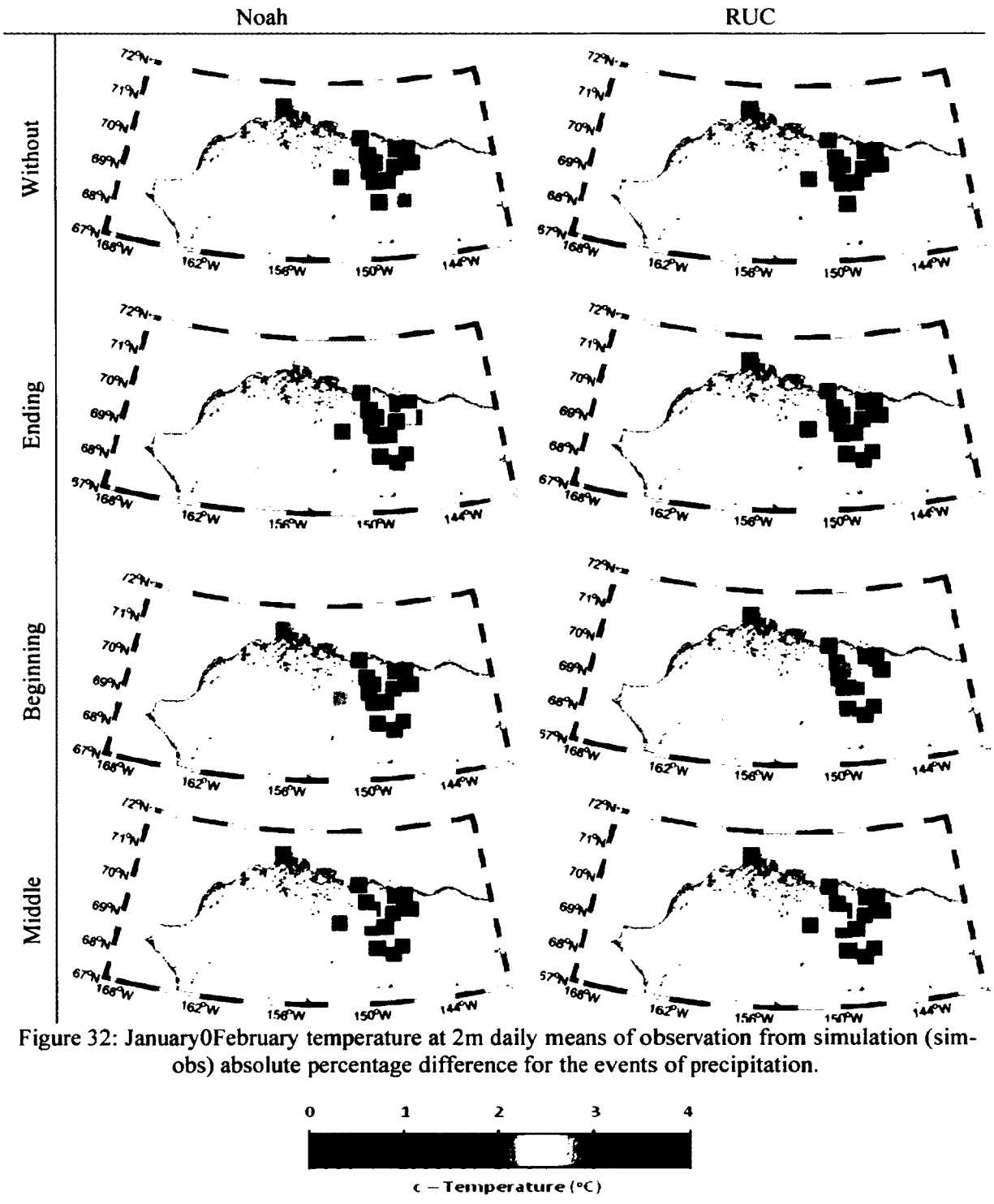

Figure 32: January0February temperature at 2m daily means of observation from simulation (sim-obs) absolute percentage difference for the events of precipitation.

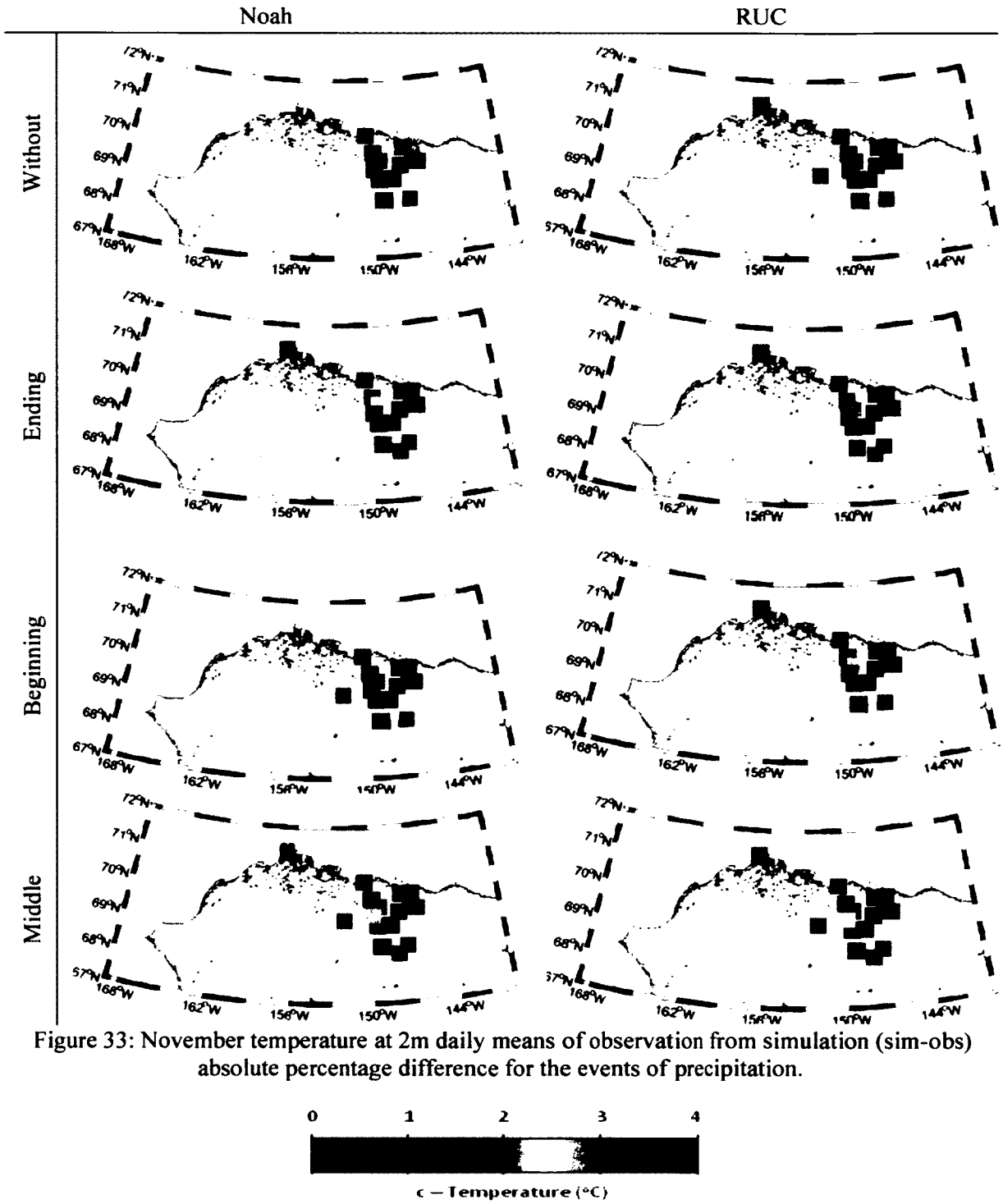

Figure 33: November temperature at 2m daily means of observation from simulation (sim-obs) absolute percentage difference for the events of precipitation.

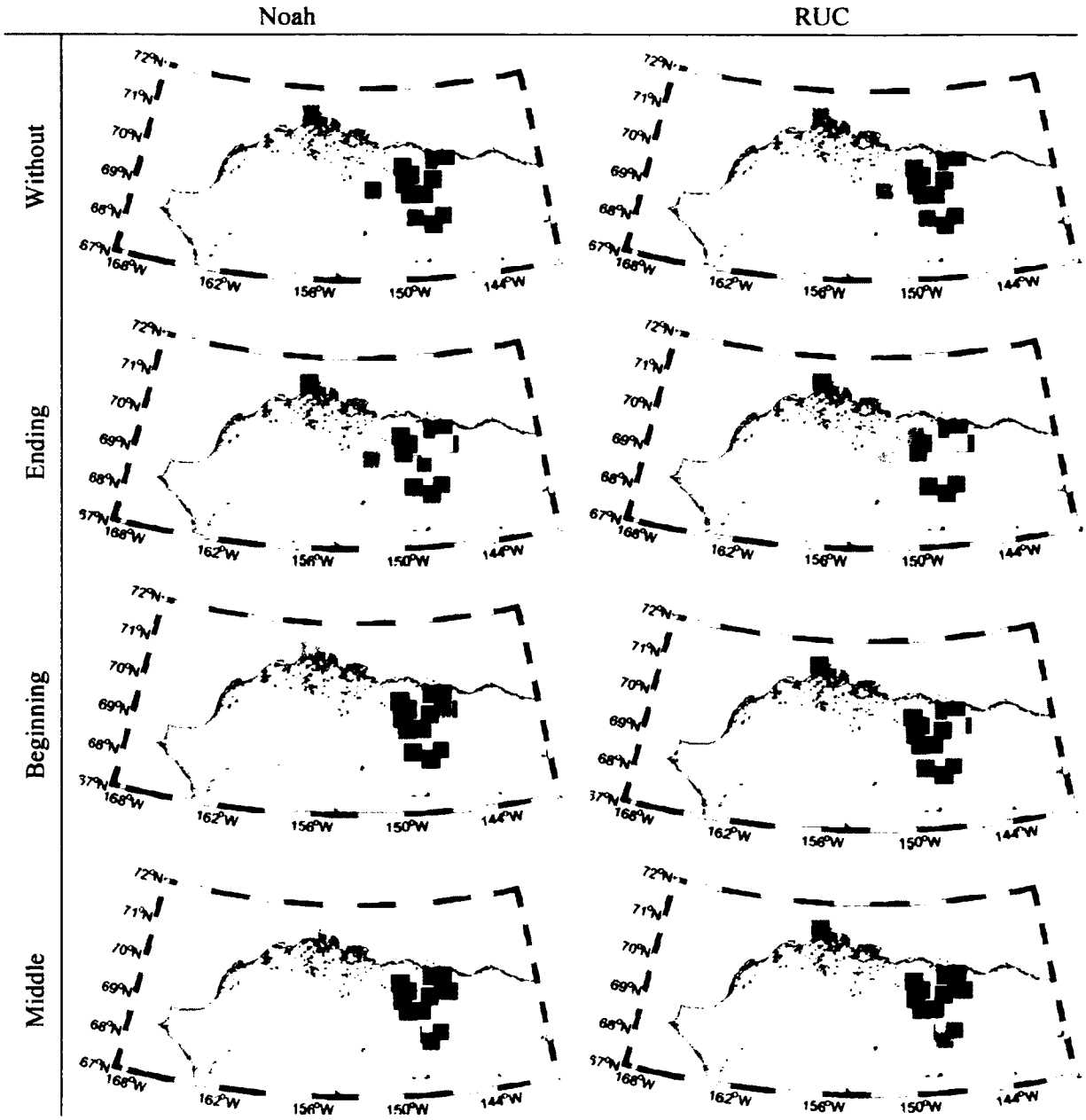

Figure 34: January-February wind speed daily means of observation from simulation (sim-obs) difference for the events of precipitation.

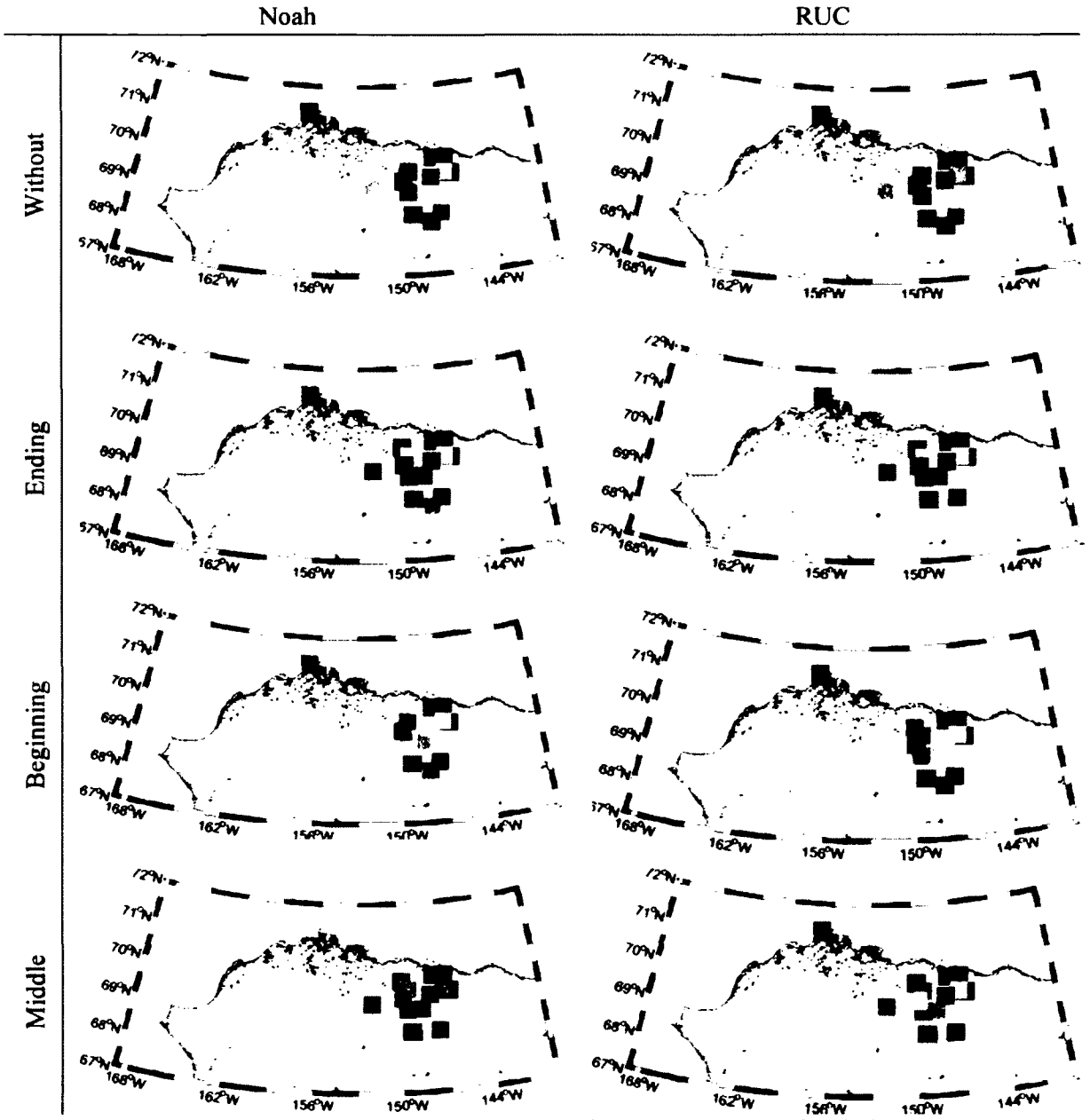

Figure 35: November wind speed daily means of observation from simulation (sim-obs) difference for the events of precipitation.

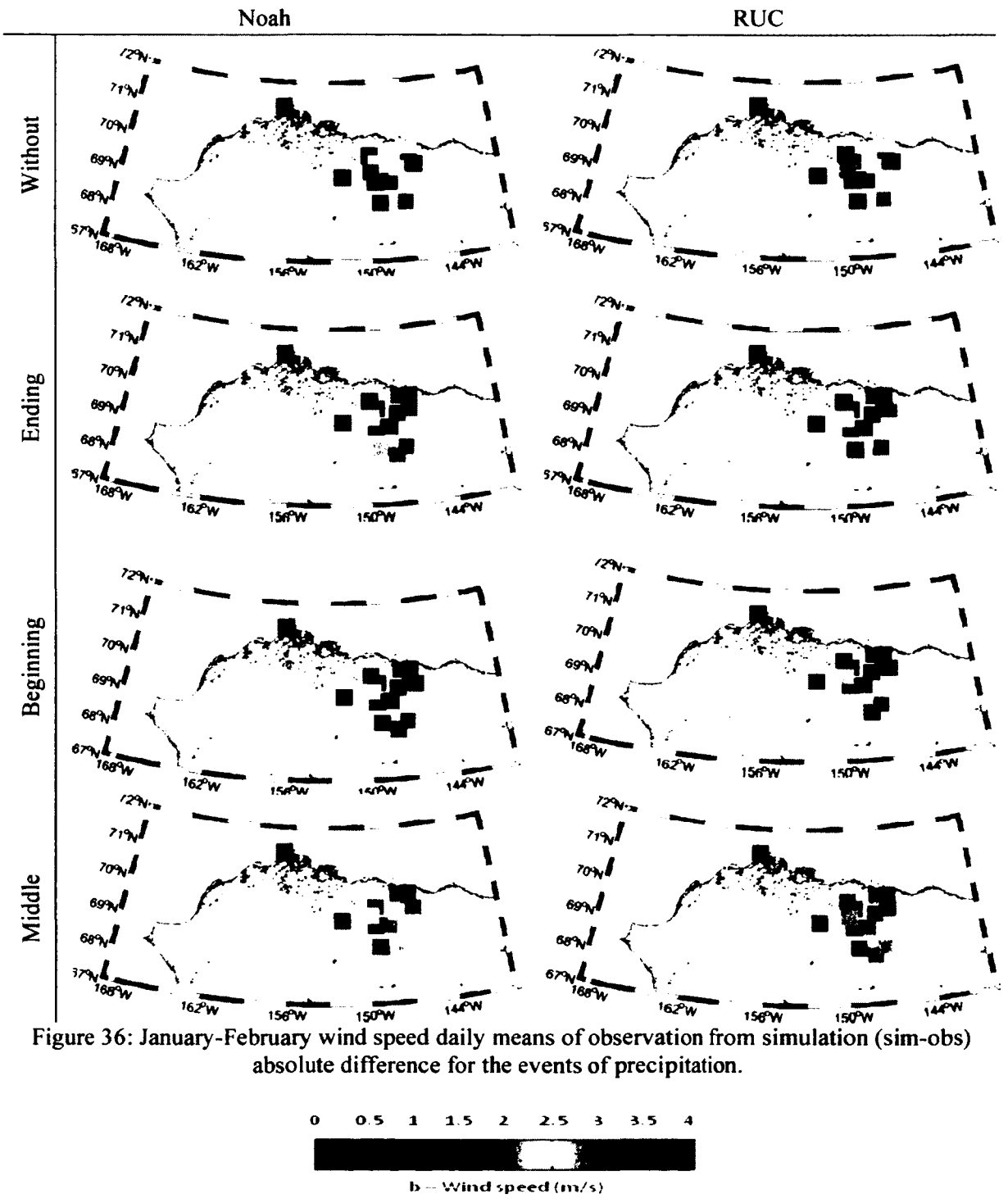

Figure 36: January-February wind speed daily means of observation from simulation (sim-obs) absolute difference for the events of precipitation.

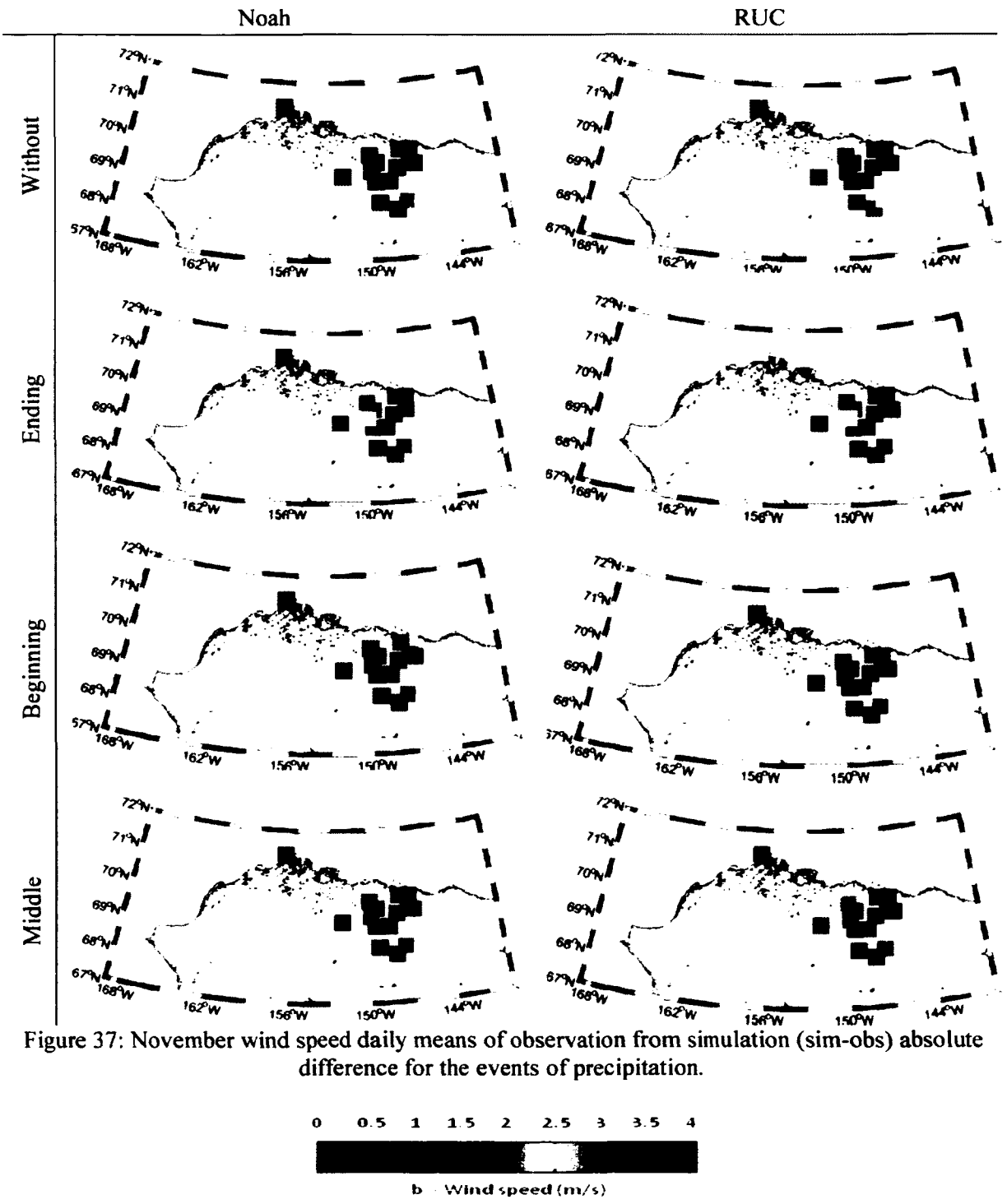

Figure 37: November wind speed daily means of observation from simulation (sim-obs) absolute difference for the events of precipitation.

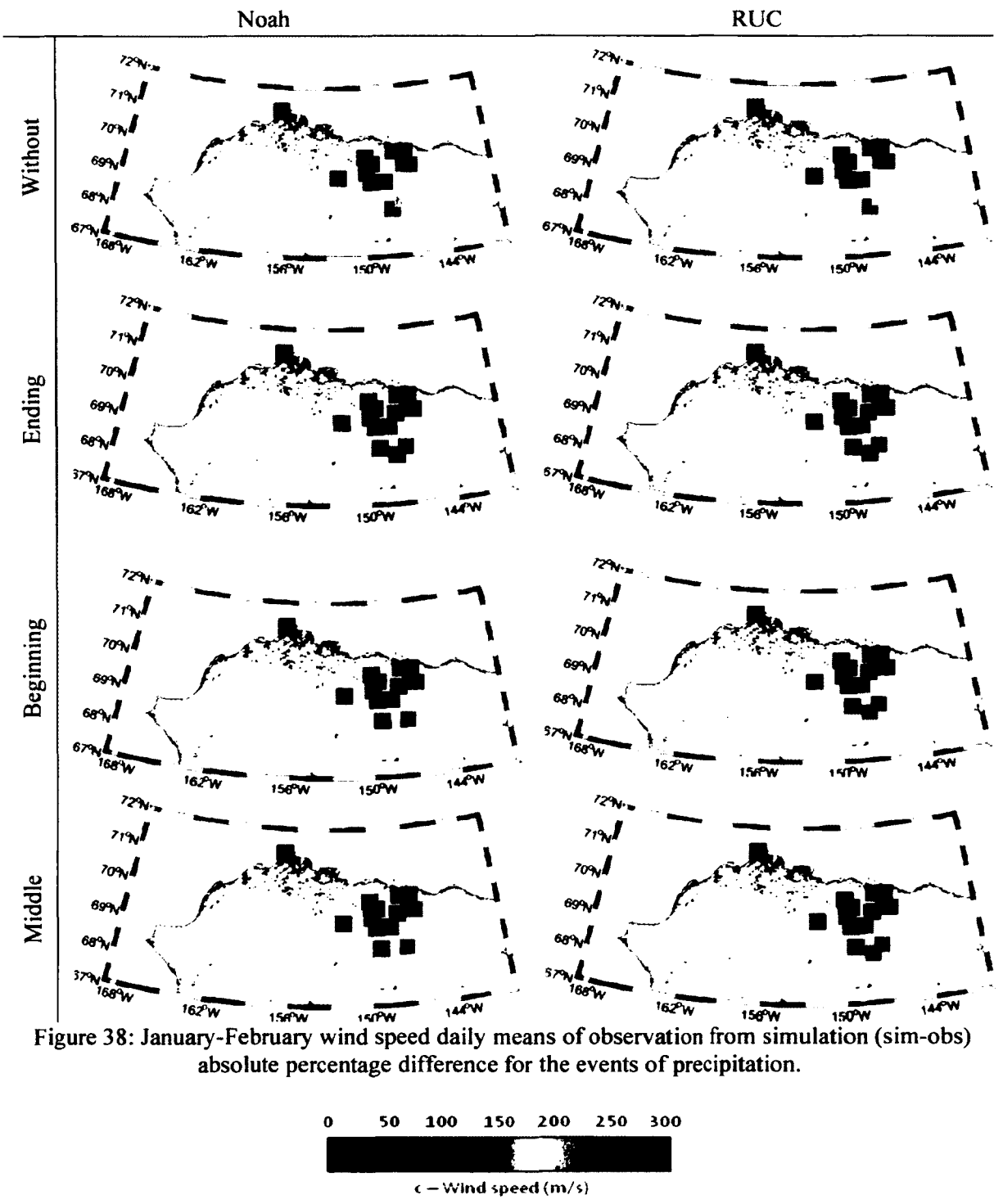

Figure 38: January-February wind speed daily means of observation from simulation (sim-obs) absolute percentage difference for the events of precipitation.

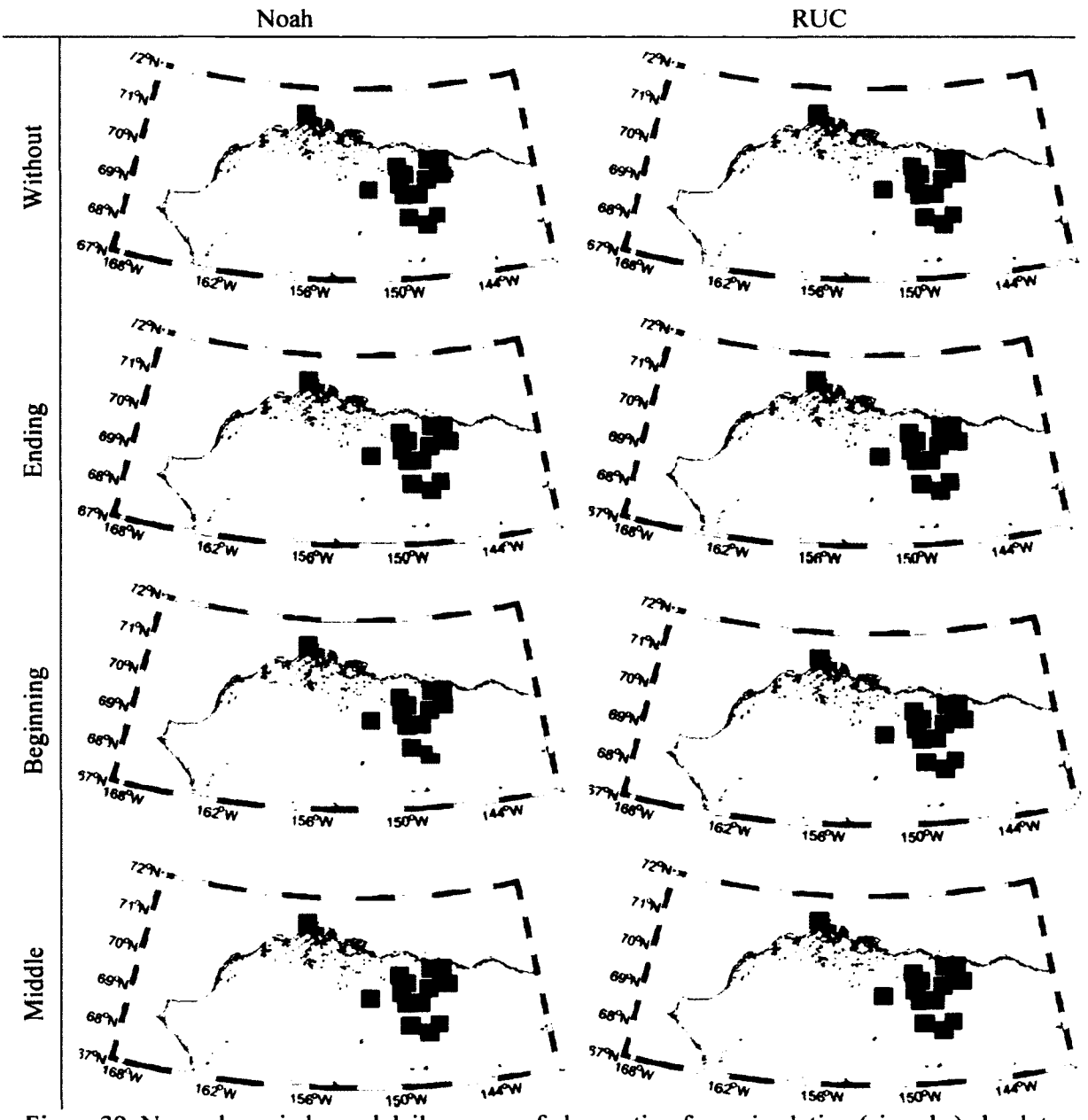

Figure 39: November wind speed daily means of observation from simulation (sim-obs) absolute percentage difference for the events of precipitation.

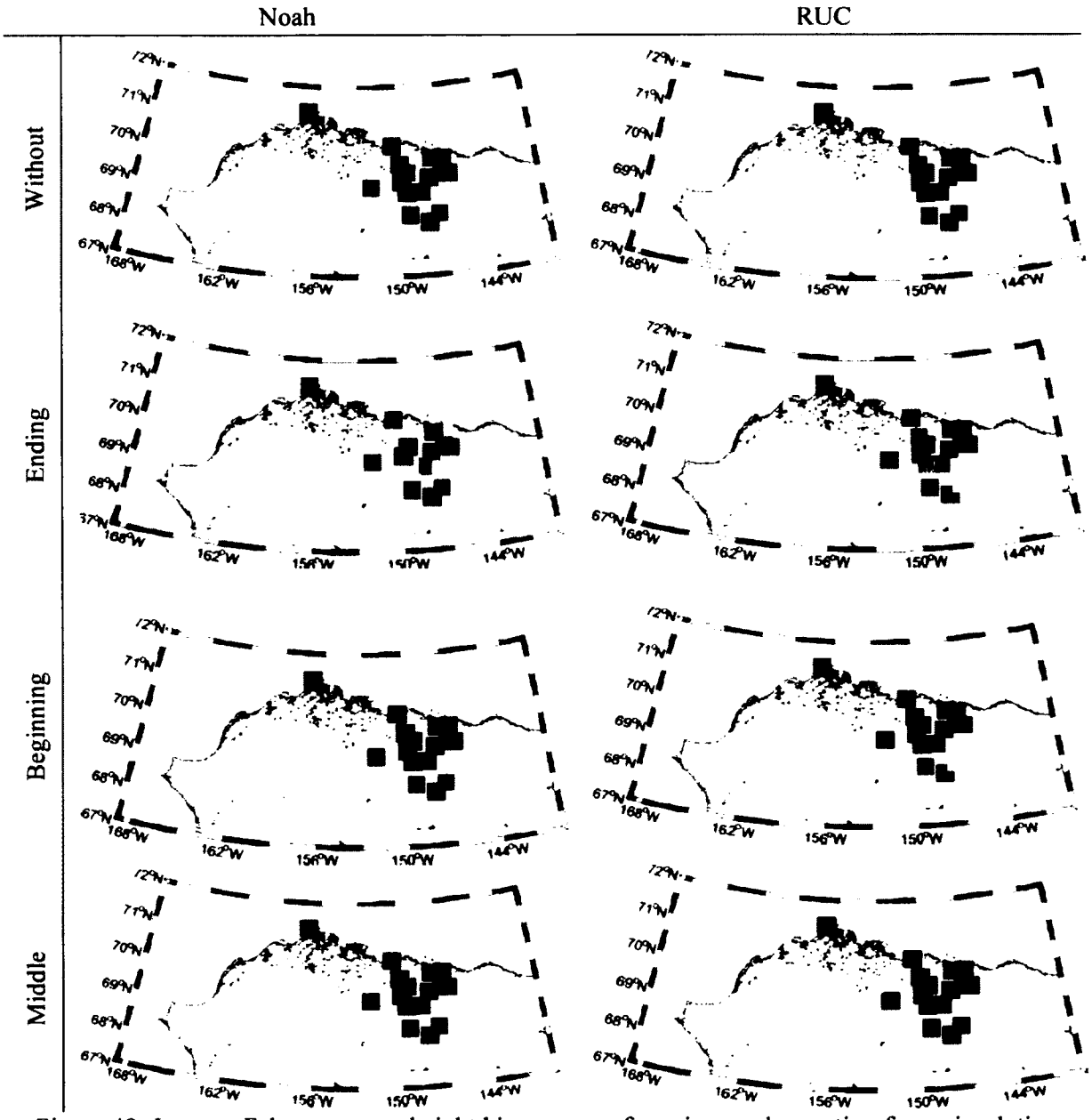

Figure 40: January-February snow height bias means of maximum observation from simulation (sim-obs) difference for the events of precipitation.

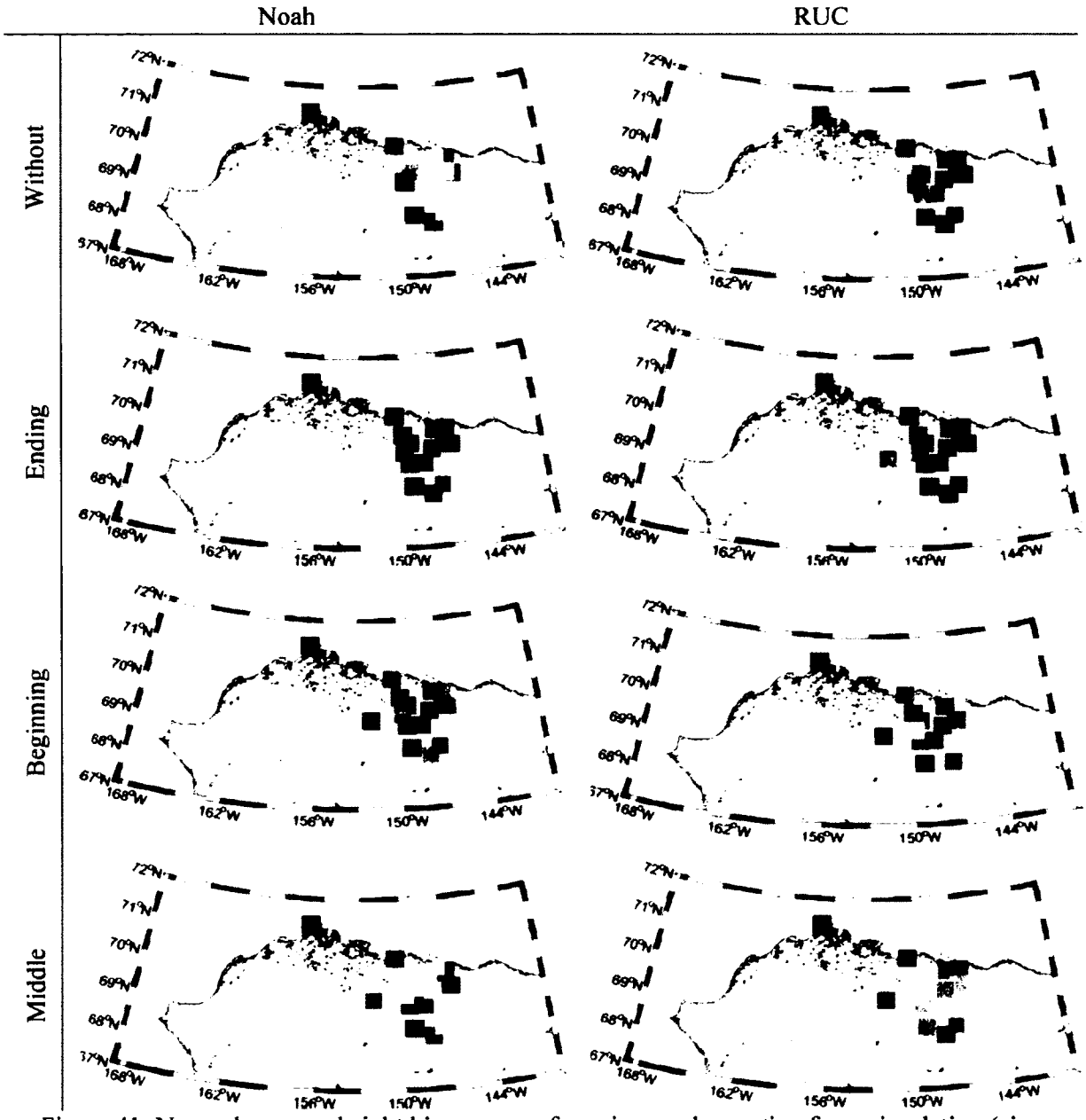

Figure 41: November snow height bias means of maximum observation from simulation (sim-obs) difference for the events of precipitation.

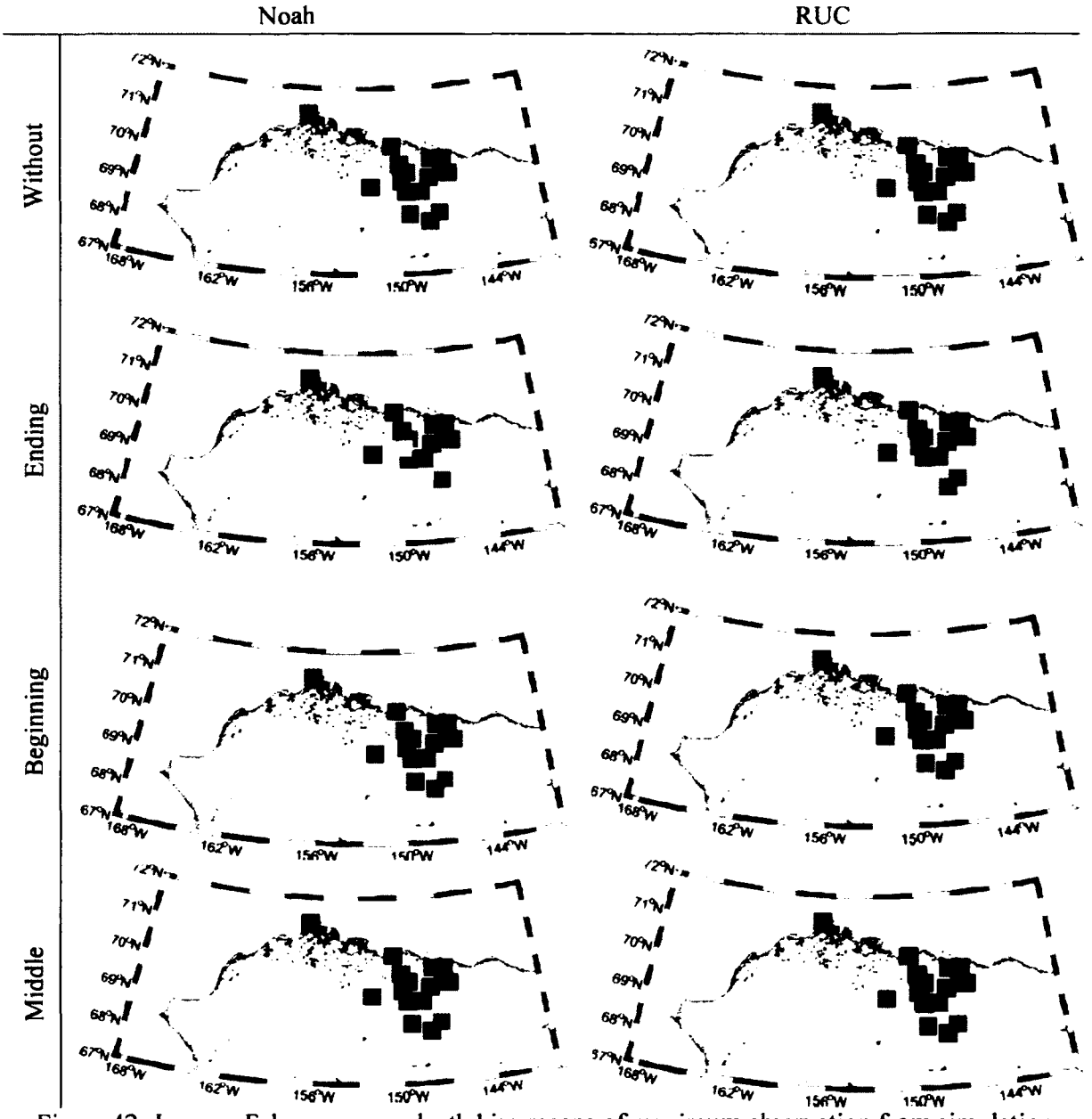

Figure 42: January-February snow depth bias means of maximum observation from simulation (sim-obs) absolute difference for the events of precipitation.

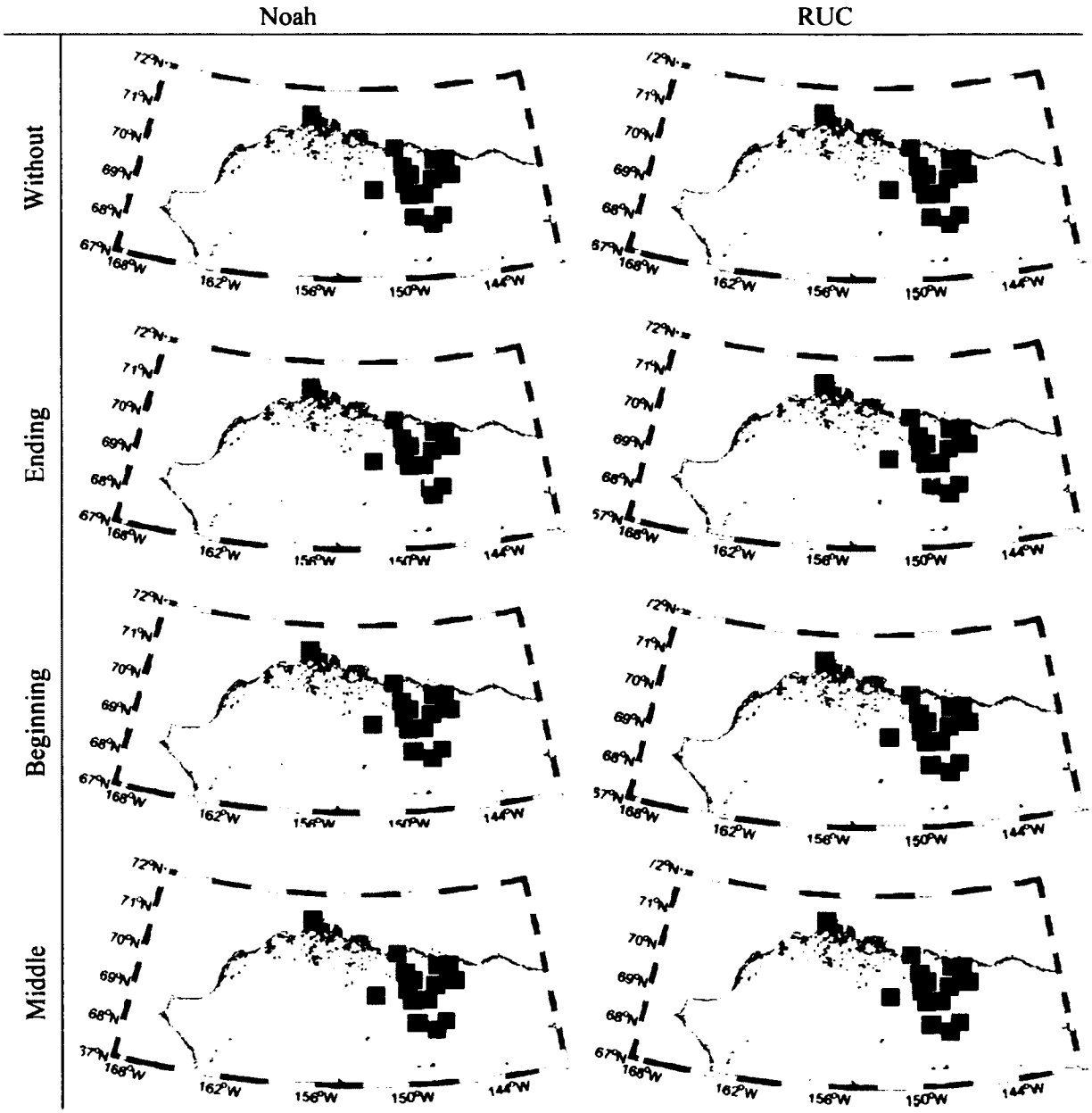

Figure 43: November snow depth bias means of maximum observation from simulation (sim-obs) absolute difference for the events of precipitation.

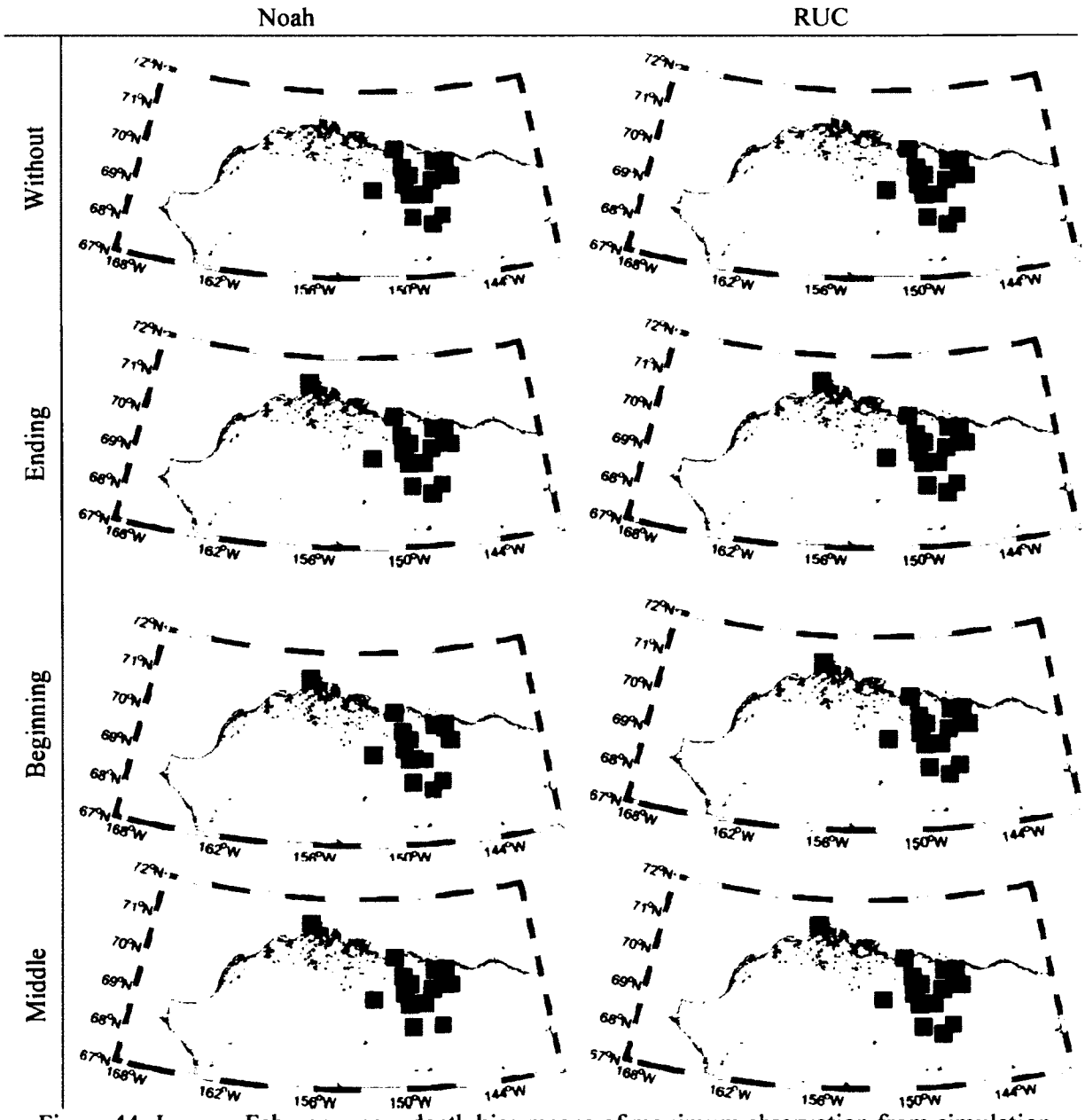

Figure 44: January-February snow depth bias means of maximum observation from simulation (sim-obs) absolute percentage difference for the events of precipitation.

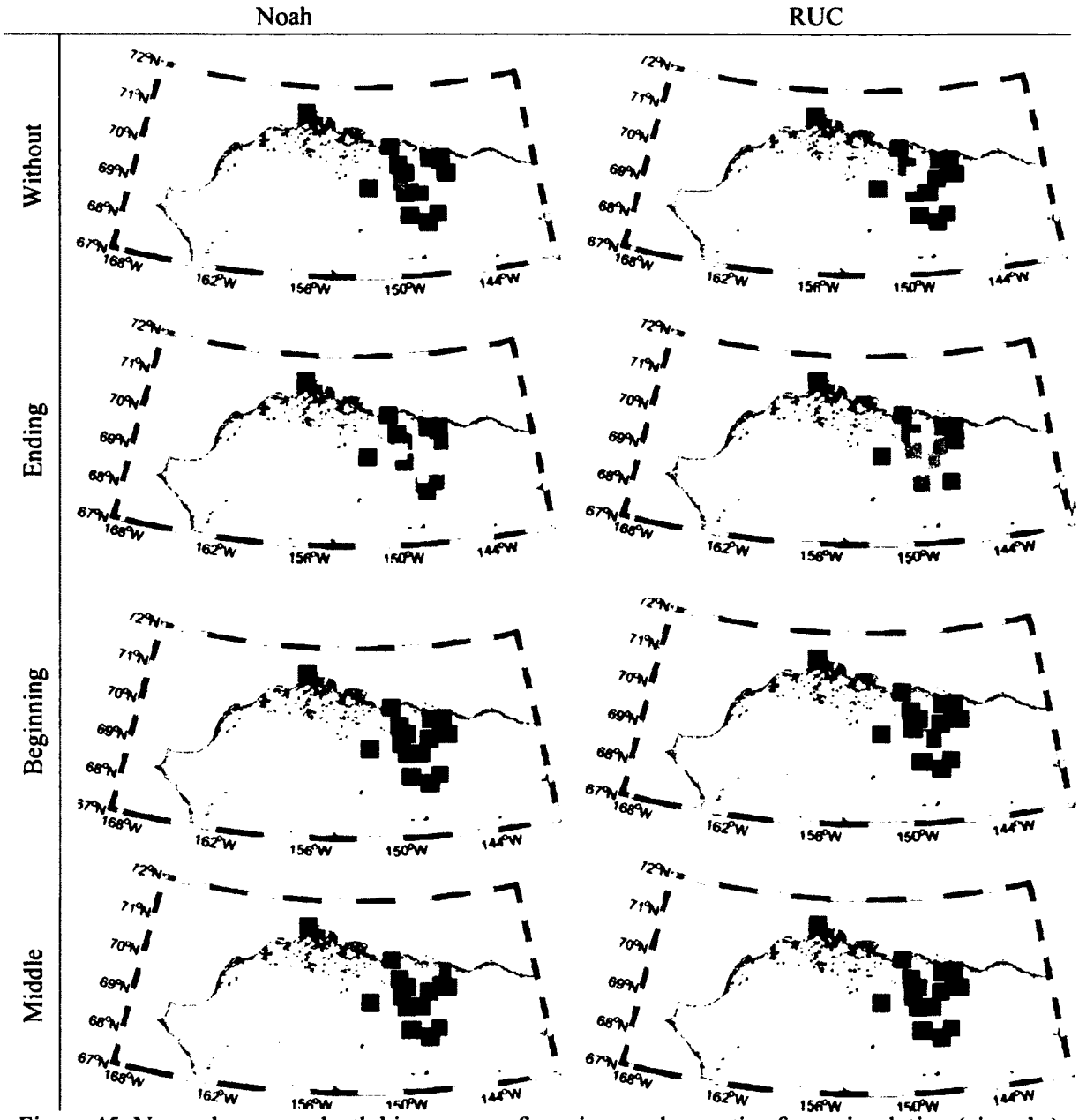

Figure 45: November snow depth bias means of maximum observation from simulation (sim-obs) absolute percentage difference for the events of precipitation.

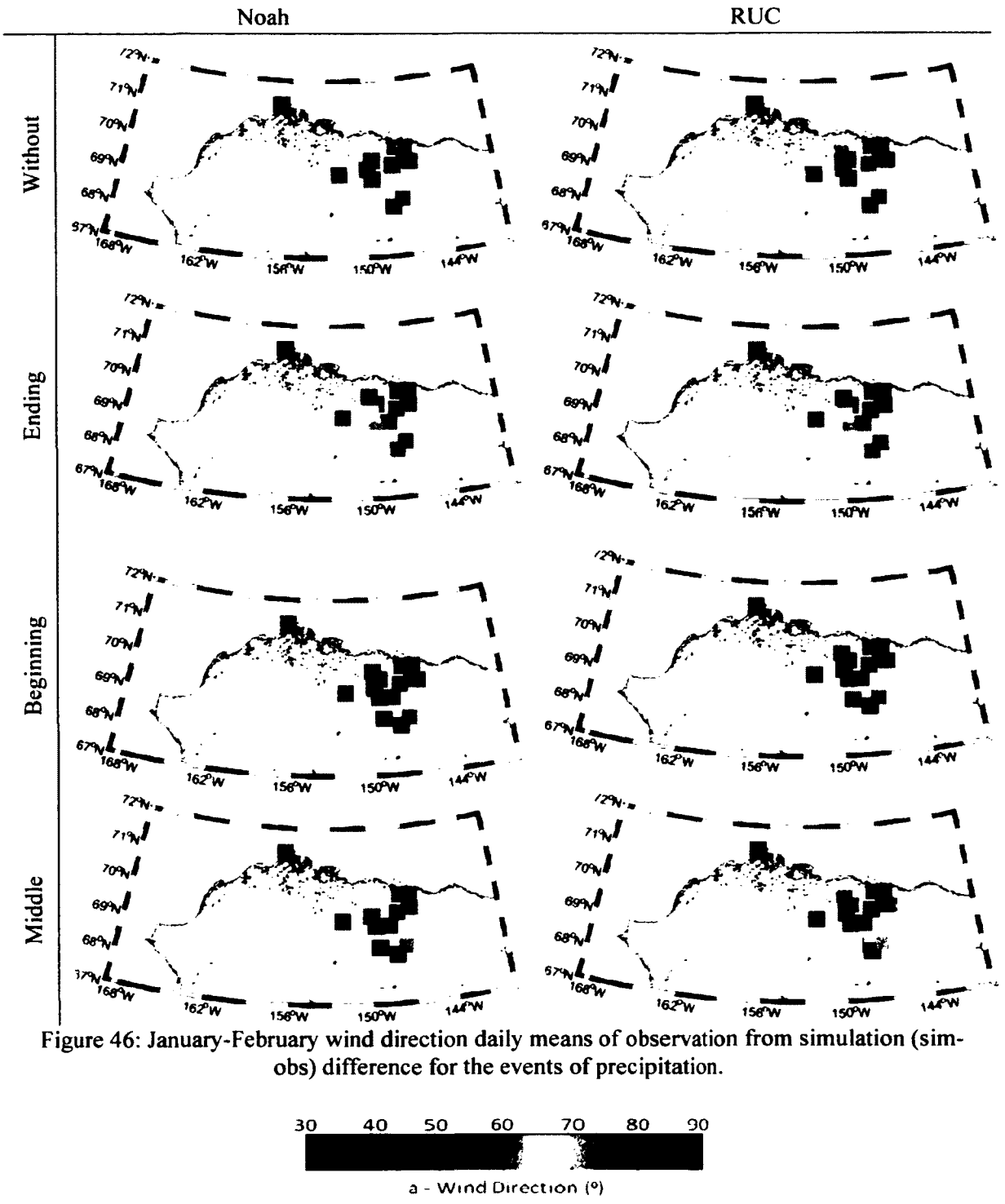

Figure 46: January-February wind direction daily means of observation from simulation (sim-obs) difference for the events of precipitation.

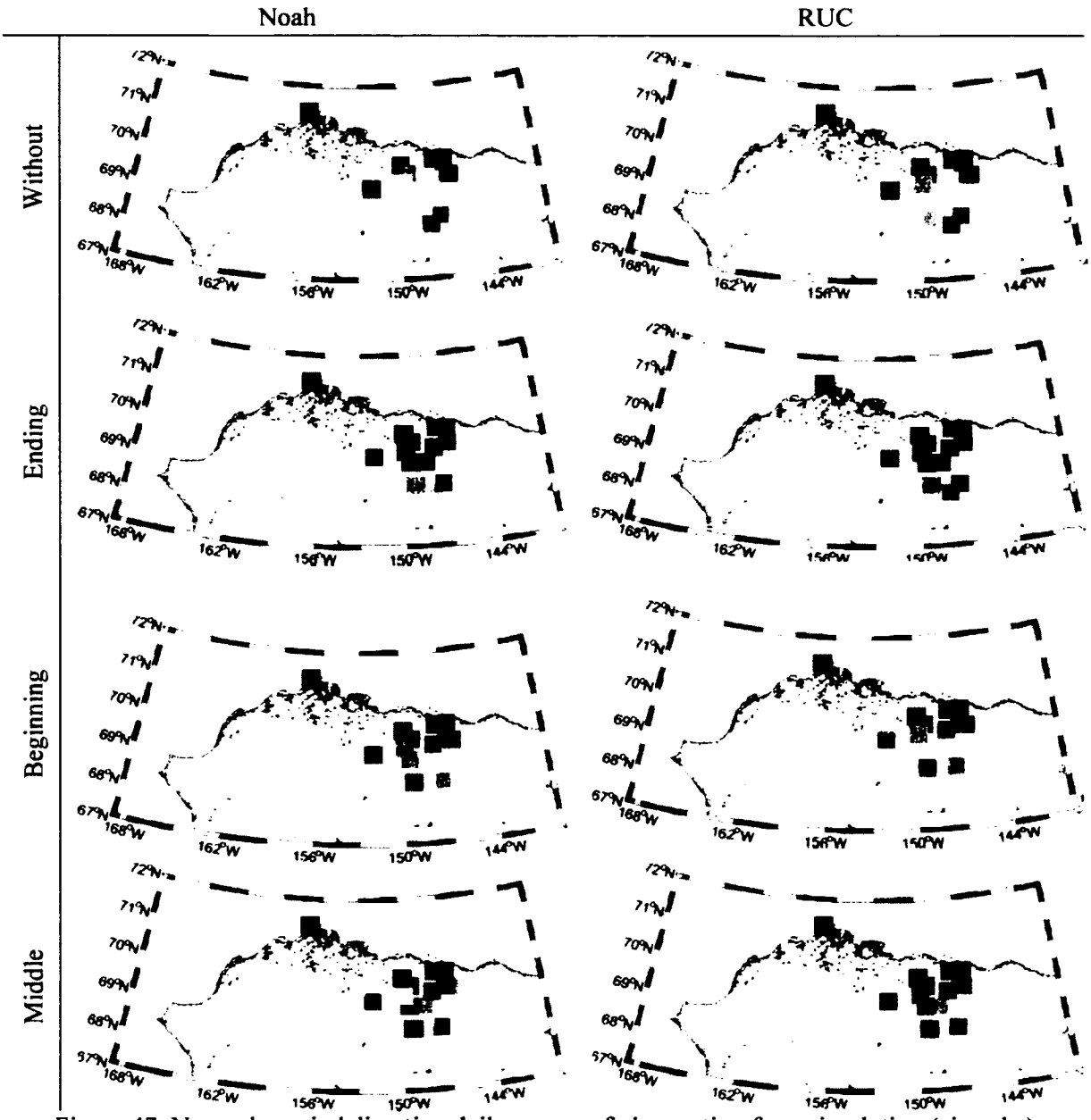

Figure 47: November wind direction daily means of observation from simulation (sim-obs) difference for the events of precipitation.

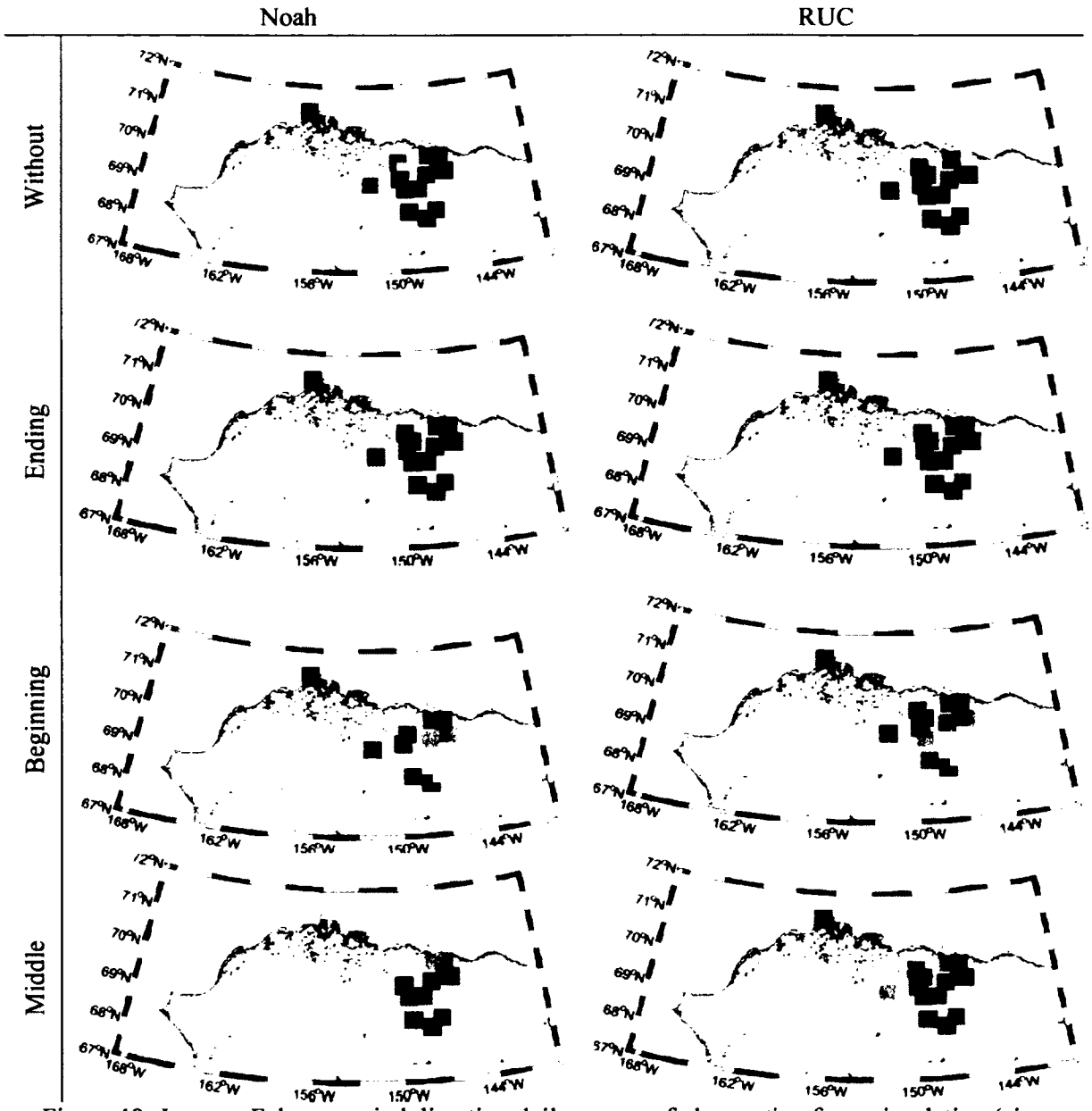

Figure 48: January-February wind direction daily means of observation from simulation (sim-obs) absolute difference for the events of precipitation.

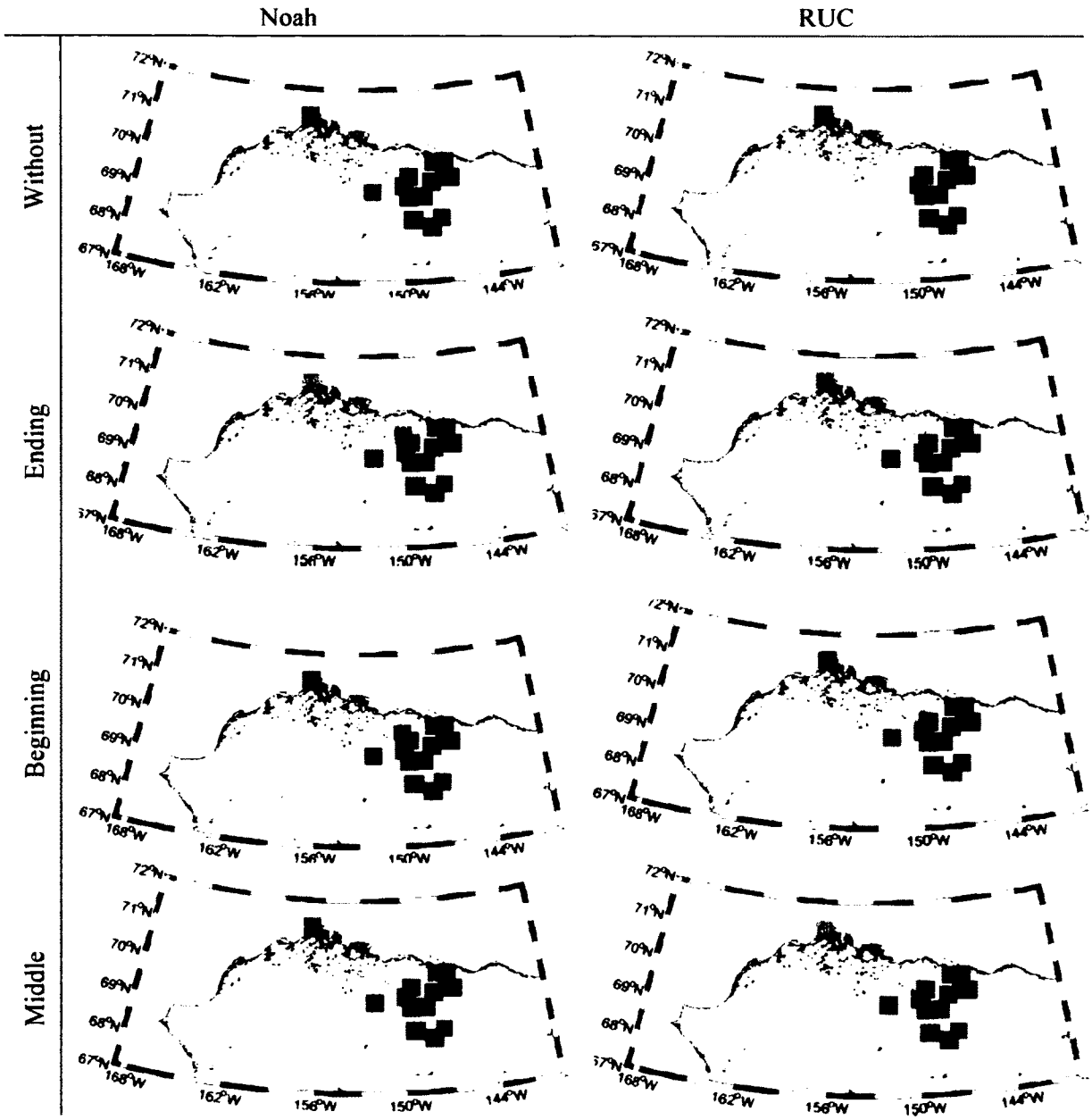

Figure 49: November wind direction daily means of observation from simulation (sim-obs) absolute difference for the events of precipitation.

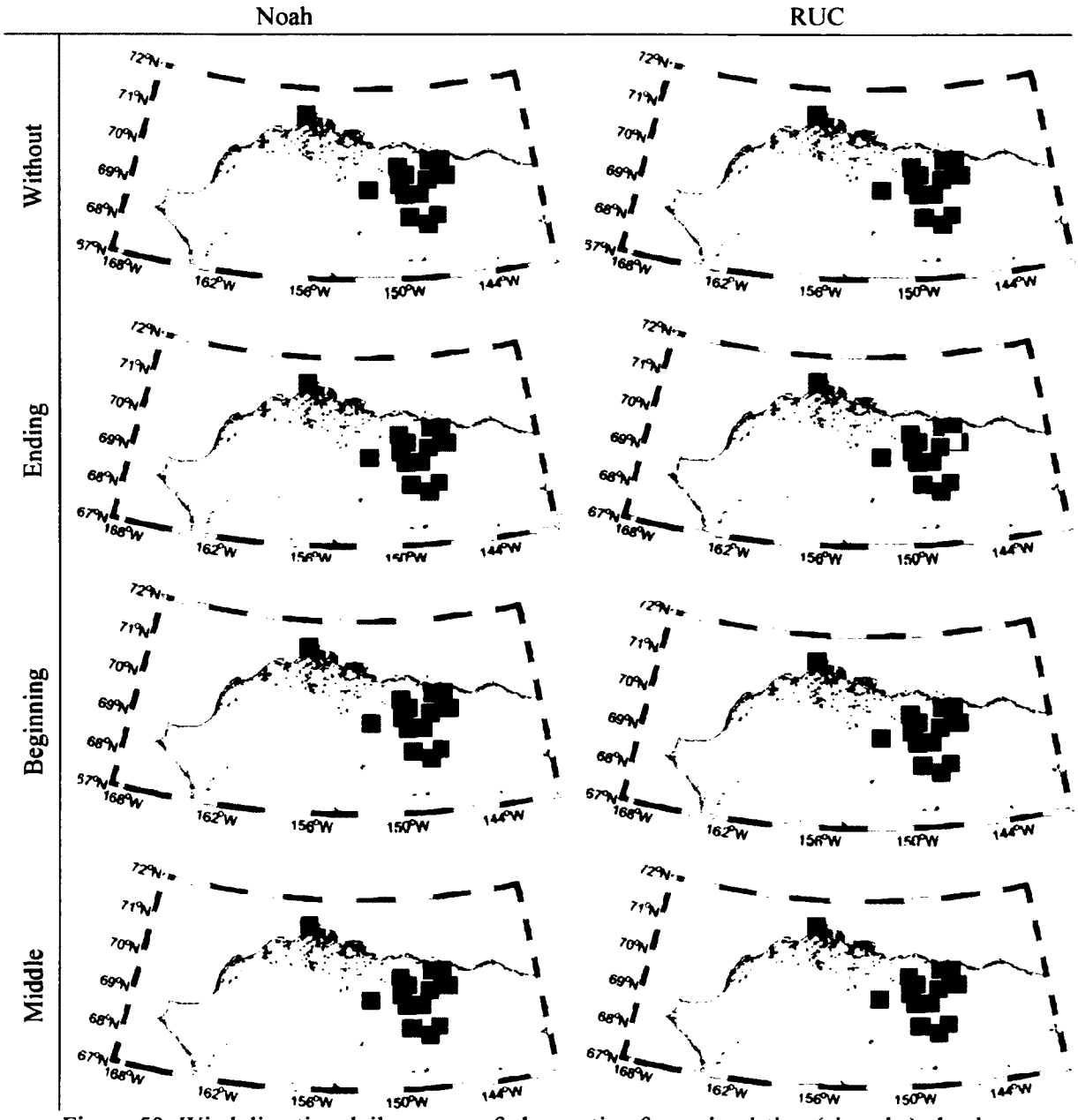

Figure 50: Wind direction daily means of observation from simulation (sim-obs) absolute percentage difference for the events of precipitation.

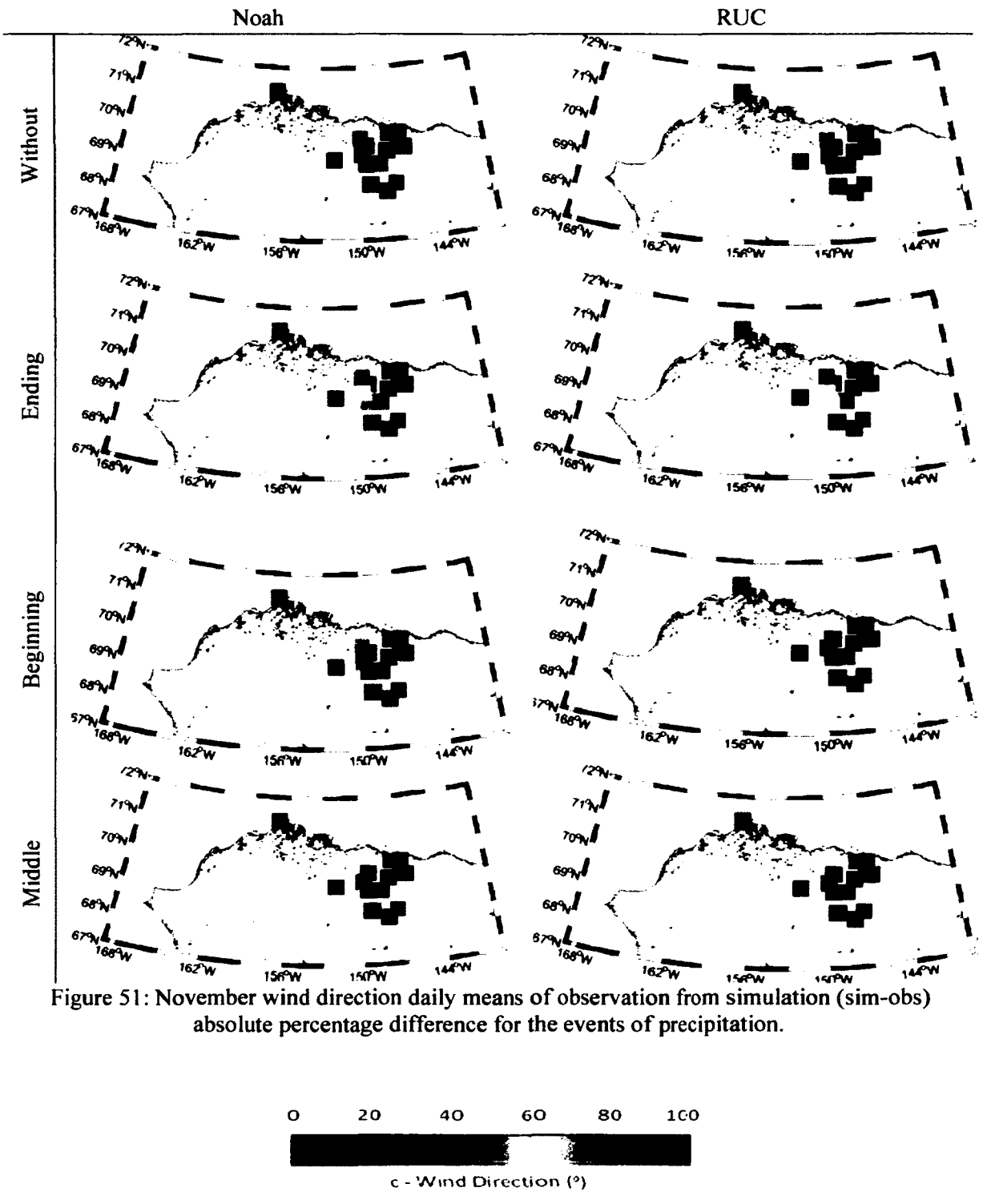

Figure 51: November wind direction daily means of observation from simulation (sim-obs) absolute percentage difference for the events of precipitation.

Table 7: Performance statistics of Noah and RUC during the five-day periods compared with the observations. Numbers shown are the hourly averages of the statistics calculated individually for each site from Table 4. The range of the means is shown in the minimum (italics) and maximum (bold) values.

		Average		Difference		RMSE	
		Noah	RUC	Noah	RUC	Noah	RUC
2m Temperature (K)	Nov 24-28	261.49	261.66	-0.16	-0.29	1.02	0.86
	Nov 19-23	260.37	260.55	2.57	2.44	0.55	0.54
	Nov 23-27	262.67	262.49	1.01	1.38	1.30	1.19
	Nov 21-25	264.64	264.50	1.19	1.34	0.94	0.92
		255 **269**	*256* **269**	*-7* **11**	*-7.1* **11.1**	*0* **3.77**	*0* **3.68**
	Jan 7-11	239.05	240.18	-2.02	-3.08	1.03	0.84
	Jan 15-19	248.95	248.96	1.66	1.62	1.22	1.18
	Jan 22-26	249.78	250.55	-0.32	-1.05	0.77	0.60
	Feb 19-23	260.15	261.00	-0.69	-1.44	1.06	0.89
		235 **264**	*238* **264**	*-8.1* **19.5**	*-8* **19.5**	*0* **7.15**	*0.1* **4.2**
Wind speed (m/s)	Nov 24-28	4.67	5.04	-0.99	-1.34	0.32	0.32
	Nov 19-23	3.93	4.28	-0.24	-0.57	0.66	0.71
	Nov 23-27	5.20	5.56	-0.81	-1.14	0.48	0.53
	Nov 21-25	5.16	5.57	-0.47	-0.87	0.46	0.46
		1.5 **13.7**	*1.8* **12.7**	*-8.7* **5.58**	-8 **4.75**	*0* **2.04**	*0* **1.84**
	Jan 7-11	2.05	2.09	-0.35	-0.42	0.17	0.16
	Jan 15-19	3.87	4.18	-0.91	-1.20	0.44	0.38
	Jan 22-26	6.11	6.39	-0.24	-0.52	0.40	0.40
	Feb 19-23	3.96	4.13	0.56	0.37	0.12	0.16
		0.7 **11.1**	*0.8* **10.5**	*-6.2* **3.53**	*-5.7* **3.01**	*0* **1.55**	*0* **1.46**
Wind direction (°)	Nov 24-28	118.10	120.93	27.19	24.60	14.30	16.13
	Nov 19-23	149.78	150.41	-42.52	-42.94	11.33	11.78
	Nov 23-27	131.56	136.75	3.31	-1.73	13.78	13.26
	Nov 21-25	152.41	154.72	-30.82	-33.13	8.63	9.36
		79 **199**	*88* **201**	*-138* **138**	*-140* **123**	*0* **45.4**	*0.3* **46.4**
	Jan 7-11	192.80	159.80	30.13	51.33	26.45	29.38
	Jan 15-19	130.08	125.56	7.04	12.35	13.12	13.19
	Jan 22-26	88.29	89.46	127.94	129.81	24.57	24.19
	Feb 19-23	139.73	144.24	47.38	40.30	35.96	30.83
		54 **285**	*46* **257**	*-173* **171**	*-151* **190**	*0.5* **109**	*1.5* **88**
Snow depth bias (cm)	Nov 24-28	1.34	0.75	-1.58	-0.88	0.65	0.42
	Nov 19-23	1.13	0.52	-0.27	0.36	0.68	0.48
	Nov 23-27	1.26	0.80	-2.81	-2.19	1.28	1.08
	Nov 21-25	0.82	0.77	-1.00	-0.82	1.44	1.13
		-1.9 **6.72**	*-1.3* **3.64**	*-23* **5.83**	*-20* **5.36**	*0* **12.2**	*0* **10.1**
	Jan 7-11	2.70	1.10	-1.61	0.21	0.82	0.30
	Jan 15-19	0.83	0.43	0.08	0.58	0.96	0.81
	Jan 22-26	2.04	0.78	-1.76	-0.17	0.84	0.35
	Feb 19-23	2.57	1.44	-1.93	-0.45	1.56	1.07
		-0.1 **6.16**	*-0.1* **2.75**	*-5.5* **5.97**	*-3.7* **5.8**	*0* **4.49**	*0* **5.2**

Across the domain hourly comparisons of snow bias, temperature, and wind speed and direction show overall few differences between the observed and simulated data. Snow depth bias hour-to-hour differences between the model and observations are small, being within less than five centimeters (5 cm) of each other. The average RSME value for all of the events was 0.86 with RUC values lower than Noah and November generally lower than January events. The daily snow bias comparison shows that only observations of Umiat near the middle of February and observations of an event in Barrow in November to be significantly above 5 cm in difference. The Umiat February data has a considerable amount of noise (Figure 52), and therefore, was removed for the quantitative analysis. Barrow observations show a dramatic change (45 to 25 cm) in snow height and decrease in temperature after precipitation; therefore, the Barrow November beginning and middle precipitation event was removed from the statistical analysis. However, due to the dramatic wind event in late November, the Barrow beginning five-day period was chosen for the coupling with SnowTran-3D.

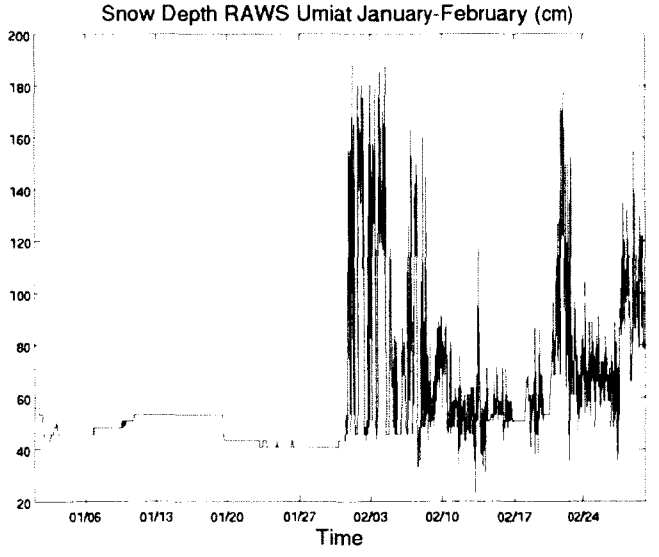

Figure 52: Noise in the snow depth observations at Umiat.

Exceptions where simulated snow depth exceeded greater than five centimeters of the observed data included the November 'without precipitation' event at Accomplishment Creek and November 'without precipitation' event at White Hills. Both events have small differences in wind speeds between simulation and observation. Accomplishment Creek observations show little to no changes over five days in snow height, but simulations show a jump during the second day. A comparison of the White Hills observations with simulated snow depth shows both to be increasing in the later part of the five days. Each of the events has large differences in temperature from observation to simulation (Figure 53).

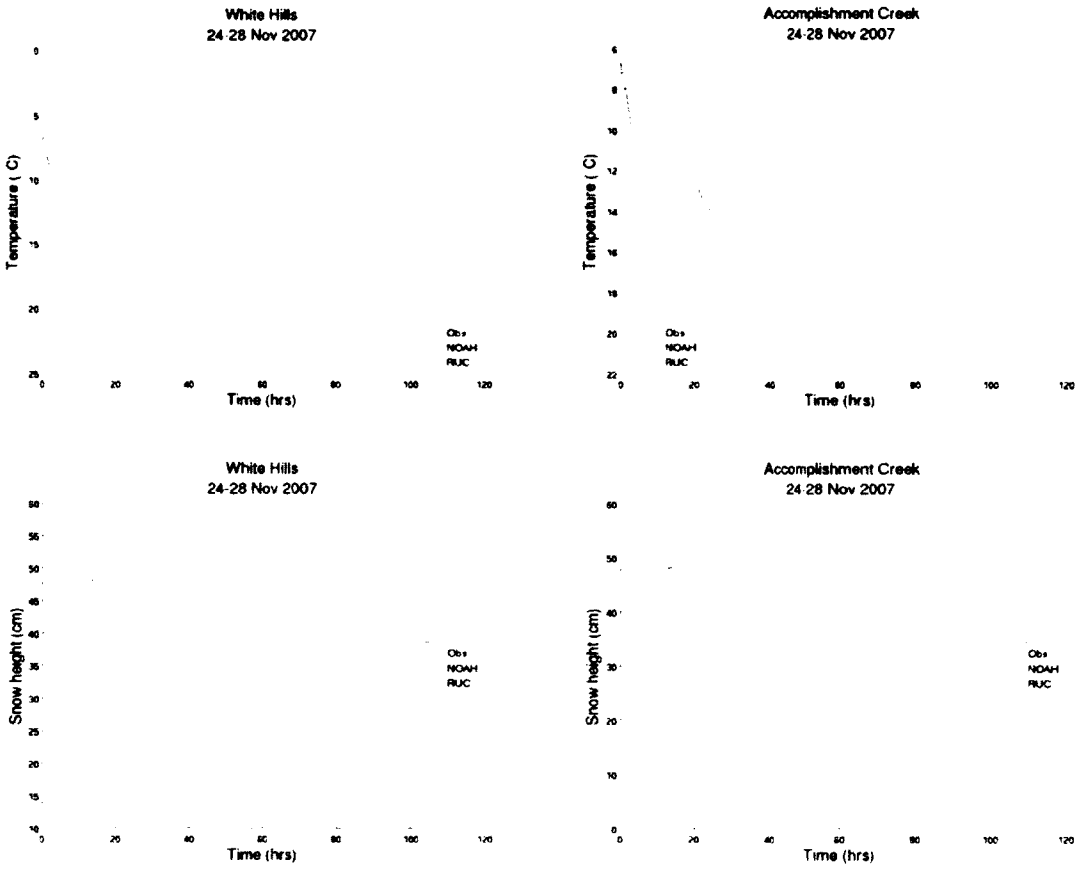

Figure 53: Observation to simulation comparison of temperature during events that have greater than 5 cm in snow depth bias difference.

The spatial comparisons of the maximum snow depth simulation to observations have overall small differences. The November 'beginning precipitation' event for all stations, excluding Barrow, has differences of roughly 3 to 4 cm. In the quantitative analysis of the simulation to the observations, the snow depth bias differences are within the accuracy error values (roughly 2 cm).

The comparisons of the simulated and observed temperature show small average of differences with less than 0.3°C overall. The average RSME value for all of the events was 0.93 with RUC values lower than Noah and November lower than January events. The spatial comparisons of the temperatures that had the greatest maximum averages are the November 'without precipitation' event (10.8°C) and the 'beginning precipitation' events for White Hills (11°C) (Figure 54) and the 'ending precipitation' January event at Imnavait (19.5°C) (Figure 55). When comparing the observed and simulated data of all the parameters for both Imnavait and White hills events, the difference is most pronounced for the temperature parameter. For example, the White Hills and Imnavait average differences in simulation minus observation for wind are less than 1 m/s and 2.4 m/s, respectively. The White Hills and Imnavait average differences in simulation minus observation for snow depth are less than 0.89 cm and 1.5 cm, respectively. The White Hills events overestimate the drop in temperatures in the middle of the five-day period during the night. The overestimation in the event's decrease in temperature coincides with an observed sustained high wind event. The Imnavait simulation overestimates the temperature associated with a precipitation and high wind event.

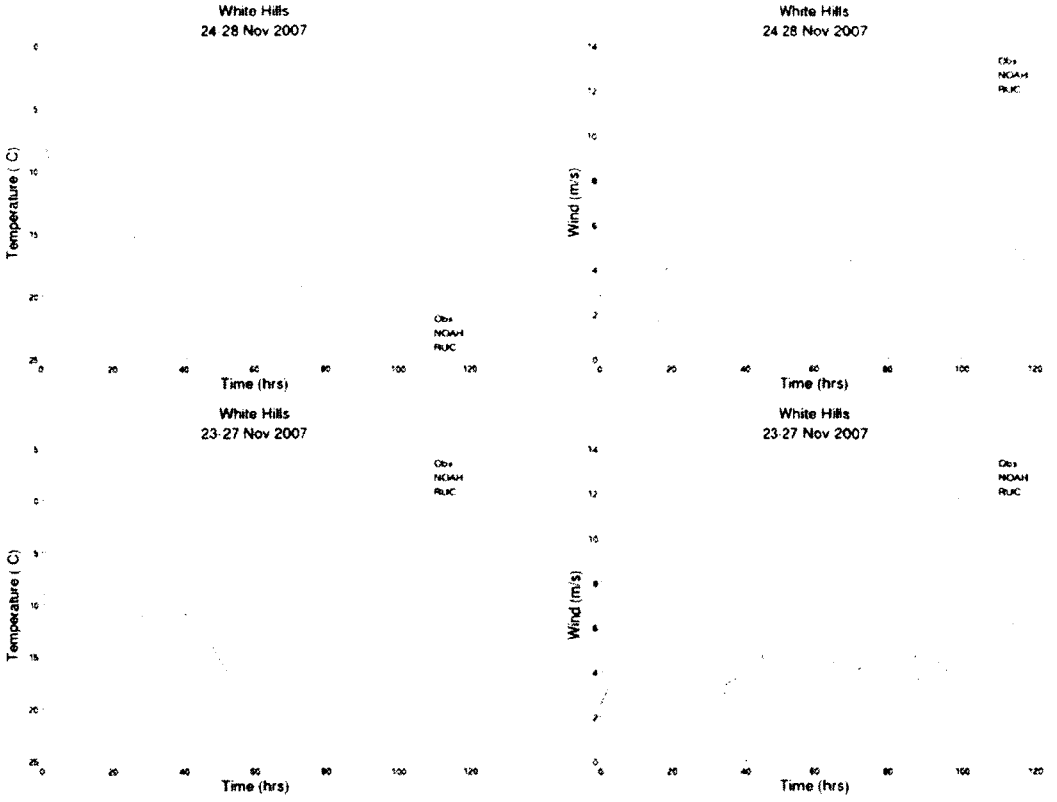

Figure 54: White Hills' temperature for simulation and observation

The spatial comparisons of the wind speed and direction simulation to observations are relatively scattered; however, the absolute percentage differences are all low. The average RSME for wind speed values for all of the events was 0.38 with Noah values lower than RUC and January lower than November events. The average RSME for wind direction values for all of the events was 18.51 with Noah values lower than RUC and November lower than January events.

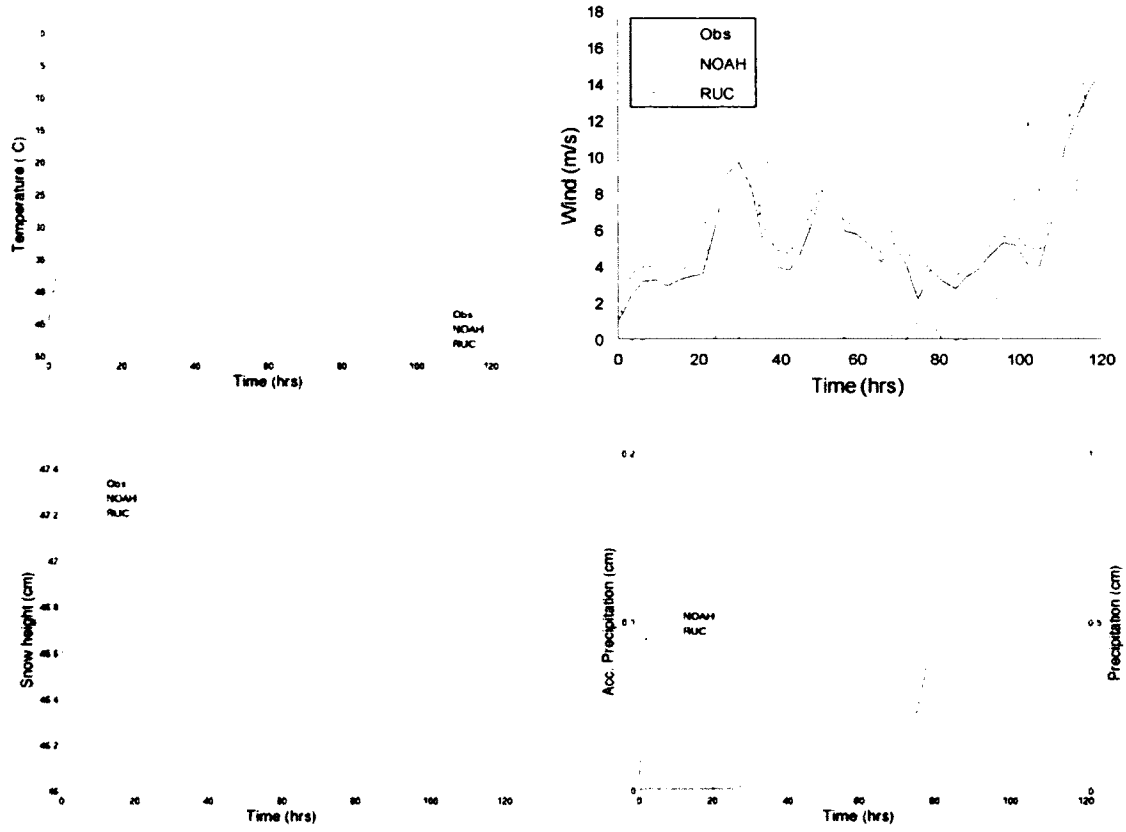

Figure 55: Imnavait parameters for simulation and observation. Observed precipitation (green) is compared to the accumulative simulated precipitation (blue).

For temporal comparison, the simulated and observed data for snow depth bias, temperature, and wind speed were plotted against each other to determine correlation values (Figure 56-79). The snow depth plots are separated into groups by station-elevation, where stations are categorized into mountain where elevations are greater than 200 m (elevation > 200 m), foothill where elevations are less than 200 m and greater than 50 m (50 m < elevation < 200 m), and coastal where elevations are near sea level (elevation < 50 m).

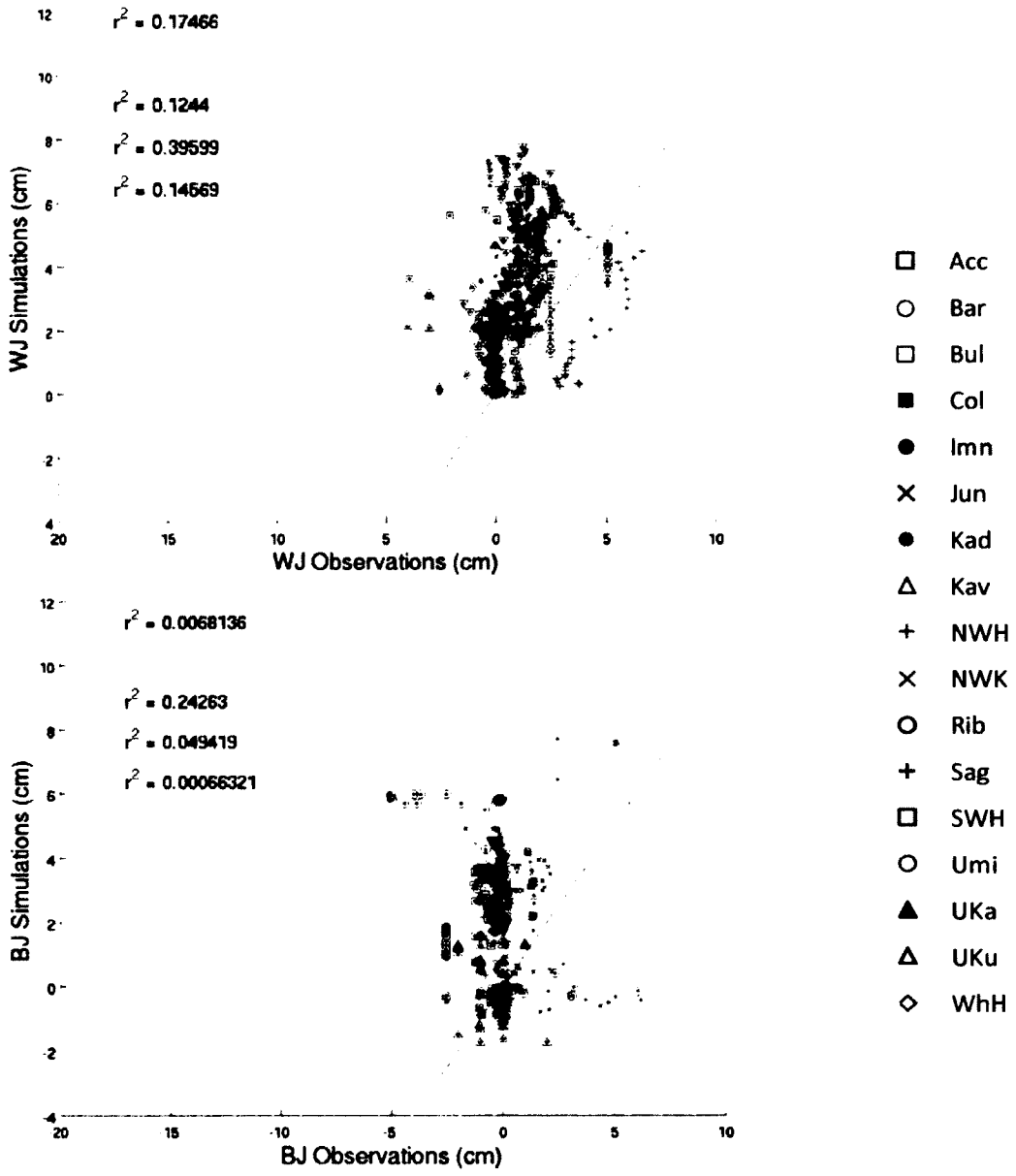

Figure 56: January Noah snow depth with bias removed scatter plots showing model predictions on the y-axis and observation data on the x-axis for each precipitation event: W-without and B-beginning. R^2 are overall, mountain (blue), coastal (magenta), and foothills (green). The black line is 1:1.

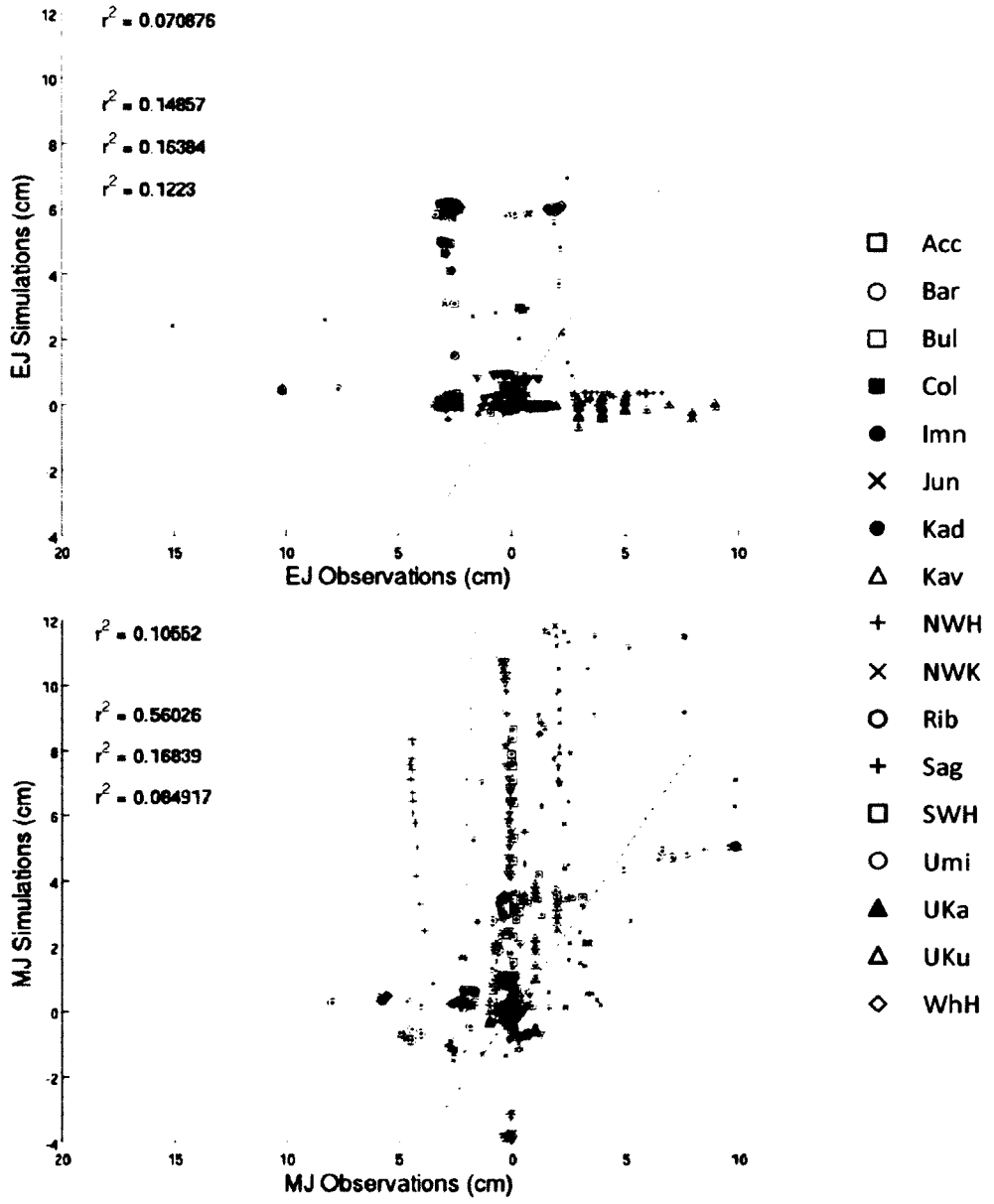

Figure 57: January Noah snow depth with bias removed scatter plots showing model predictions on the y-axis and observation data on the x-axis for each precipitation event: E-ending and M-middle. R^2 are overall, mountain (blue), coastal (magenta), and foothills (green). The black line is 1:1.

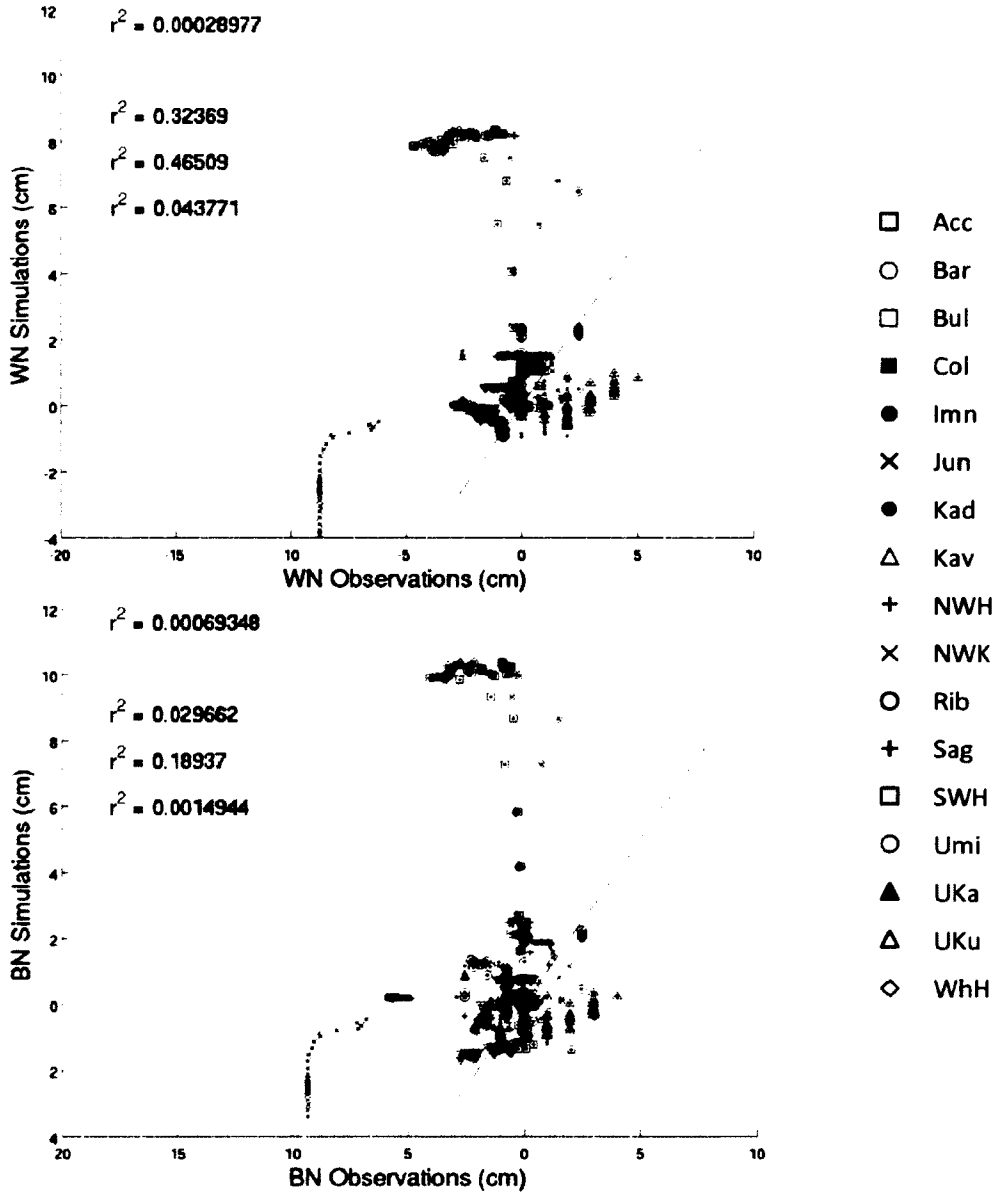

Figure 58: November Noah snow depth with initial bias removed scatter plots showing model predictions on the y-axis and observation data on the x-axis for each precipitation event: W-without and B-beginning. R^2 are overall, mountain (blue), coastal (magenta), and foothills (green). The black line is 1:1.

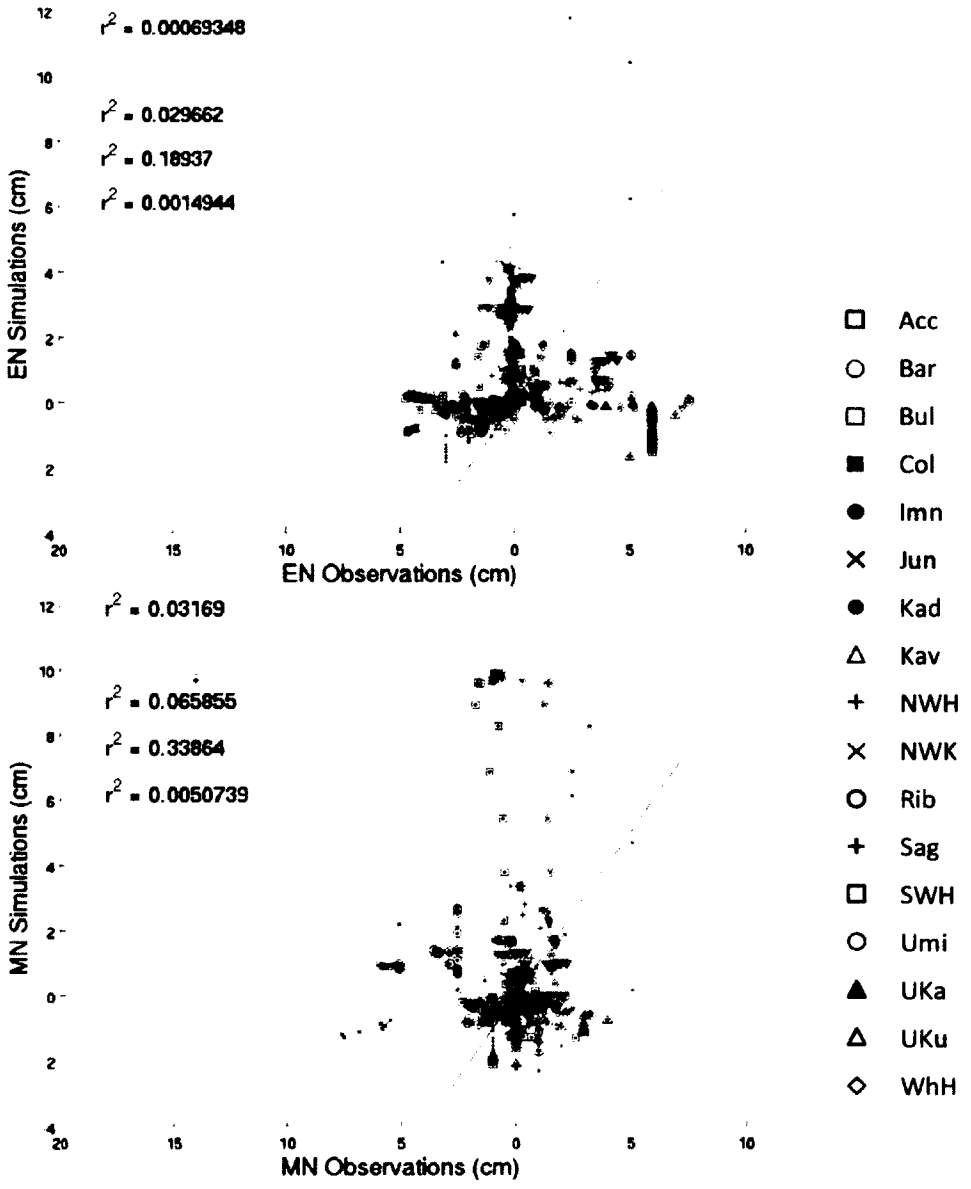

Figure 59: November Noah snow depth with initial bias removed scatter plots showing model predictions on the y-axis and observation data on the x-axis for each precipitation event: E-ending and M-middle. R^2 are overall, mountain (blue), coastal (magenta), and foothills (green). The black line is 1:1.

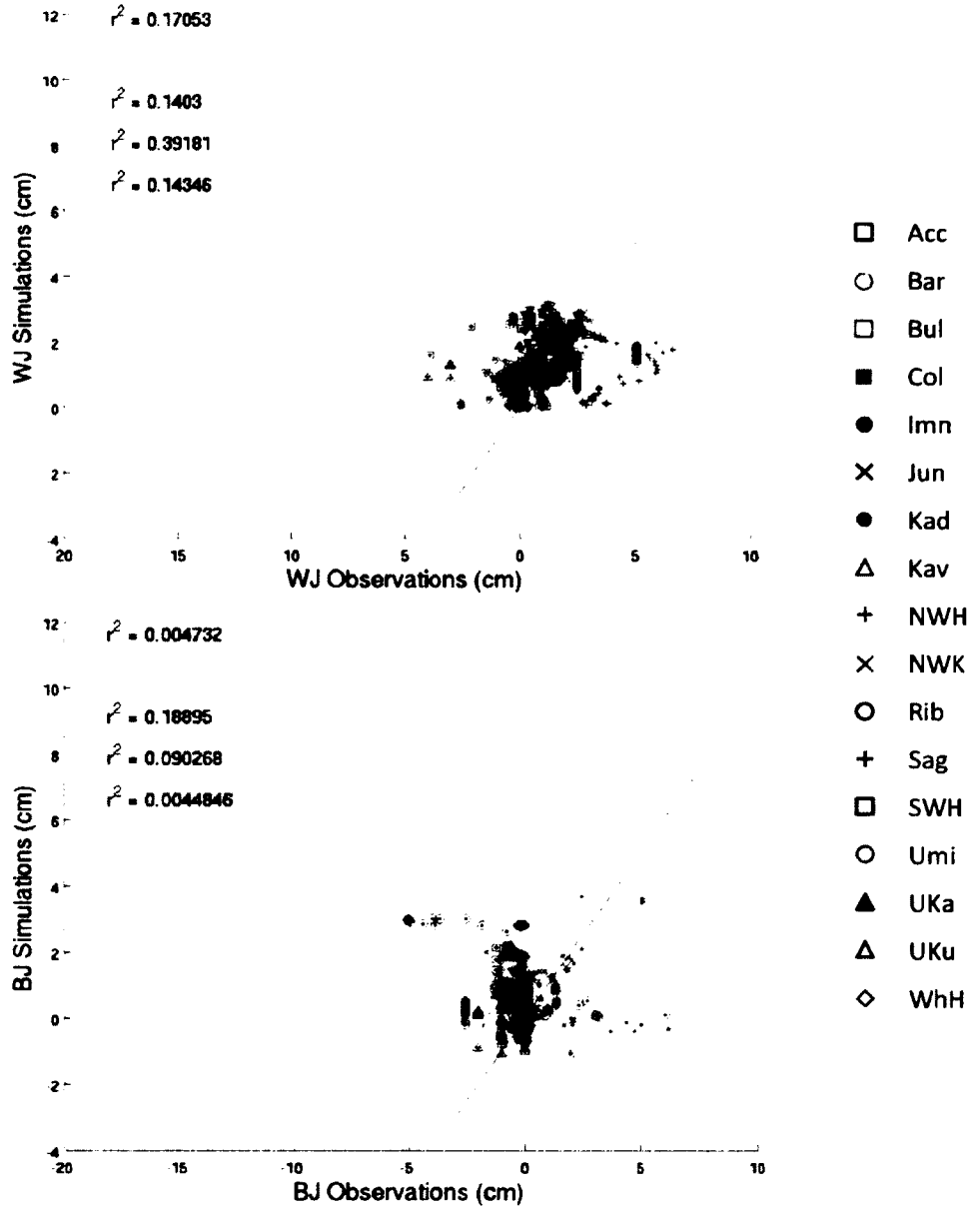

Figure 60: January RUC snow depth with bias removed scatter plots showing model predictions on the y-axis and observation data on the x-axis for each precipitation event: W-without and B-beginning. R^2 are overall, mountain (blue), coastal (magenta), and foothills (green). The black line is 1:1.

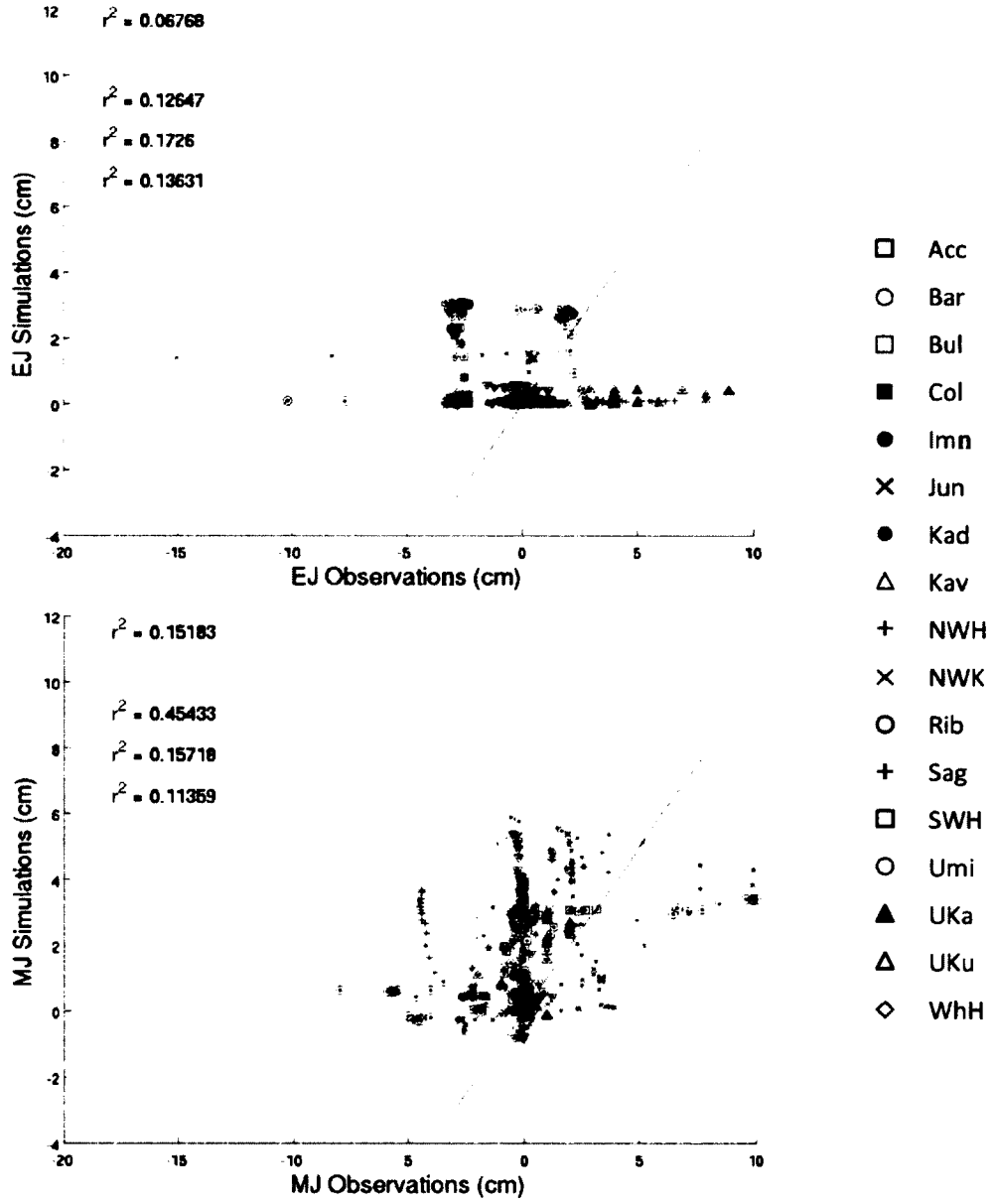

Figure 61: January RUC snow depth with bias removed scatter plots showing model predictions on the y-axis and observation data on the x-axis for each precipitation event: E-ending and M-middle. R^2 are overall, mountain (blue), coastal (magenta), and foothills (green). The black line is 1:1.

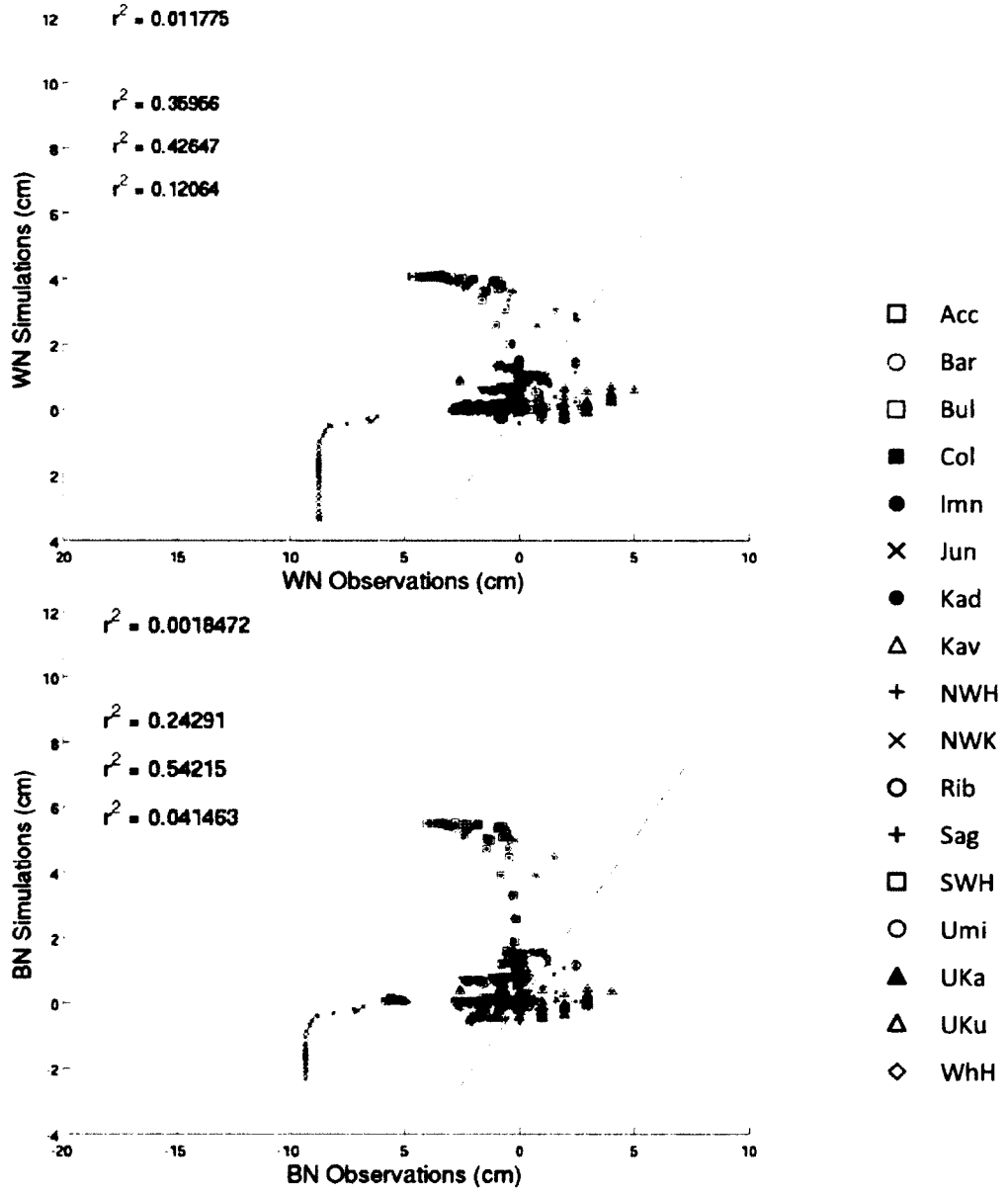

Figure 62: November RUC snow depth with initial bias removed scatter plots showing model predictions on the y-axis and observation data on the x-axis for each precipitation event: W-without and B-beginning. R^2 are overall, mountain (blue), coastal (magenta), and foothills (green). The black line is 1:1.

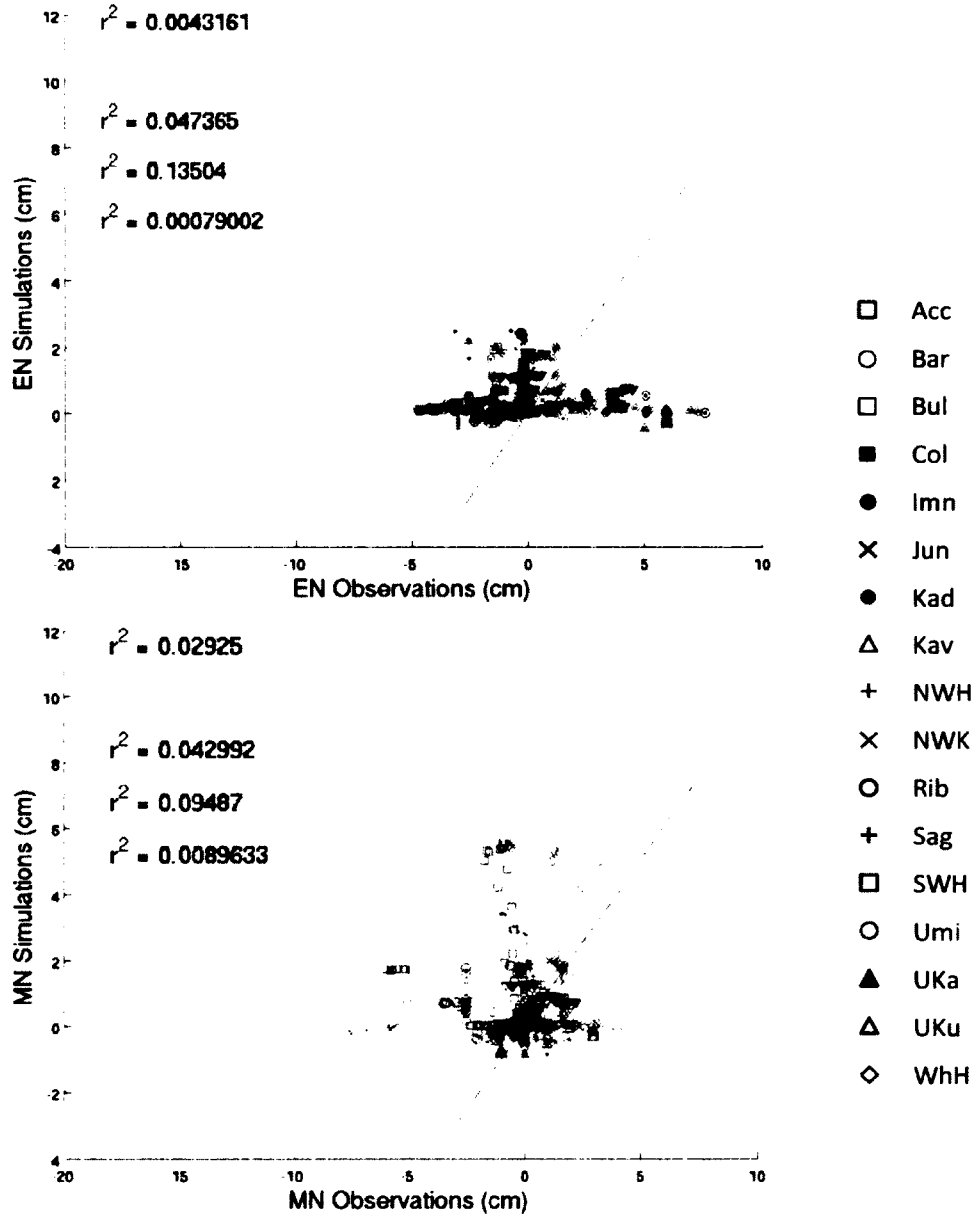

Figure 63: November RUC snow depth with initial bias removed scatter plots showing model predictions on the y-axis and observation data on the x-axis for each precipitation event: E-ending and M-middle. R^2 are overall, mountain (blue), coastal (magenta), and foothills (green). The black line is 1:1.

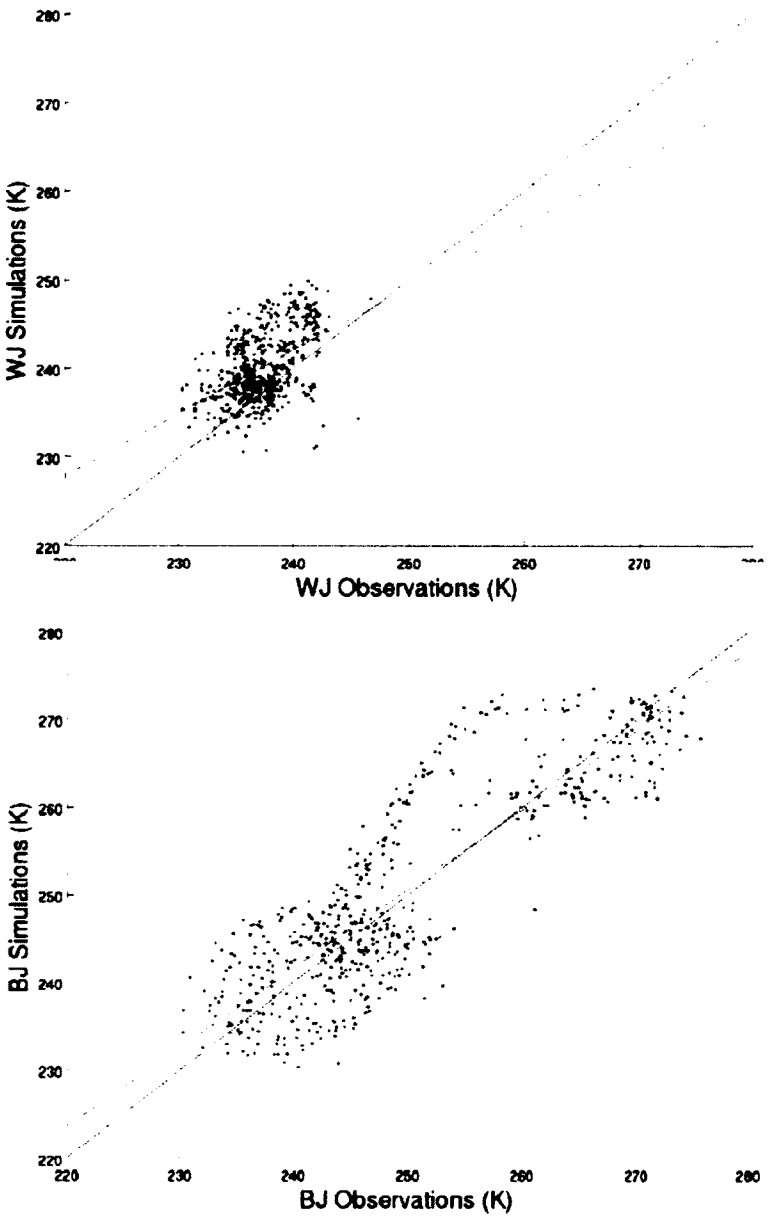

Figure 64: January Noah temperature at 2m scatter plots showing model predictions for all stations on the y-axis and observation data on the x-axis for each precipitation event: W-without and B-beginning. The black line is 1:1; the red is a trendline.

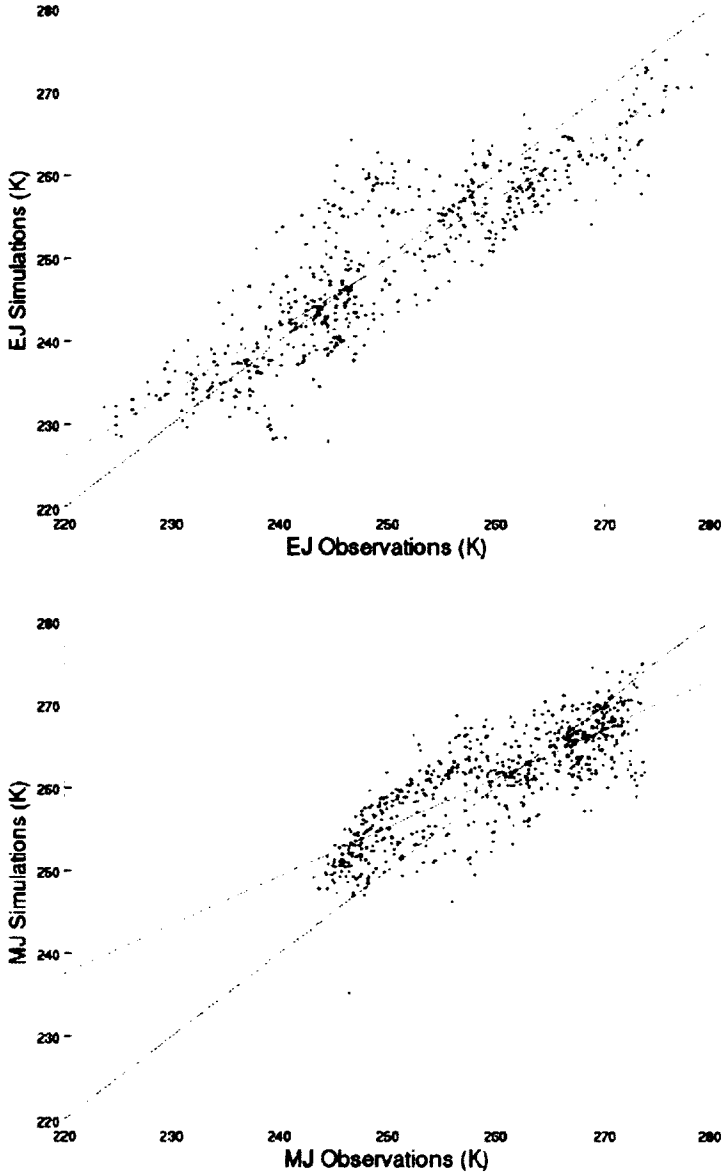

Figure 65: January Noah temperature at 2m scatter plots showing model predictions for all stations on the y-axis and observation data on the x-axis for each precipitation event: E-ending and M-middle. The black line is 1:1; the red is a trendline.

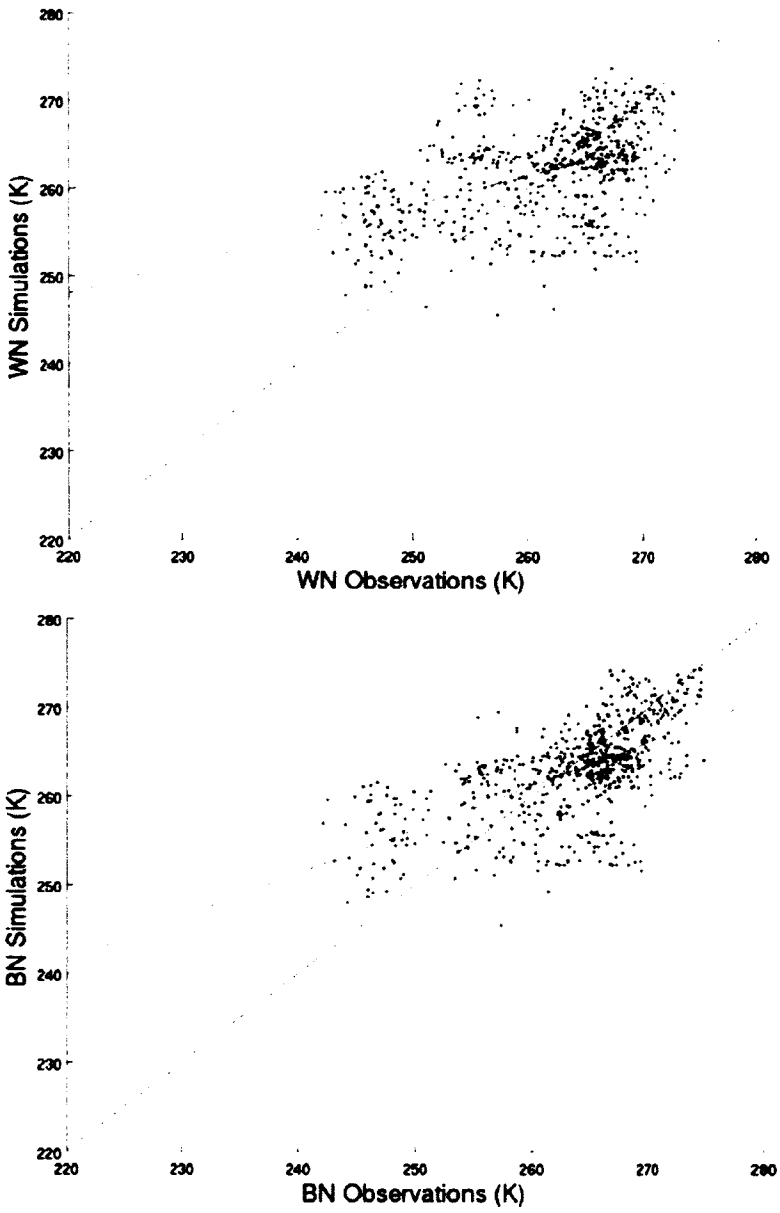

Figure 66: November Noah temperature at 2m scatter plots showing model predictions for all stations on the y-axis and observation data on the x-axis for each precipitation event: W-without and B-beginning. The black line is 1:1; the red is a trendline.

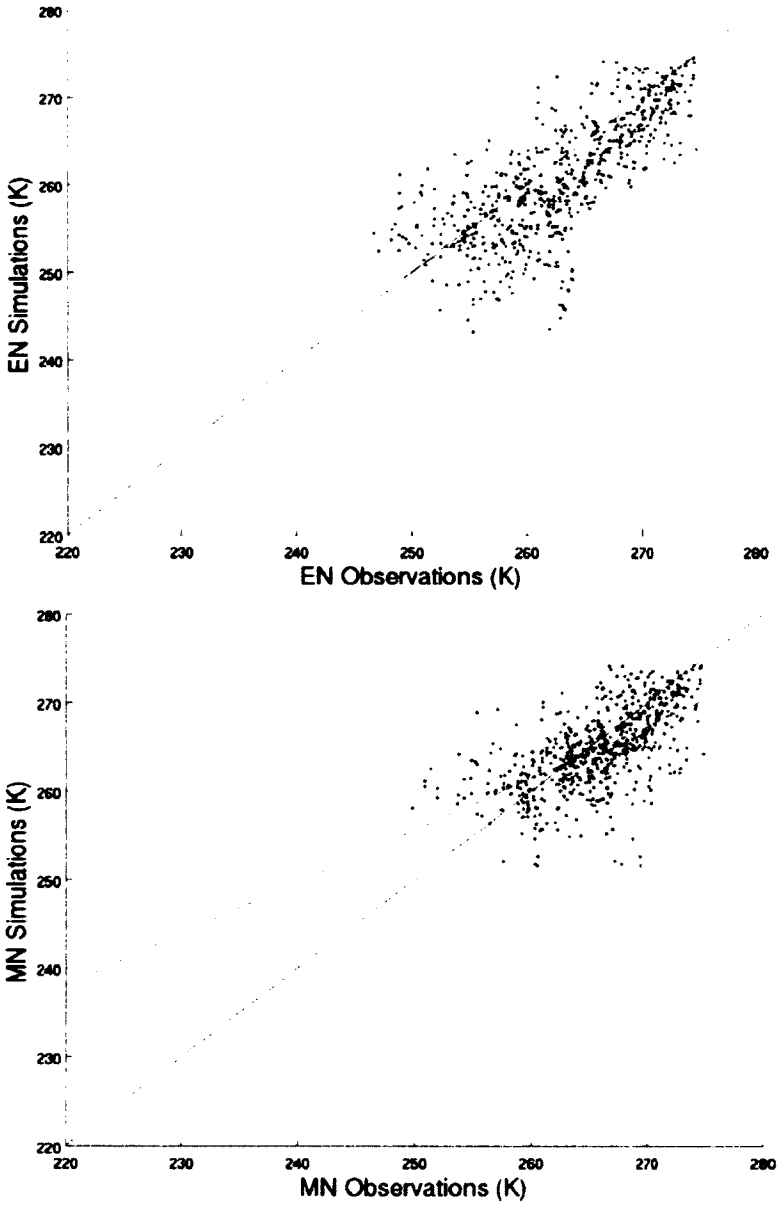

Figure 67: November Noah temperature at 2m scatter plots showing model predictions for all stations on the y-axis and observation data on the x-axis for each precipitation event: E-ending and M-middle. The black line is 1:1; the red is a trendline.

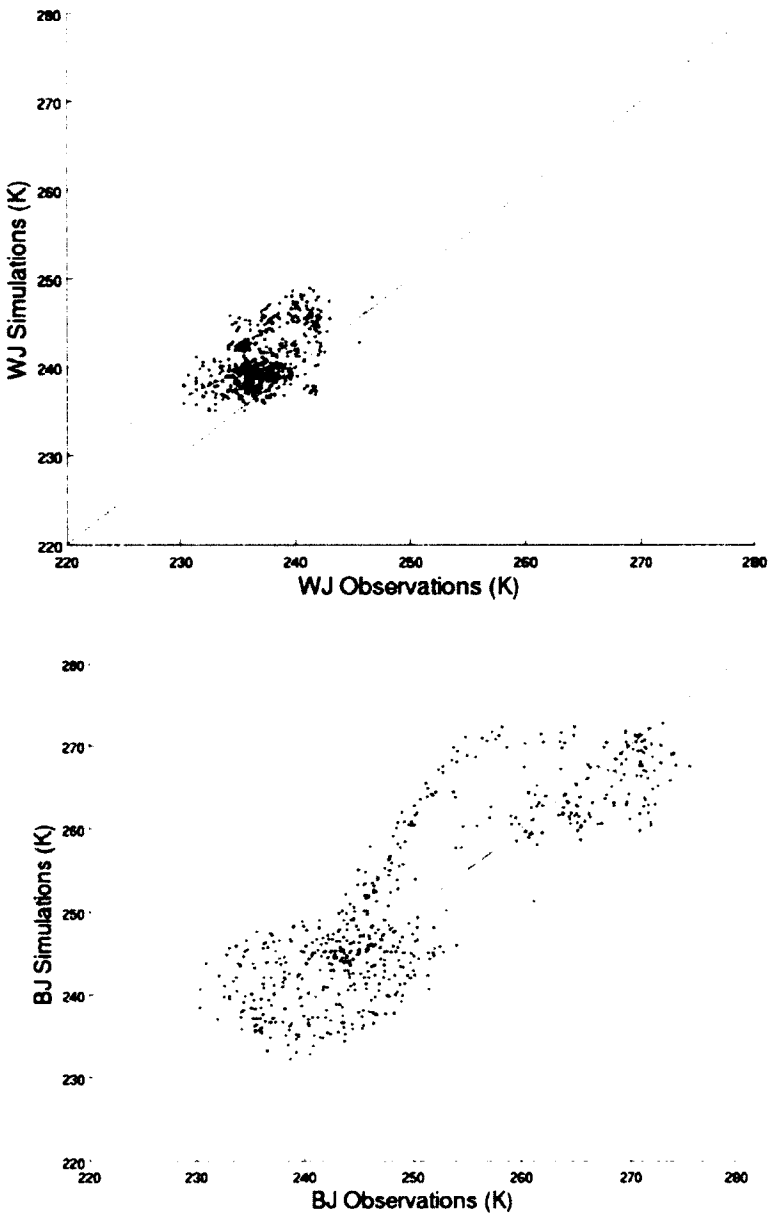

Figure 68: January RUC temperature at 2m scatter plots showing model predictions for all stations on the y-axis and observation data on the x-axis for each precipitation event: W-without and B-beginning. The black line is 1:1; the red is a trendline.

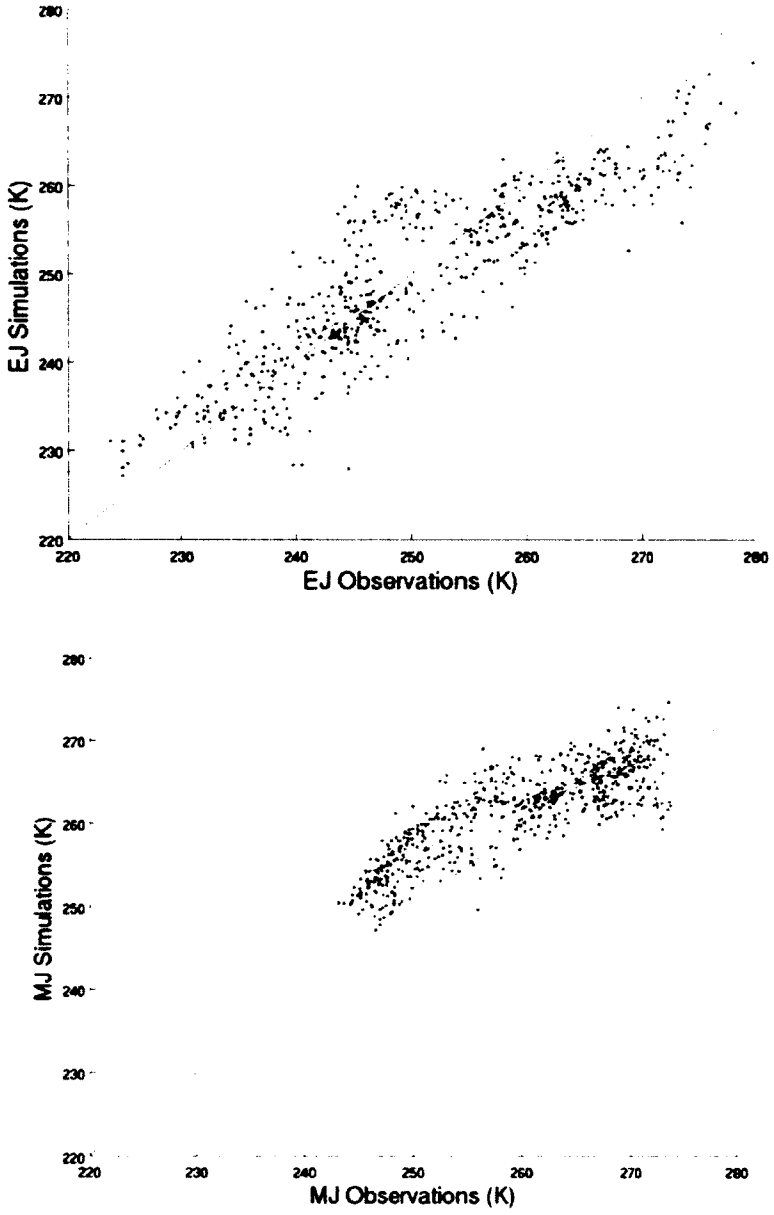

Figure 69: January RUC temperature at 2m scatter plots showing model predictions for all stations on the y-axis and observation data on the x-axis for each precipitation event: W-without, E-ending, B-beginning, and M-middle. The black line is 1:1; the red is a trendline.

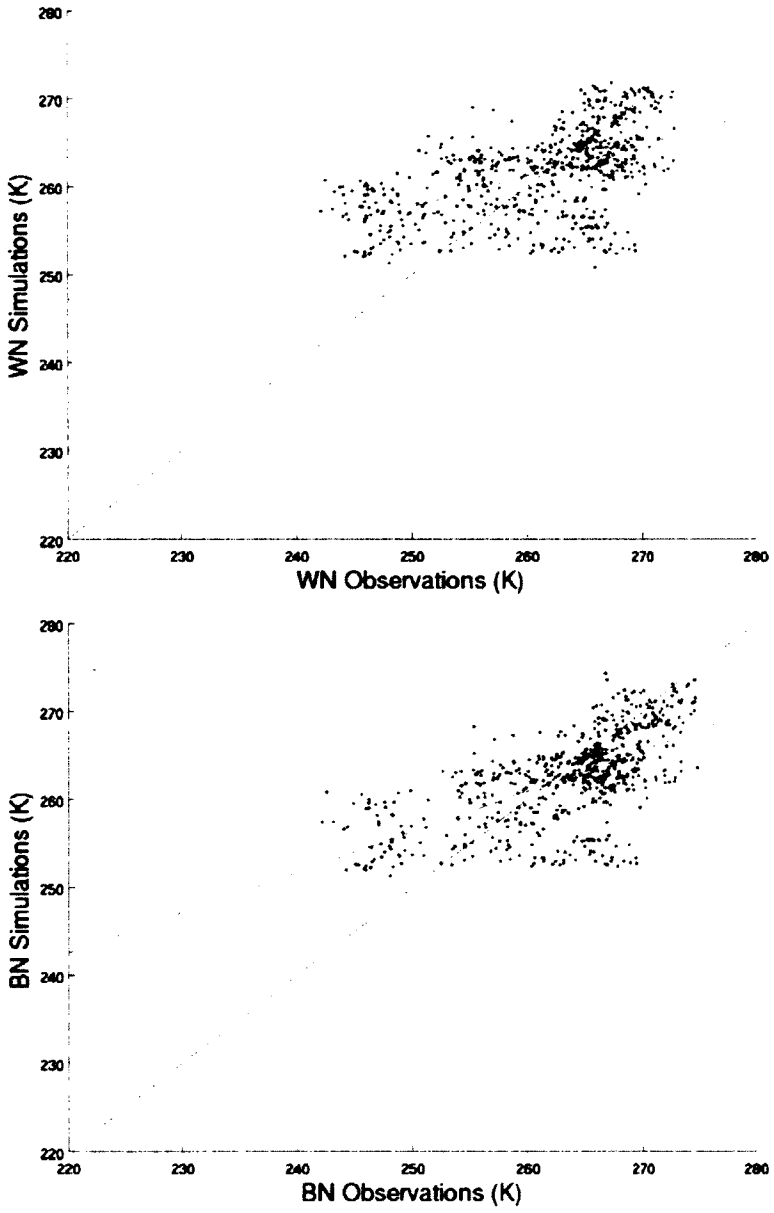

Figure 70: November RUC temperature at 2m scatter plots showing model predictions for all stations on the y-axis and observation data on the x-axis for each precipitation event: W-without and B-beginning. The black line is 1:1; the red is a trendline.

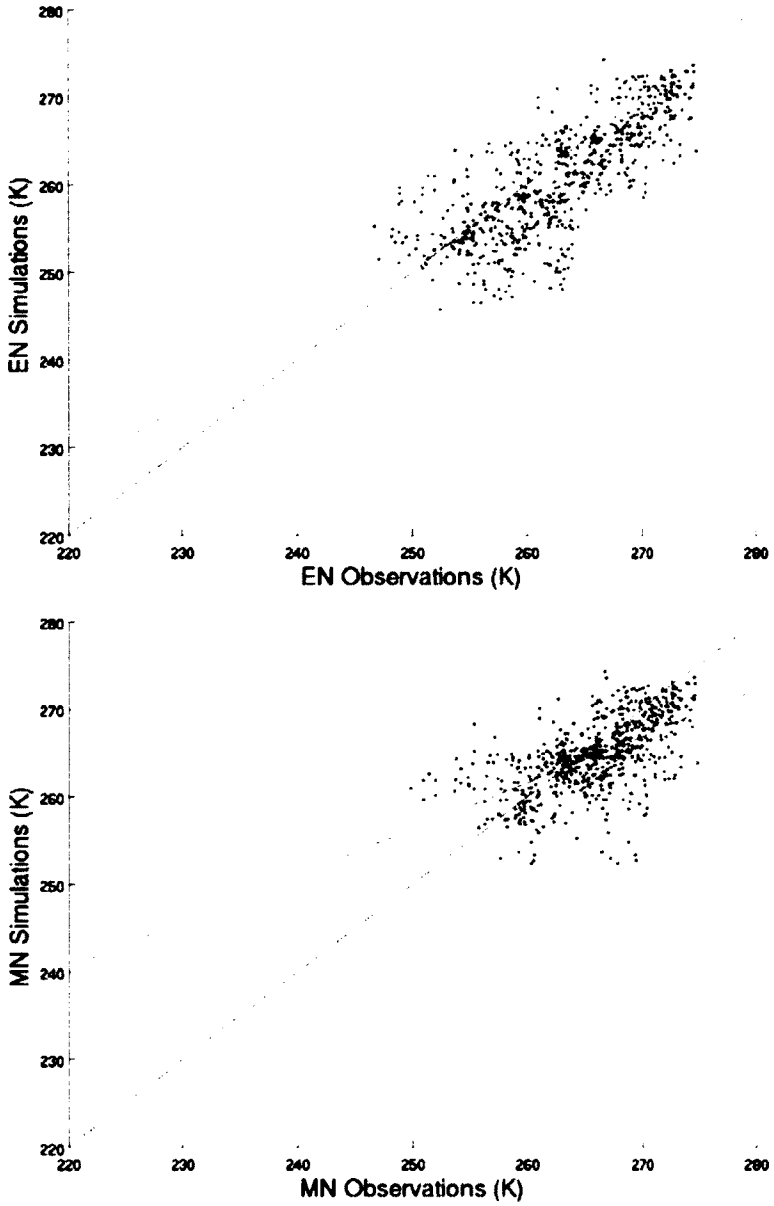

Figure 71: November RUC temperature at 2m scatter plots showing model predictions for all stations on the y-axis and observation data on the x-axis for each precipitation event: E-ending and M-middle. The black line is 1:1; the red is a trendline.

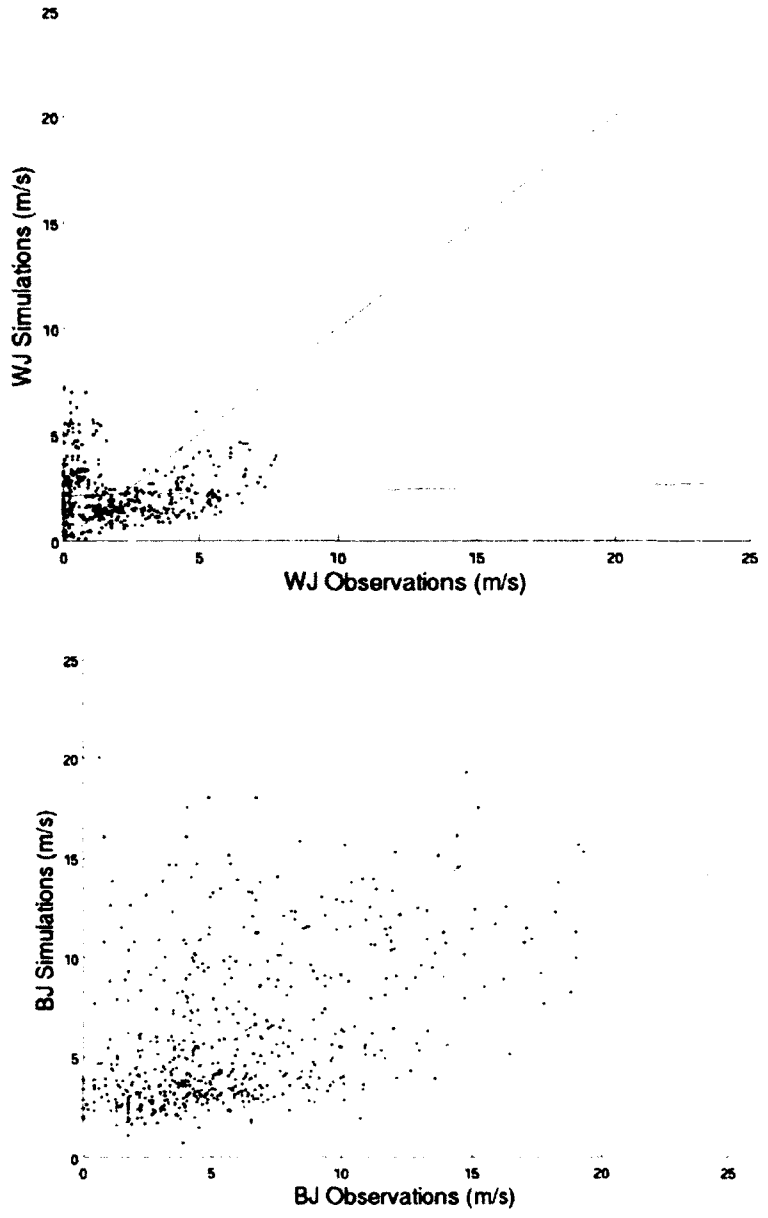

Figure 72: January Noah wind speed scatter plots showing model predictions for all stations on the y-axis and observation data on the x-axis for each precipitation event: W-without and B-beginning. The black line is 1:1; the red is a trendline.

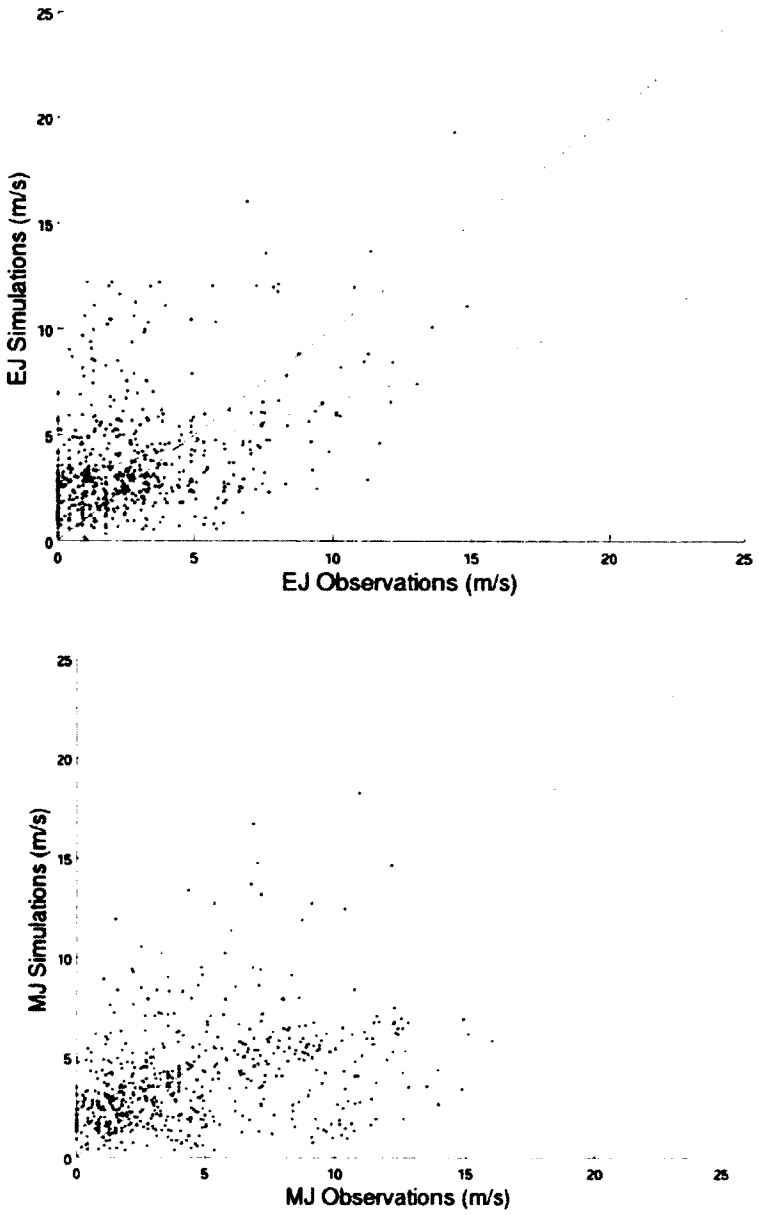

Figure 73: January Noah wind speed scatter plots showing model predictions for all stations on the y-axis and observation data on the x-axis for each precipitation event: E-ending and M-middle. The black line is 1:1; the red is a trendline.

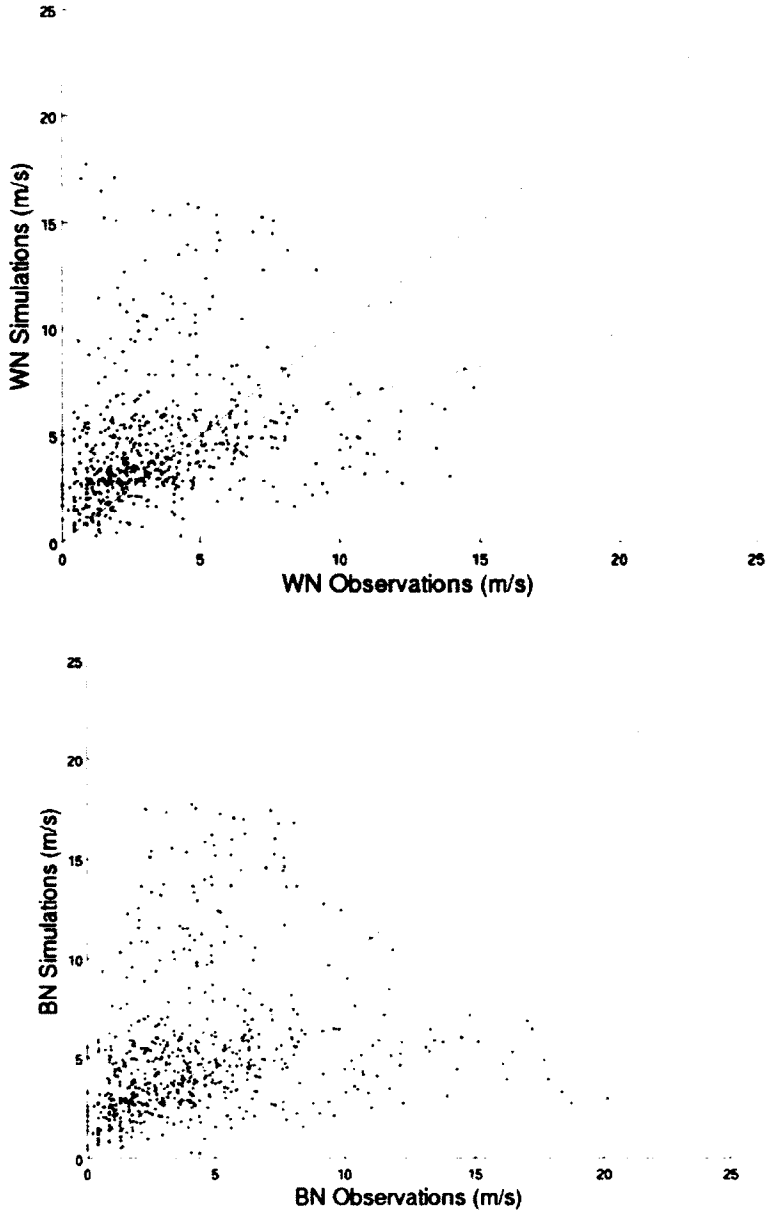

Figure 74: November Noah wind speed scatter plots showing model predictions for all stations on the y-axis and observation data on the x-axis for each precipitation event: W-without and B-beginning. The black line is 1:1; the red is a trendline.

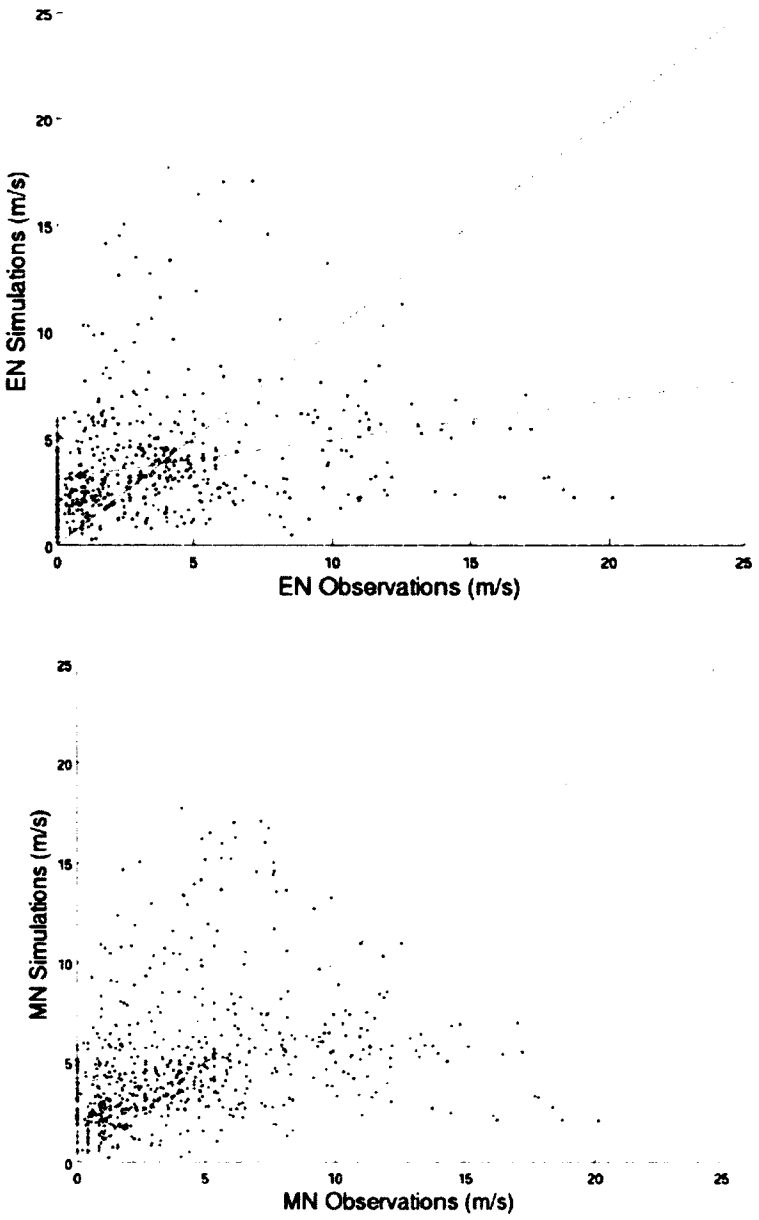

Figure 75: November Noah wind speed scatter plots showing model predictions for all stations on the y-axis and observation data on the x-axis for each precipitation event: E-ending and M-middle. The black line is 1:1; the red is a trendline.

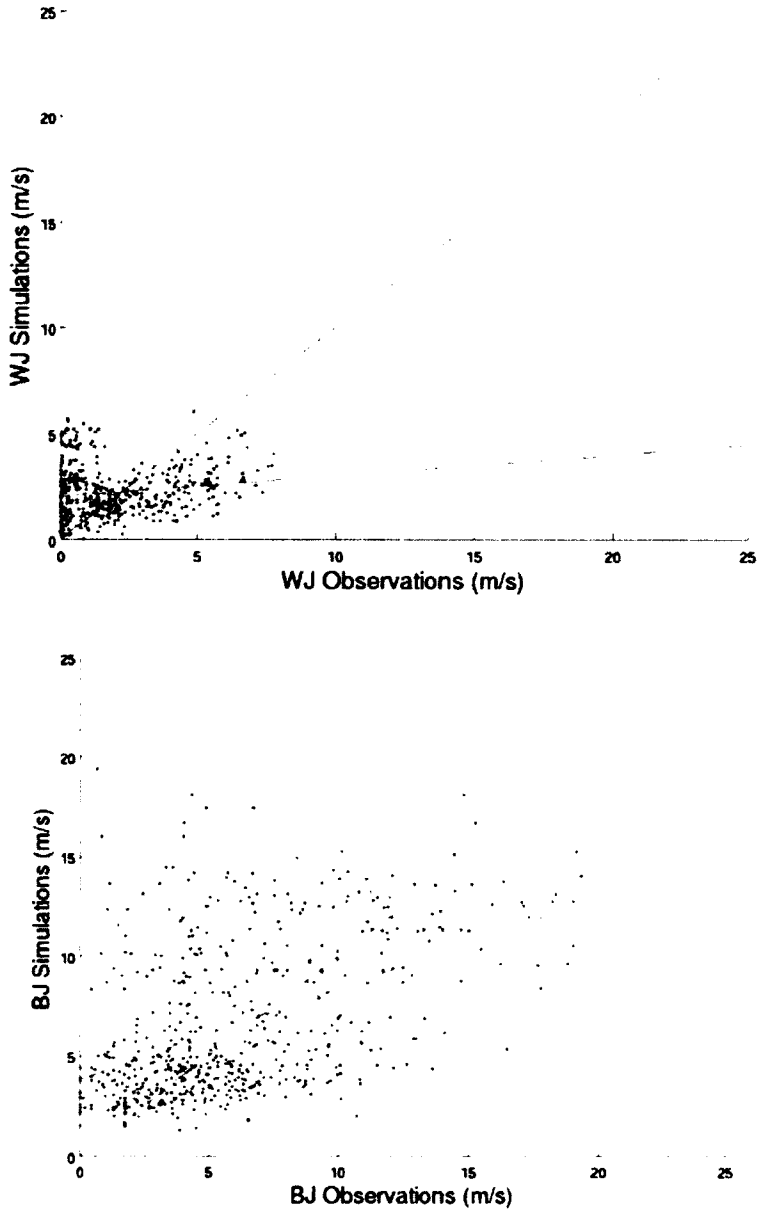

Figure 76: January RUC wind speed scatter plots showing model predictions for all stations on the y-axis and observation data on the x-axis for each precipitation event: W-without and B-beginning. The black line is 1:1; the red is a trendline.

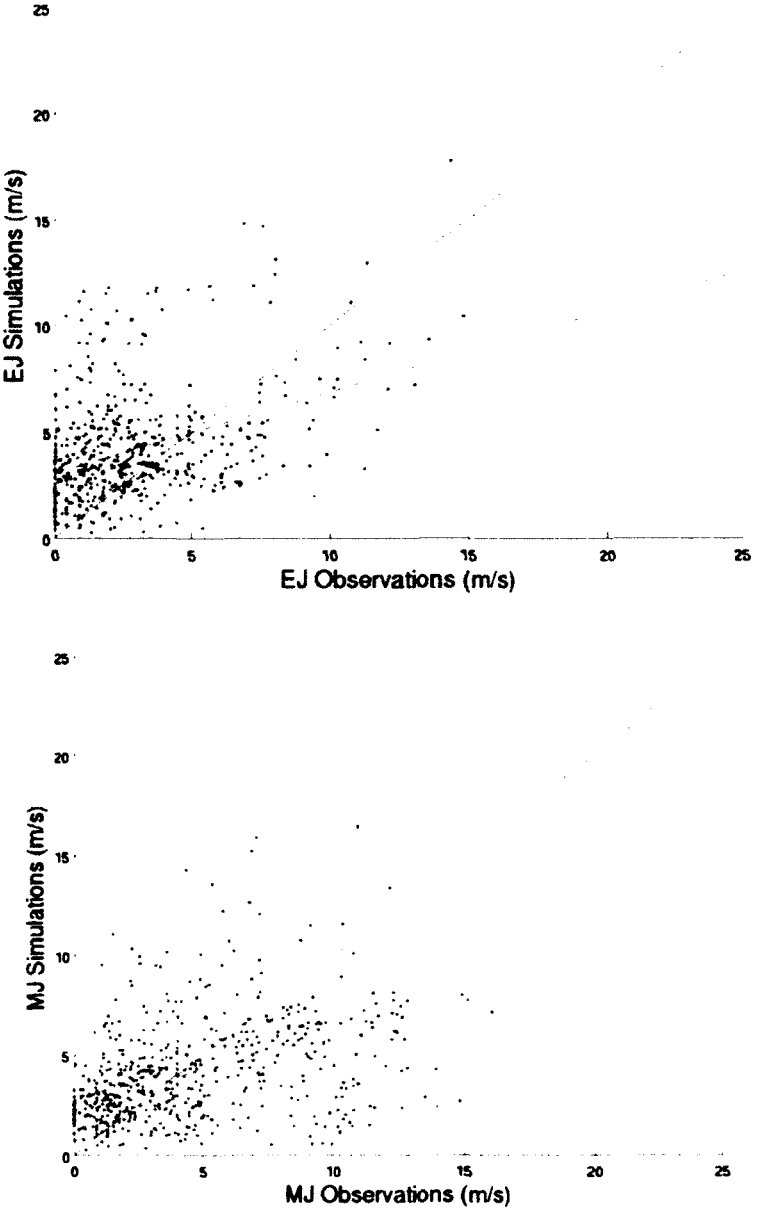

Figure 77: January RUC wind speed scatter plots showing model predictions for all stations on the y-axis and observation data on the x-axis for each precipitation event: E-ending and M-middle. The black line is 1:1; the red is a trendline.

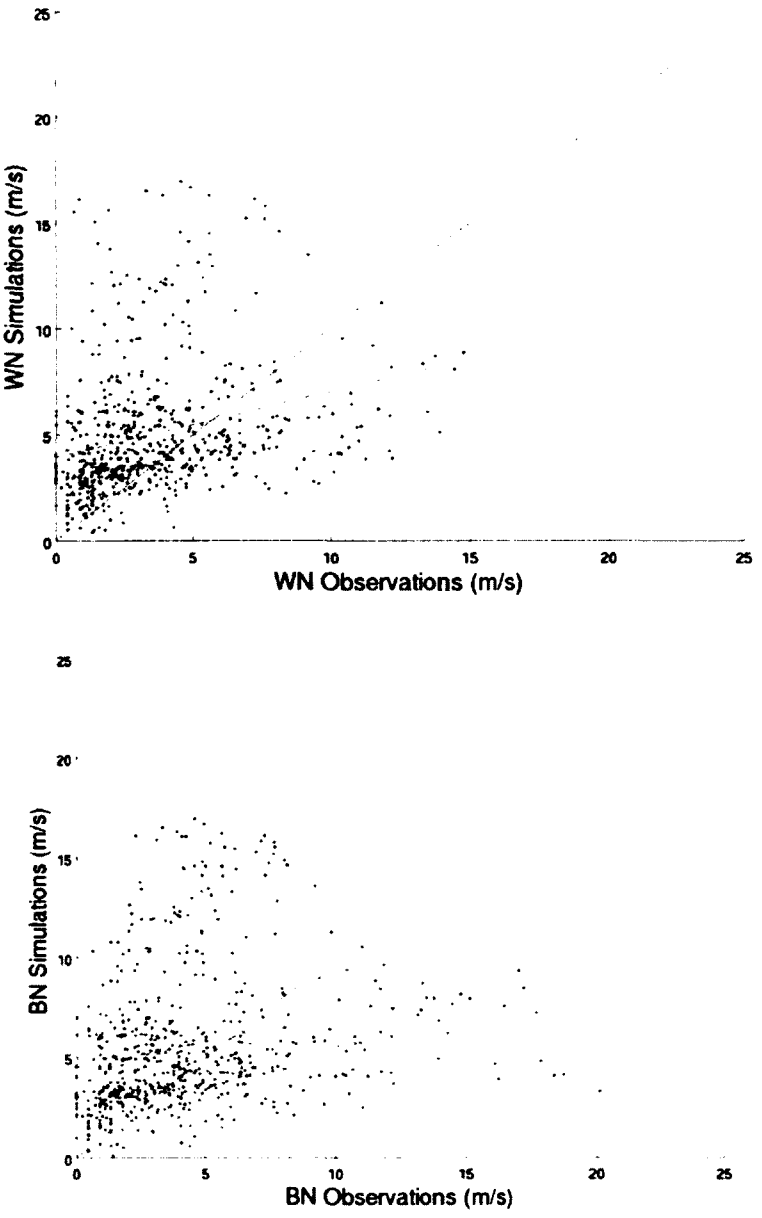

Figure 78: November RUC wind speed scatter plots showing model predictions for all stations on the y-axis and observation data on the x-axis for each precipitation event: W-without and B-beginning. The black line is 1:1; the red is a trendline.

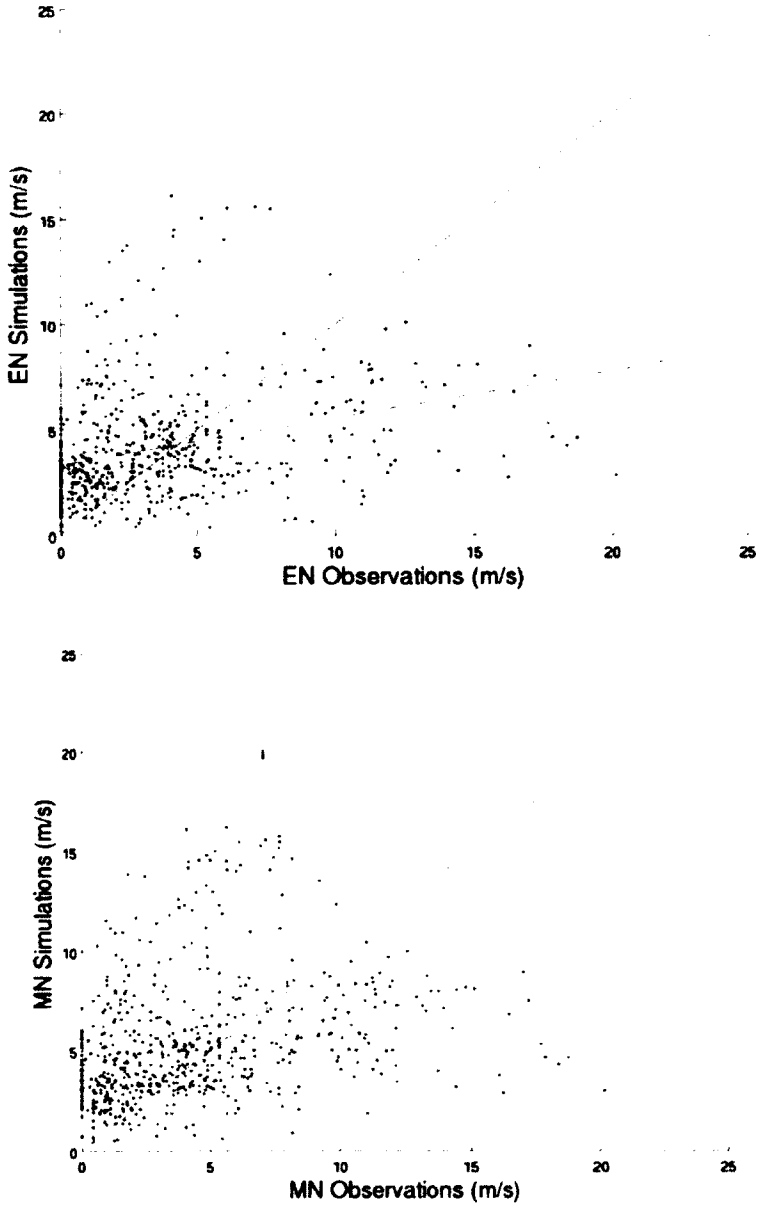

Figure 79: November RUC wind speed scatter plots showing model predictions for all stations on the y-axis and observation data on the x-axis for each precipitation event: E-ending and M-middle. The black line is 1:1; the red is a trendline.

Hour-to-hour snow depth bias correlation values were relatively low (Table 8). Mountain station correlation values were in general higher during January events than the correlations values for the coastal and foothills stations. Coastal values were higher in November than in the mountains and foothills. Noah correlation values for the January precipitation events tended to be higher than RUC values; whereas, RUC correlation values are higher for November events.

Table 8: Correlation values for snow depth bias

Without		January Noah	January RUC	November Noah	November RUC
	Overall	0.17466	0.17053	0.0002898	0.011775
	Mountains	0.1244	0.1403	0.32369	0.35956
	Coastal	0.39599	0.39181	0.46509	0.42647
	Foothills	0.14569	0.14346	0.043771	0.12064
End					
	Overall	0.070676	0.06768	0.0006935	0.004316
	Mountains	0.14857	0.12647	0.029662	0.047365
	Coastal	0.16384	0.1726	0.18937	0.13504
	Foothills	0.1223	0.13631	0.0014944	0.00079
Beginning					
	Overall	0.006814	0.004732	0.0006935	0.001847
	Mountains	0.24263	0.18895	0.029662	0.24291
	Coastal	0.049419	0.090268	0.18937	0.54215
	Foothills	0.000663	0.0044846	0.0014944	0.041463
Middle					
	Overall	0.10552	0.15183	0.03169	0.02925
	Mountains	0.56026	0.45433	0.065855	0.042992
	Coastal	0.16839	0.15718	0.33864	0.09487
	Foothills	0.084917	0.11359	0.0050739	0.008963

Hour-to-hour temperature correlation values for all stations were relatively high compared to snow depth bias for both Noah and RUC (Table 9). Linear relationships for RUC values, on average, are better than Noah values with January correlating better than November (Figure 64-Figure 70). In hour-to-hour wind speed, January correlation was better than November, and RUC correlation was better than Noah (Table 10).

Table 9: Correlation values for temperature

Without	January Noah	January RUC	November Noah	November RUC
End	0.22685	0.26579	0.2142	0.28278
Beginning	0.77875	0.78724	0.5492	0.58623
Middle	0.74652	0.7291	0.5492	0.38762
	0.64756	0.68185	0.37181	0.34991

Table 10: Correlation values for wind speed

Without	January Noah	January RUC	November Noah	November RUC
End	0.001302	0.025106	0.074122	0.075486
Beginning	0.13831	0.15512	0.065576	0.098343
Middle	0.19553	0.2205	0.065576	0.057847
	0.12447	0.14189	0.069172	0.090108

The five-day periods have relatively small differences in snow depth. However, the Barrow November 'beginning precipitation' event (Figure 80) experienced a roughly 20 cm decrease in snow depth during the five-day period. Even with a high potential sublimation value of 50% of snowfall (Liston and Sturm 2002; 2004) this snow depth decrease is not explained. The difference in the simulation and observation of the Barrow event is shown as the maximum value of the snow depth bias in Figure 3. Significant snow depth changes, such as Barrow during the November event, are usually associated with high wind speeds or change of direction of wind (Figure 81). The maximum wind speed during this event was greater than 10 m/s, indicating blowing snow during the snowfall. For each of the five-day periods, the high wind events were for the most part

significantly reduced in the absence of a precipitation event (Table 11, Table 12). For the months prior to the event, wind direction values (Figure 82) for the observation station in the mountains are mostly toward the north-northeast. On the coast and foothills, the wind direction is mostly toward northeast-northwest. Barrow wind direction predominately occurs in the north-northeast for the five-day period.

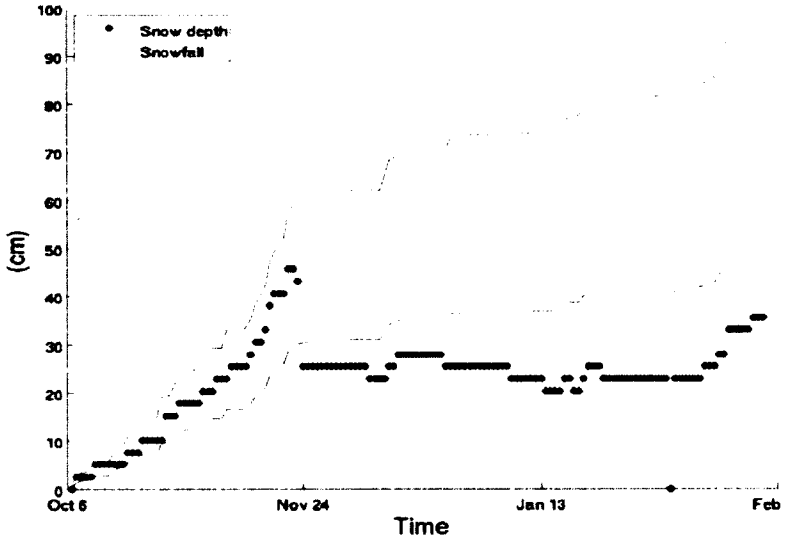

Figure 80: Barrow snow depth and accumulation of precipitation comparison from the beginning of the snow season to end of February. The blue lines indicate snow depth and snowfall accumulation, and the black indicates the high potential sublimation value of 50% of snowfall (Liston and Sturm 2002; 2004).

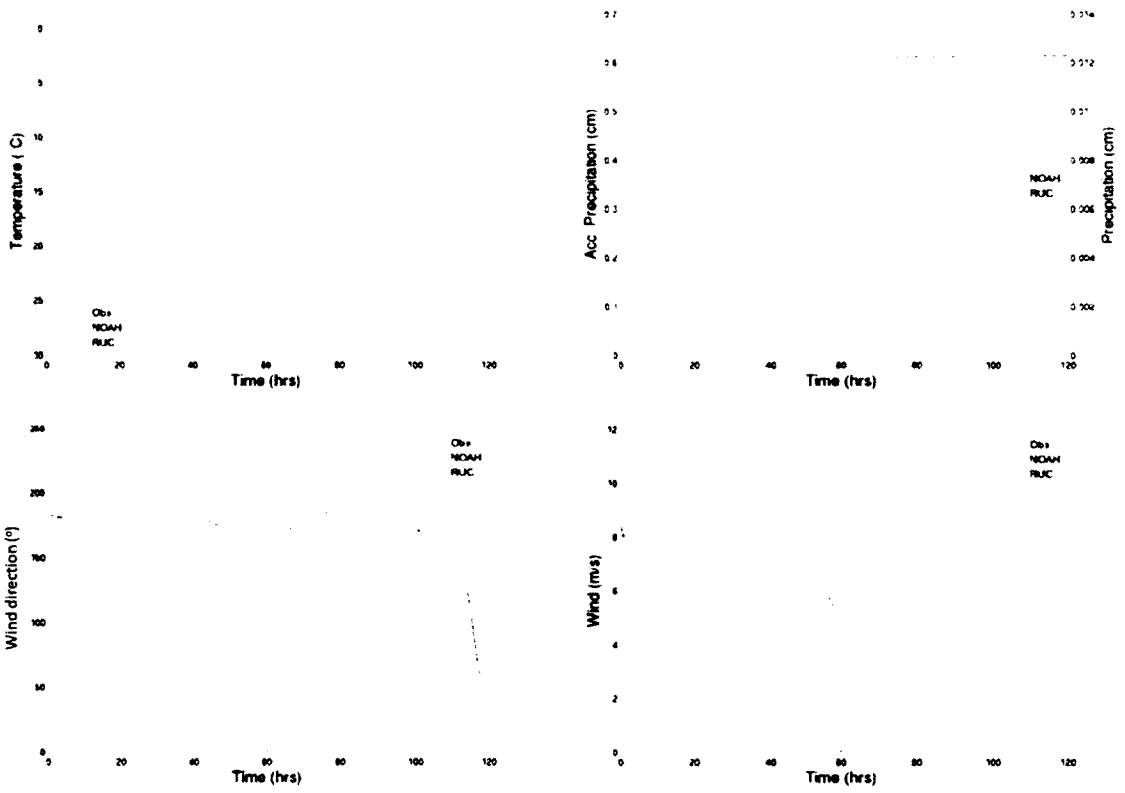

Figure 81: Barrow beginning November precipitation event with a dramatic change in snow depth parameters comparison of simulation to observation. Barrow temperature is recorded as minimum and maximum values. Observed precipitation (green) is compared to the accumulative simulated precipitation (blue).

Table 11: Number of hourly wind speed from meteorological observations greater or equal to 5 ms^{-1}.

$\geq 5ms^{-1}$	Acc	Bull	Imn	Jun	Kad	Kav	NWH	NwK	Rib	Sag	SWH	Umi	Uka	Uku	WhH	Total
jan_wo	0	63	0	0	53	1	26	0	0	0	0	0	0	0	0	143
nov_wo	86	50	20	35	34	18	16	0	36	39	40	0	0	11	46	431
jan_end	32	37	19	10	23	16	16	10	22	19	16	4	6	0	38	268
nov_end	34	89	34	15	88	22	42	0	22	4	0	0	0	19	17	386
jan_beg	55	89	36	29	87	70	65	88	44	68	60	24	58	0	74	847
nov_beg	93	74	29	49	58	22	30	0	52	43	40	0	0	17	60	567
jan_mid	27	70	10	21	65	55	44	57	38	58	53	2	48	21	69	638
nov_mid	56	102	37	40	95	25	51	0	54	38	28	0	0	28	45	599

Table 12: Number of hourly wind speed from meteorological observations greater or equal to 10 ms^{-1}.

$\geq 10ms^{-1}$	Acc	Bull	Imn	Jun	Kad	Kav	NWH	NwK	Rib	Sag	SWH	Umi	Uka	Uku	WhH	Total
jan_wo	0	0	0	0	0	0	0	0	0	0	0	0	0	0	0	0
nov_wo	0	33	0	0	14	0	0	0	6	0	0	0	0	0	21	74
jan_end	0	0	0	5	0	0	6	0	13	9	8	0	0	0	7	48
nov_end	0	66	0	0	55	0	4	0	0	0	0	0	0	0	10	135
jan_beg	9	32	0	7	33	14	20	30	25	21	16	1	18	0	33	259
nov_beg	0	57	0	0	36	0	0	0	6	0	0	0	0	0	29	128
jan_mid	0	45	0	0	43	9	4	24	8	1	1	0	12	0	26	173
nov_mid	0	83	0	0	65	0	4	0	6	0	0	0	0	0	25	183

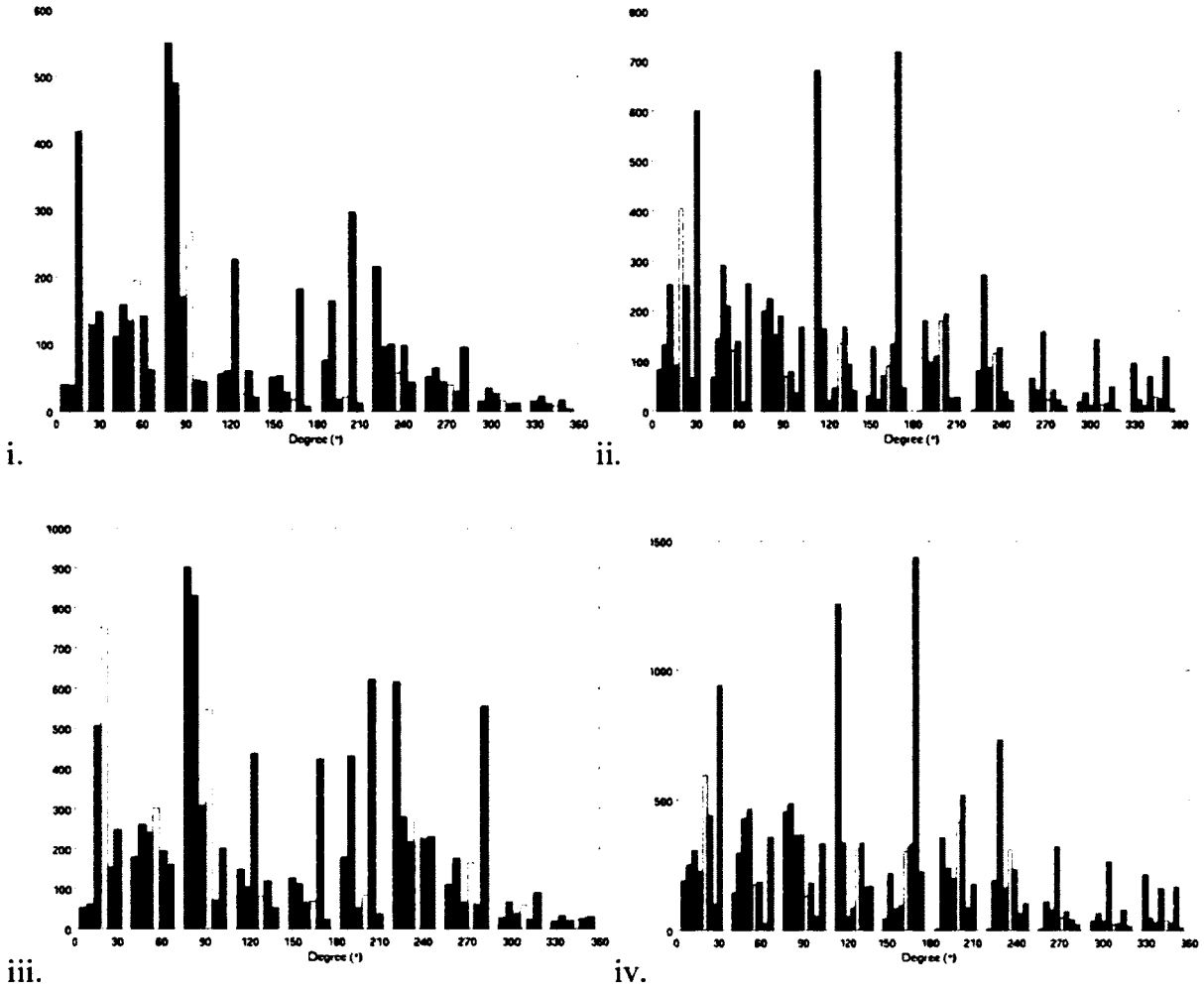

Figure 82: Wind direction history for the stations on the coast from October to November (i,ii) and mountains and foothills October to January (iii,iv). Stations are categorized into mountains (foothills and coastal) by elevation greater (less) 200 meters. Each color bar is a station.

1.2 SnowTran-3D Algorithm

According to the Alaska Arctic Tundra Vegetation Map (Raynolds et al. 2006), the vegetation in Barrow is classified as a wetland. Therefore, the vegetation holding capacity, C_v, is 0.20 m, the vegetation roughness length, z_{0_veg}, is 0.150 m, and the snow roughness length, z_{0_snow}, is 0.005 m (Liston and Sturm 1998). The WRF climate

simulations' meteorological data, with the exception of the snow depth, was used for the calculation of the snow depth using the SnowTran-3D rate of change of snow depth (Eqn. 1). Meteorological data for Barrow during the five-day event show wind speeds greater than 5 m/s and temperatures of the five day event, the snow density was defined by Eqn. (12). For comparison, the snow density was also user-defined as 280 kgm^{-3}, the average Arctic snow density (Liston and Strum 1998). Utilizing Eqn. (1) and (12) and model predictions, the rate of change in snow depth was calculated (Table 13 and 14). The calculated snow depth with the snow density comparison was compared to the observed snow depth (Figure 83).

Table 13: SnowTran-3D rate of change in snow depth equation utilizing simulated meteorological data from Noah in three hour increments from 23 November to 27 November

P (m/s)	ρ_s (kg m^{-3})	dQ_s/dx (kg m^{-1} s^{-1})	dQ_s/dy (kg m^{-1} s^{-1})	dQ_t/dx (kg m^{-1} s^{-1})	dQ_t/dy (kg m^{-1} s^{-1})	$d\zeta/dt$ (m/s)
0.00E+00	2.33E+02	-4.98E-02	6.45E-03	-1.51E-06	2.13E-04	4.63E-08
0.00E+00	1.52E+02	-1.23E-01	4.08E-03	8.23E-10	1.07E-04	1.95E-07
0.00E+00	1.90E+02	-3.19E-02	5.53E-03	1.06E-06	1.81E-04	3.45E-08
0.00E+00	2.18E+02	-1.56E-02	6.75E-03	1.95E-07	2.52E-04	9.82E-09
1.80E-08	2.27E+02	-8.23E-03	6.97E-03	-7.33E-07	2.62E-04	8.05E-08
8.99E-08	2.50E+02	-8.43E-03	8.73E-03	-1.09E-06	3.98E-04	3.58E-07
1.09E-07	2.53E+02	-7.71E-03	9.17E-03	-1.27E-06	4.43E-04	4.31E-07
1.13E-07	2.60E+02	-5.83E-03	9.29E-03	-1.98E-06	4.42E-04	4.31E-07
2.26E-07	2.58E+02	-1.27E-02	9.01E-03	-4.96E-07	4.16E-04	8.78E-07
4.39E-07	2.46E+02	-1.28E-02	8.24E-03	-3.16E-07	3.57E-04	1.78E-06
5.48E-07	2.19E+02	-6.09E-03	6.28E-03	-1.08E-06	2.15E-04	2.49E-06
6.45E-07	2.22E+02	-9.06E-03	6.31E-03	-5.18E-07	2.16E-04	2.91E-06
6.85E-07	2.26E+02	-2.11E-02	6.64E-03	4.61E-07	2.38E-04	3.05E-06
8.11E-07	2.15E+02	-1.86E+00	6.18E-03	2.73E-09	2.13E-04	5.93E-06
9.36E-07	2.25E+02	-2.03E-01	6.86E-03	3.59E-10	2.57E-04	4.37E-06
9.76E-07	2.07E+02	-1.51E-02	5.90E-03	2.38E-07	1.97E-04	4.71E-06
1.01E-06	1.80E+02	-6.26E-03	4.63E-03	-4.64E-07	1.28E-04	5.59E-06
1.04E-06	1.62E+02	-7.51E-03	4.26E-03	-1.01E-07	1.14E-04	6.39E-06
1.10E-06	1.20E+02	-3.12E-02	3.13E-03	-1.04E-08	6.88E-05	9.24E-06
1.25E-06	1.11E+02	-1.61E-02	2.97E-03	6.70E-07	6.32E-05	1.13E-05
1.41E-06	7.77E+01	-1.73E-02	2.08E-03	-1.68E-08	3.29E-05	1.81E-05
1.54E-06	7.95E+01	-8.16E-03	1.69E-03	3.07E-07	2.10E-05	1.93E-05
1.66E-06	8.16E+01	-3.74E-03	1.82E-03	-1.41E-07	2.44E-05	2.04E-05
1.69E-06	7.50E+01	-2.14E-02	1.11E-03	-1.32E-08	9.62E-06	2.25E-05
1.69E-06	7.50E+01	-2.46E-02	1.45E-03	-8.33E-09	1.57E-05	2.26E-05
1.69E-06	7.50E+01	-2.51E-02	1.67E-03	-8.14E-09	2.03E-05	2.26E-05
1.69E-06	7.50E+01	-7.05E-03	1.35E-03	2.16E-07	1.33E-05	2.26E-05
1.69E-06	7.50E+01	-6.04E-03	1.69E-03	1.42E-07	2.05E-05	2.26E-05
1.70E-06	7.50E+01	-2.84E-03	1.25E-03	-3.89E-07	1.15E-05	2.26E-05
1.70E-06	7.50E+01	-1.20E-03	2.21E-03	-6.10E-07	3.60E-05	2.26E-05
1.70E-06	7.50E+01	-1.62E-03	1.21E-03	-7.37E-07	1.09E-05	2.26E-05
1.70E-06	7.50E+01	-1.43E-03	1.46E-03	-7.32E-07	1.52E-05	2.26E-05
1.70E-06	7.50E+01	-5.44E-03	6.82E-04	-8.00E-10	4.30E-06	2.26E-05
1.70E-06	7.50E+01	-2.17E-02	6.95E-04	-1.77E-08	4.41E-06	2.27E-05
1.70E-06	7.50E+01	-5.58E-03	2.29E-04	-2.78E-08	1.06E-06	2.26E-05
1.70E-06	7.50E+01	-1.34E-03	-4.77E-04	-1.28E-06	-1.36E-06	2.26E-05
1.70E-06	7.50E+01	-3.79E-04	-9.98E-04	-8.91E-07	-2.01E-06	2.26E-05
1.70E-06	7.50E+01	-5.71E-04	-2.19E-03	-1.30E-06	-2.11E-06	2.26E-05
1.70E-06	7.50E+01	-1.69E-03	-1.91E-03	-1.56E-06	-2.15E-06	2.26E-05
1.70E-06	7.50E+01	-1.94E-03	-7.60E-03	-2.01E-06	-6.50E-07	2.27E-05
1.70E-06	7.50E+01	-1.08E-02	-3.20E-03	2.93E-07	-1.75E-06	2.27E-05

Table 14: SnowTran-3D rate of change in snow depth equation utilizing simulated meteorological data from RUC in three hour increments from 23 November to 27 November

P (m/s)	ρ_s (kg m^{-3})	dQ_s/dx (kg m^{-1} s^{-1})	dQ_s/dy (kg m^{-1} s^{-1})	dQ_t/dx (kg m^{-1} s^{-1})	dQ_t/dy (kg m^{-1} s^{-1})	$d\zeta/dt$ (m/s)
0.00E+00	2.33E+02	-4.98E-02	6.45E-03	-1.51E-06	2.13E-04	4.63E-08
0.00E+00	1.87E+02	-2.00E-01	4.71E-03	1.50E-09	1.28E-04	2.61E-07
0.00E+00	2.22E+02	-2.64E-02	6.10E-03	7.06E-07	1.97E-04	2.27E-08
0.00E+00	2.21E+02	-6.74E-03	6.47E-03	-9.73E-07	2.26E-04	4.52E-11
4.92E-08	2.17E+02	-4.11E-03	6.04E-03	-1.62E-06	1.96E-04	2.24E-07
1.37E-07	2.27E+02	-3.15E-03	6.99E-03	-2.00E-06	2.62E-04	5.97E-07
1.48E-07	2.33E+02	-3.82E-03	7.24E-03	-1.98E-06	2.77E-04	6.28E-07
1.55E-07	2.61E+02	-5.21E-03	9.11E-03	-2.21E-06	4.20E-04	5.90E-07
2.95E-07	2.40E+02	-4.58E-03	7.66E-03	-1.92E-06	3.08E-04	1.22E-06
4.76E-07	2.40E+02	-6.12E-03	7.76E-03	-1.44E-06	3.19E-04	1.98E-06
5.73E-07	2.22E+02	-3.34E-03	6.54E-03	-1.86E-06	2.32E-04	2.57E-06
6.50E-07	2.09E+02	-2.87E-03	5.75E-03	-1.74E-06	1.84E-04	3.11E-06
6.92E-07	1.84E+02	-6.57E-03	4.79E-03	-4.52E-07	1.36E-04	3.75E-06
8.53E-07	1.67E+02	-1.16E-02	4.21E-03	-2.12E-07	1.09E-04	5.10E-06
9.80E-07	1.72E+02	-8.02E-02	4.36E-03	-2.92E-09	1.16E-04	5.80E-06
1.01E-06	1.89E+02	-1.41E-02	5.03E-03	2.79E-07	1.48E-04	5.36E-06
1.05E-06	1.75E+02	-9.26E-03	4.57E-03	-9.14E-09	1.27E-04	5.99E-06
1.09E-06	1.78E+02	-1.65E-02	4.84E-03	4.68E-07	1.42E-04	6.15E-06
1.15E-06	1.34E+02	-7.22E-03	3.49E-03	-2.58E-07	8.19E-05	8.58E-06
1.29E-06	1.13E+02	-9.22E-03	2.99E-03	2.93E-07	6.38E-05	1.14E-05
1.43E-06	8.17E+01	-3.37E-03	2.19E-03	-1.71E-07	3.62E-05	1.75E-05
1.55E-06	8.13E+01	-1.62E-02	2.15E-03	-2.06E-08	3.51E-05	1.91E-05
1.67E-06	8.19E+01	-5.13E-03	1.95E-03	5.42E-08	2.83E-05	2.04E-05
1.69E-06	8.14E+01	-2.80E-03	1.14E-03	-5.65E-07	1.01E-05	2.08E-05
1.70E-06	7.82E+01	-5.63E-03	1.76E-03	-1.67E-07	2.29E-05	2.17E-05
1.70E-06	7.92E+01	-2.43E-02	1.16E-03	-1.03E-08	1.03E-05	2.15E-05
1.70E-06	8.05E+01	-1.06E-02	1.49E-03	4.53E-07	1.63E-05	2.11E-05
1.70E-06	8.33E+01	-8.98E-03	1.62E-03	3.48E-07	1.92E-05	2.04E-05
1.70E-06	7.76E+01	-4.08E-03	1.55E-03	-8.49E-08	1.79E-05	2.19E-05
1.70E-06	7.57E+01	-1.51E-03	1.65E-03	-6.16E-07	2.02E-05	2.24E-05
1.70E-06	7.50E+01	-2.52E-03	1.50E-03	-3.81E-07	1.67E-05	2.26E-05
1.70E-06	7.50E+01	-5.09E-03	1.74E-03	6.53E-08	2.25E-05	2.26E-05
1.70E-06	7.50E+01	-4.32E-02	1.15E-03	-1.02E-09	1.02E-05	2.27E-05
1.70E-06	7.50E+01	-5.19E-03	7.88E-04	-2.50E-07	5.45E-06	2.26E-05
1.70E-06	7.50E+01	-6.79E-03	2.28E-04	1.43E-07	1.06E-06	2.26E-05
1.70E-06	7.50E+01	-1.46E-03	4.44E-04	-9.33E-07	2.41E-06	2.26E-05
1.70E-06	7.50E+01	-5.42E-04	-2.37E-05	-9.31E-07	-9.24E-08	2.26E-05
1.70E-06	7.50E+01	-6.51E-04	-1.44E-03	-1.29E-06	-2.15E-06	2.26E-05
1.70E-06	7.50E+01	-6.86E-04	-1.57E-03	-1.34E-06	-2.16E-06	2.26E-05
1.70E-06	7.50E+01	-1.74E-03	-5.79E-03	-1.97E-06	-9.94E-07	2.26E-05
1.70E-06	7.50E+01	-3.34E-03	-2.66E-03	-1.03E-06	-1.91E-06	2.26E-05

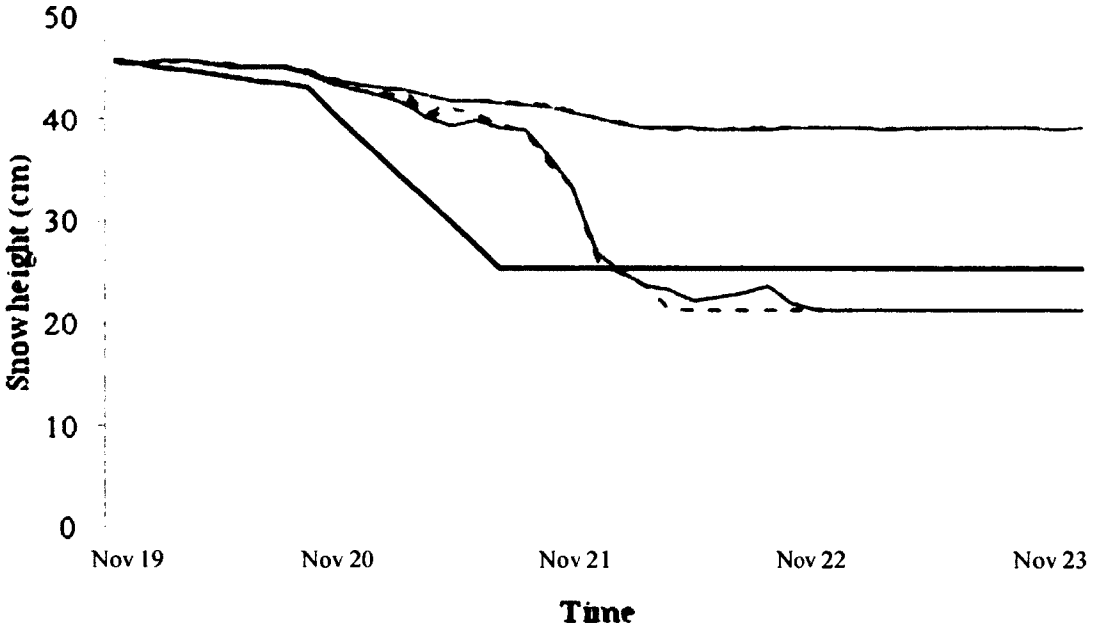

Figure 83: SnowTran-3D rate of change equation utilized with Noah (dashed) and RUC (solid) simulated meteorological data with observational snow depth data (solid black) where snow density is defined by Eqn. (12) (blue) and user-defined at 280 kgm^{-3} (red).

2.0 Discussion

2.1 Observation to Simulation Evaluation

Initial bias between most of the model outputs and observations became the first hurdle in comparing the results. Initial bias in snow depth for the events existed in patterns between stations and regions. Foothills and mountain values had higher simulated initial bias (15 to 30 cm) while coastal areas, with the exception of Barrow station, had lower simulated snow depths (0 to 8 cm). For example, Accomplishment Creek observational data had a 60 cm lower snow depth than simulation values. The imperfection of the initial conditions is largely dependent on the initialization dataset (GFS). WRF performance for the prediction of precipitation is found to be dependent on initialization (Jankov et al. 2007; Etherton and Santos 2008). The removal of the initial bias assisted in the

comparison of the simulated and observed results allowing for the evaluation to be focused on output, not the initial conditions.

The removal of the initial values from the time sets showed the simulation results and observations to have only a few centimeters of variance. Taking into consideration the two centimeters of potential error in the sensors (Ryan et al. 2008), the values with the biases removed were quantitatively comparable. Exception only occurs during a dramatic change in snow depth in the observations, such as during the Barrow November event. The model's inability to predict sudden drops in the snow level potentially could be an indication of the model's inability to redistribute snow.

Performance analysis of the two land surface models shows minimal differences between the parameters snow depth bias, temperature, and wind speed. The RUC scheme tends to do perform better than Noah scheme in predicting temperature. The average, minimum, and maximum of the two models' values are within the same order of magnitude. RUC RMSE values are lower, and RUC correlation values are higher than Noah. The wind speed average differences of Noah are smaller than the RUC, and the RMSE, average, maximum, and minimum values are relatively the same for the two LSMs. The snow bias differences and RSME values are lower for RUC than Noah, but both failed to simulate the drop of snow depth in Barrow. Low magnitude differences between Noah and RUC and greater correlation in RUC were consistent with similar studies (Hines and Bromwich 2008; Boone and Etchevers 2001).

Potential differences in the snow heights between the Noah and RUC scheme outputs could be related to layering and liquid water retention (SnowMIP 2001). The Noah scheme, which works with one snow layer only, can only accommodate one snowpack temperature. The RUC scheme works with five layers and is, therefore, able to create a snow temperature profile, allowing the interaction of snow and air to be better defined. The single layer models allow for only one temperature while multiple layer models generate a temperature gradient within the pack, further impacting the snow height where

or when melting occurs. Single layer models cause the snow depth to be overestimated late in the snow season and snow density to be underestimated because it is fixed (Boone and Etchevers 2001). In the single layer snow model, higher snow water equivalent values are generated by high liquid water retention values, which could allow for higher snow depth values (Boone and Etchevers 2001). Therefore, the thermal construction of the snow in single layer models is limited to a specific thickness versus the whole depth.

The simulation versus observation spatial comparisons shows minimal differences in snow bias, wind speed and direction, and temperature. The snow depth bias differences are within the accuracy error values (roughly 2 cm). Simulated precipitation events within all the five-day periods generally overestimated increases in the snow depth. Inadequacy in solid precipitation event predictions was also found in the Mansell et al. (2006) study of fugitive windblown dust emissions. Average differences between simulated and observed temperatures were less than 0.3°C overall. The three exceptions of greater than 0.3°C difference in temperature are the November 'without precipitation' and November 'beginning precipitation' events for White Hills and the 'end precipitation' snow event in the middle of winter at Imnavait. The White Hills exception overestimates the drop in temperature in the middle of the five-day period during the night. During relatively stable night conditions, the underestimating of temperature is consistent with other studies (de Meij et al. 2009, Henderson et al. 2007; Zepka and Pinto 2010). Observational events with sustained periods of strong winds following drops in temperatures are underestimated by the LSMs. Similar results were found in a Russian study (Vel'tishchev et al. 2011). Both LSMs tend to overestimate wind speed and underestimate temperatures (de Meij et al. 2009). Both LSMs show wind speed profiles as having low errors, less than 2.0 ms^{-1} (Gilliam et al. 2009).

2.2 SnowTran-3D

The result of utilizing the SnowTran-3D rate of snow depth change with the WRF model meteorological predictions shows the reduction in snow depth as seen in the observed

snow depth in the middle of the five-day period in the 'beginning precipitation' November event in Barrow. The simulated sustained high winds in one direction allowed for considerable snow removal through transport, which was confirmed in the observational snow depth data; however, the snow depth reduction was not captured in the WRF simulation directly. To capture the snow reduction, the WRF simulated meteorological data was asynchronously coupled with the SnowTran-3D snow depth rate of change equation. Two snow densities were used for the snow depth rate of change, one temperature and wind dependent and the other constant. The user-defined Arctic snow density is more appropriate for low temperatures and nearly constant surface-shear strength (Liston and Strum 1998). Therefore, for events in the middle of winter, the constant snow density could be a more appropriate for the calculation of snow depth. For the Barrow November event, the equated snow density with dependency of wind speed and temperature mimicked the observational data well and was the better choice for the snow depth calculation.

The roughly 20 cm observed reduction in snow depth with the SnowTran-3D equation was reproduced by the simulation. The equation overestimated the amount of snow that was removed by roughly 4 centimeters. The significant drop in temperature at the end of the 'beginning precipitation' November event (20°C) potentially affected the determination of the amount of snow transported. There is also a slight lag in the equated snow depth. The slight lag in the equated snow depth reduction could be potentially explained with the inclusion of sublimation. More study and assimilation would be needed to verify these results by including additional historical snow transfer events to the model simulation and adding sublimation to the equation.

2.3 Climate Change

A warming climate has the potential to effect the North Slope building season by further reducing the access duration to the tundra. However, the oil and gas industry can use alternative techniques such as making thinner ice roads, while extending the winter work

season without compromises to the tundra condition (Schultz 2010). This can be achieved by altering current ice road building practices to include using the earlier snowfall as pre-packing material, ice chips from shallow lakes, and breaking down heavy drill rigs into lighter weight pieces. Snow transport via wind, while temperature sensitive, will continue so long as very cold arctic winters persist.

3.0 Conclusion

Comparison of observations with model predictions indicates that the temporal and spatial characteristics generally were well modeled with exceptions of initial bias of snow depth and overestimation of nocturnal temperature decreases. The initial bias in snow depth was most likely caused by the initialization dataset (GFS) rather than WRF itself. The temperature underestimations were likely dependent on the nocturnal stability conditions of the model and did not significantly influence snow depth predictions. The Noah LSM generally bettered the RUC LSM in predicting spatial characteristics for temperature, wind speed, and wind direction. The RUC LSM generally bettered the Noah LSM in predicting spatial characteristics for snow height bias. Magnitude differences between RUC and Noah LSM performance were low. The RUC LSM bettered Noah LSM in predicting all temporal characteristics. Model agreement with observations could be improved with higher temporal resolution, more meteorological data, and model improvements.

Regarding the historical snow transfer event, the application of the WRF-simulated meteorological fields and SnowTran-3D rate of change of snow depth equation improved results of the snow transport prediction significantly, especially when compared to the stand alone results of the WRF simulation.

4.0 Statement

A snow transfer event prediction tool to assist in production and operations would be beneficial to arctic transportation. Further evaluation into the use of SnowTran-3D and WRF with differing historical snow transfer events such as ablation or early season snowfall will potentially broaden the tool's capability and utilization.

Acknowledgements

I acknowledge salary support for the work herein from DOE-NETL's Arctic Transportation Network project, the NSF-IARC cooperative agreement, the JAMSTEC-IARC cooperative agreement, as well as travel support from Campbell Scientific Canada. Thanks to Nicole Molders, Michael Lilly, Don Morton, and Jessica Cherry for simulation data, computational assistance, and fruitful discussion. Computational support was provided in part by a grant of HPC resources from the Arctic Region Supercomputing Center at the University of Alaska Fairbanks as part of the Department of Defense High Performance Computing Modernization Program.

References

Anderson EA. 1976. A point energy and mass balance model of a snow cover. NOAA Technical Report: NWS-19.

Arctic Research Commission. 2003. Climate change, permafrost, and impacts on civil infrastructure. United States Special report: 01-03.

Bader HR, Guimond J. 2004. Tundra Travel Modeling Project Provisional Report. Alaska Department of Natural Rcsources, Northern Region Land Section.

Baker D, Kalnay E. 2008. The multi-meteorology air quality (MMAQ) ensemble project: variance generated by a WRF varied physics ensemble. Presented at the 7th Annual CMAS Conference, Chapel Hill, NC, October 6-8, 2008.

Baker D, Downs T, Ku M, Hao W, Sistla G, Kiss M, Johnson M, Brown D. 2010. Sensitivity testing of WRF Physics parameterizations for meteorological modeling and protocol in support of regional SIP air quality modeling in the OTR. Presented at the Ozone Transport Commission. Available from: www.otc.org.

Bakkehøi S, Øien K, Førland EJ. 1985. An automatic precipitation gauge based on vibrating-wire strain gauges. Nordic Hydrology 16: 193-202.

Benson CS. 1969. The seasonal snow cover of Arctic Alaska. Arctic Institute of North America Research Paper.

Benson CS, Sturm M. 1993. Structure and wind transport of seasonal snow on the Arctic slope of Alaska. Annals of Glaciology 18: 261-267.

Berezovskaya S, Hilton K, Derry J, Youcha E, Kane D, Gieck R, Homan J, Lilly M. 2010. Snow survey data for the central North Slope watersheds: Spring 2010. University of Alaska Fairbanks, Water and Environmental Research Center, Report INE/WERC: 10.01.

Bilello MA. 1957. A survey of Arctic snow-cover properties as related to climatic conditions. USA Snow, Ice and Permafrost Research Establishment (USACRREL), Research Report RR.

Bilello MA. 1984. Regional and seasonal variations in the snow-cover density in the USSR. USA Cold Regions Research and Engineering Laboratory, CRREL Report: 84-22.

Bogdanova EG, Ilyin BM, Dragomilova IV. 2002. Application of a comprehensive bias-correction model to precipitation measured at Russian North Pole drifting stations. Journal of Hydrometeorology 3: 700-713.

Boone A, Etchevers P. 2001. An intercomparison of three snow schemes of varying complexity coupled to the same land surface model: social-scale evaluation at an alpine site. Journal of Hydrometeorology 2: 374-394.

Brazenec WA. 2005. Evaluation of ultrasonic snow depth sensors for automated surface observing systems (ASOS). Department of Forest, Rangeland, and Watershed Stewardship, M.S. Thesis, Colorado State University, Fort Collins, CO.

Chen F, Dudhia J. 2001. Coupling an advances land-surface/ hydrology model with the Penn State/ NCAR MM5 modeling system. Part I: Modeling description and implementation. Monthly Weather Review 129: 569-585.

Chigullapalli S, Mölders N. 2008. Sensitivity studies using the Weather Research and Forecasting (WRF) model. ARSC report.

Chou MD, Suarez MJ. 1994. An efficient thermal infrared radiation parameterization for use in general circulation models. NASA Technical Memo: 104606.

Colbeck S, Akitaya E, Armostrong R, Gubler H, Lafeuille J, Lied K, McClung D, Morris E. 1990. The international classification for seasonal snow on the ground. International Glaciological Society: 1-23.

Colbeck SC. 1987. A review of the metamorphism and classification of seasonal snow cover crystals. In: B Salm, Gubler H, editors. Avalanche Formation, Movements and Effects. IAHS Publications 162: 1-34.

Colbeck SC. 1990. The layered character of snow covers. Reviews of Geophysics 29: 81-96.

Conover JH. 1960. Macro- and micro-climatology of the Arctic slope of Alaska. U.S. Quartermaster Research and Engineering Center. Environmental Protection Research Division Technical Report: EP-139.

De Meij A, Gizella A, Cuvelier C, Thunis P, Bessagnet B, Vinuesa JF, Minut L, Kelder HM. 2009. The impact of MM5 and WRF meteorology over complex terrain on CHIMERE model calculations. Atmospheric Chemistry Physics 9: 6611-6632.

Doesken NJ, Judson A. 1996. The Snow Booklet: A guide to the science, climatology, and measurement of snow in the United States, Colorado State University, Fort Collins, CO.

Doorschot J, Lehning M. 2002. Equilibrium saltation: mass fluxes, aerodynamic entrainment, and dependence on grain properties. Boundary-Layer Meteorology 104(1): 111-130.

Essery R, Etchevers P. 2004. Parameter sensitivity in simulations of snowmelt. Journal Geophysical Research 109: D20111. Available from: doi: 10.1029/2004JD005036.

Etchevers P, Martin E, Brown R, Fierz C, Lajeune Y, Bazile E, Boone A, Dai Y-J, Essery R, Fernandez A, Gusev Y, Jordan R, Koren V, Kowalczyk E, Nasonova NO, Pyles RD, Schlosser A, Shmakin AB, Smirnova TG, Strasser U, Verseghy D, Yamazaki T, Yang ZL. 2004. Validation of the surface energy budget simulated by several LSMs. Annals of Glaciology 38: 150-158.

Etherton B, Santos P. 2008. Sensitivity of WRF Forecasts for South Florida to Initial Conditions. Weather Forecasting 23: 725-740. Available from: doi: 10.1175/2007WAF2006115.1

Evans BM, Walker DA, Benson CS, Norstrand EA, Petersen GW. 1989. Spatial interrelationships between terrain, snow distribution and vegetation patterns at an Arctic Foothills site in Alaska. Holarctic Ecology 12(3): 270-278.

Ferrians OJ Jr. 1994. Permafrost in Alaska. In: Plafker G, HC Berg, editors. The Geology of Alaska. v. G-1. Boulder, Colorado, Geological Society of America: 845-853.

Frenzen P, Vogel CA. 1995. On the magnitude and apparent range of the von Karman constant in the atmospheric surface layer. Boundary-Layer Meteorology 72(4): 371-392. Available from: doi: 10.1007/BF00709000.

Gilliam R, Pleim J, Otte T. 2009. Multiscale meteorological modeling for air quality applications, Presented at the EPA Atmospheric and Modeling Analysis Division Peer Review Conference, January 27-29, Research Triangle Park, NC.

Goodison BE, Metcalfe JR. 1988. Canadian participation in the WMO solid precipitation measurement Intercomparison. In: Thomsen T, Søgaard H, Braithwaite R, editors. Applied Hydrology Development of Northern Basins. Proceeding from The Seventh Northern Research Basins Symposium/Workshop; May 25-June 1, 1988; Ilulissat, Greenland: Danish Society for Arctic Technology, c/o Greenland technical organization, Copenhagen, Denmark; P. 199-207.

Goodison BE, Louie PYT, Yang D. 1998. WMO solid precipitation measurement intercomparison final report. World Meteorological Organization Instruments and Observing Methods. Report No.: 67.

Gray DM, Male DH. 1981. The Distribution of snowcover. In: Gray DM, Male DH, editors, Handbook of Snow: principles, processes, management and use. Toronto, Oxford, New York, Sydney, Paris, Frankfurt: Pergamon Press. p 153-190.

Greeley R, Iversen JD. 1985. Wind as a geological process on Earth, Mars, Venus and Titan. Cambridge, Cambridge University Press.

Henderson D, PaiMazumder D, Mölders N. 2007. Evaluation of the WRF model over Siberia. REU-Report. Available from: http://www.gi.alaska.edu/~molders/REU_report_2007.pdf

Hines KM, Bromwich DH. 2008. Development and testing of Polar WRF. Part I: Greenland ice sheet meteorology. Monthly Weather Review 136: 1971-1989.

Hinzman LD, Kane DL, Benson CS, Everett KR. 1991. Hydrologic and thermal properties of the active layer in the Alaskan Arctic. Cold Regions Science and Technology 19: 95-110.

Hirashima H, Ohata T, Kodama Y, Yabuki H, Sato N, Georgiadi A. 2004. Non-uniform distribution of tundra snow cover in eastern Siberia. Journal of Hydrometeorology 5: 373-389.

Janjić ZI. 1996. The surface layer in the NCEP Eta Model. Proceedings of the 11th Conference on Numerical Weather Prediction, Norfolk, VA: American Meteorology Society; P. 354-355.

Janjić ZI. 2002. Nonsingular implementation of the Mellor-Yamada level 2.5 scheme in the NCEP Mesomodel. NCEP Office Note 437, National Centers for Environmental Prediction.

Jankov I, Gallus WA Jr, Segal M, Koch SE. 2007. Influence of initial conditions on the WRF-ARW Model QPF response to physical parameterization changes. American Meteorological Society 22: 501-519. Available from: doi: 10.1175/WAF998.1

Jeffries MO, Morris K, Liston GE. 1996. A method to determine lake depth and water availability on the North Slope of Alaska with space-borne imaging radar and numerical ice growth modeling. Arctic 49: 367-374.

Jeffries MO, Zhang T, Frey K, Kozlenko N. 1999. Estimating late-winter heat flow to the atmosphere from the lake-dominated Alaska North Slope. Journal of Glaciology 45: 315-324.

Jorgenson MT, Heiner M. 2003. Ecosystems of northern Alaska. Unpublished map by the Nature Conservancy. Anchorage, AK.

Jorgenson MT, Roth JE, Miller PF, Macander MJ, Duffy MS, Wells AF, Frost GV, Pullman ER. 2009. An ecological land survey and land cover map of the Arctic network. Natural resource technical report: NPS/ARCN/NRTR-2009/270.

Kane DL, Youcha EK, Stuefer S, Toniolo H, Schnabel W, Gieck R, Myerchin-Tape G, Homan J, Lamb E, Tape K. 2012. Analysis Report for Foothills/Umiat Corridor and Bullen Projects: 2006-2011. University of Alaska, Water and Environmental Research Center, Report INE/WERC: 12.01.

Kane DL, Hinzman LD, Benson CS, Liston GE. 1991. Snow Hydrology of a Headwater Arctic Basin 1, Physical Measurements and Process Studies. Water Resources Research 27(6): 1099-1109.

Kind RJ. 1992. One-dimensional Aeolian suspension above beds of loose particles – a new concentration-profile equation. Atmospheric Environment, 26A (5): 927-931.

Koren V, Schaake J, Mitchel K, Duan Q-Y, Chen F, Baker JM. 1999. A parameterization of snowpack and frozen ground intended for NCEP weather and climate models. Journal of Geophysical Research 104: 19569-19585.

LaChapelle ER. 1969. Properties of snow. Seattle, WA, University of Washington. College of Forest Resources.

Lee LW. 1975. Sublimation of snow in turbulent atmosphere. Ph.D. thesis, University of Wyoming, Laramie, WY.

Lemke P, Ren J, Alley RB, Allison I, Carrasco J, Flato G, Fujii Y, Kaser G, Mote P, Thomas RH, Zhang T. 2007. Observations: Changes in Snow, Ice and Frozen Ground. In: Climate change 2007: the physical science basis; summary for policymakers, technical summary and frequently asked questions. Proceedings of the Working Group I contribution to the Fourth Assessment Report of the Intergovernmental Panel on Climate Change: ISBN 92-9169-121-6.

Ling F, Zhang T. 2006. Sensitivity of ground thermal regime and surface energy fluxes to tundra snow density in northern Alaska. Cold Regions Science and Technology 44: 121-130.

Liston GE, Sturm M. 1998. A snow-transport model for complex terrain. Journal of Glaciology 44(148): 489-516.

Liston GE, Sturm M. 2002. Winter precipitation patterns in arctic Alaska determined from blowing-snow model and snow-depth observations. Journal of Hydrometeorology 3: 646-659.

Liston GE, Sturm M. 2003. The snow cover on lakes of the Arctic coastal plain of Alaska, USA. Journal of Glaciology 49(166): 370-380.

Liston GE, Sturm M. 2004. The role of winter sublimation in the Arctic moisture budget. Nordic Hydrology 35(4): 325-334.

Liston GE, Haehnel RB, Sturm M, Hiemstra CA, Berezovskaya S, Tabler RD. 2007. Simulating complex snow distributions in windy environments using SnowTran-3D. Journal of Glaciology 53: 241-256.

Lundberg A, Halldin S. 2001. Snow measurement techniques for land-surface-atmosphere exchange studies in boreal landscapes. Theory of Applied Climatology 70: 215-230.

Male DH. 1980. The seasonal snowcover. In: Colbeck SC, editor. Dynamics of snow and ice masses. New York, Academic Press. p 305-395.

Mansell GE, Lau S, Russell J, Omary M. 2006. Final Report: Fugitive Wind Blown Dust Emissions and Model Performance Evaluation, Phase II. Presented at the Western Governors Association by ENVIRON International Corporation, Novato, CA and the University of California at Riverside Center for Environmental Research and Technology, Riverside, CA.

National Research Council. 2003. Cumulative Environmental Effects of Oil and Gas Activities on Alaska's North Slope. National Academies Press. Washington, DC.

Paolo D'O, Caylow K, Okin GS, Scanlon TM. 2007. On soil moisture – vegetation feedbacks and their possible effects on the dynamics of dryland ecosystems. Journal of Geophysical Research 112: 410-420.

Pomeroy JW, Gray DM. 1990. Saltation of snow. Water Resources Research 26(7): 1583-1594.

Pomeroy JW, Gray DM, Landine PG. 1993. The prairie blowing snow model: characteristics, validation, operation. Journal of Hydrology 144: 165-192.

Raynolds MA, Walker DA, Maier HA. 2006. Alaska Arctic Tundra Vegetation Map. Scale 1:4,000.000. Conversion of Arctic Flora and Fauna Map No. 2, U.S. Fish and Wildlife Service, Anchorage, Alaska.

Romanovsky VE, Sergueev DO, Osterkamp TE. 2003. Spatial and temporal variations in the active layer and near-surface permafrost temperatures in northern Alaska. In: Phillips M, Springman SM, Arenson LU, Balkema AA, editors. Proceedings of the 8th International Conference on Permafrost; Brookfield, Vermont: P. 989–994.

Romanovsky VE, Osterkamp TE. 2000. Effects of unfrozen water on heat and mass transport processes in the active layer and permafrost. Permafrost and Periglacial Processes 11: 219-239.

Ryan WA, Doesken NJ, Fassnacht S. 2008. Evaluation of ultrasonic snow depth sensors for U.S snow measurements. Journal of Atmospheric and Oceanic Technology 25: 667-684.

Savelyev SA, Gordon M, Hanesiak J, Papakyriakou T, Taylor PA. 2006. Blowing snow studies in the Canadian Arctic Shelf Exchange Study, 2003-04. Hydrological Processes 20: 817-827.

Schmidt RA. 1982. Vertical profiles of wind speed, snow concentration and humidity of blowing snow. Boundary-Layer Meteorology 23(2): 223-246.

Schultz G. 2010. History of Alaska Department of Natural Resources Management of Ice Roads Construction and Impacts of Different Methods of Ice Roads Construction. Presented at the Arctic Ice and Snow Roads 2010 Conference: Advancements and Future Needs.

Sellman PV, Brown J, Lewellen RI, McKim H, Merry C. 1975. The Classification and Geomorphic Implications of Thaw Lakes on the Arctic Coastal Plain, Alaska. Hanover,

New Hampshire: U.S. Army Cold Regions Research & Engineering Laboratory Research Report: 344.

Sevurk B, Hertig J-A, Spiess R. 1989. The effect of precipitation gauge orifice on the wind field deformation as investigated in a wind tunnel. Atmospheric Environment 25A: 1173-1181.

Shulski M, Wendler G. 2007. The Climate of Alaska. University of Alaska Press.

Skamarock WC, Klemp JB, Dudhia J, Gill DO, Barker DM, Duda MG, Huang X, Wang W, Powers JG. 2008. A Description of the Advanced Research WRF Version 3. NCAR Technical Note: NCAR/TN-475+STR.

Smirnova TG, Brown JM, Benjamin SG. 2000. Parameterization of cold-season processes in the MAPS land-surface scheme. Journal of Geophysical Research 105: 4077-4086.

Smith SL, Romanovsky VE, Lewkowicz AG, Burn CR, Allard M, Clow GD, Yoshikawa K, Throop J. 2010. Thermal State of Permafrost in North America – A Contribution to the International Polar Year. Permafrost and Periglacial Processes 21: 117-135.

Snow Model Intercomparison Project (SnowMIP). 2001. An Overview of models participating in the Snow Model Intercomparison Project (SnowMIP). In: Essery R, Yang Z, editors. Proceedings of the SnowMIP Workshop, 11 July 2001, 8th Scientific Assembly of IAMAS; Innsbruck, Austria. Available from: http://www.cnrm.meteo.fr/snowmip/

Steppuhn H. 1976. Areal water equivalents for prairie snow covers by centralized sampling. Proceedings of the 44th Annual Meeting Western Snow Conference; P. 63-68.

Stieglitz M, Dey SJ, Romanovsky VE, Osterkamp TE. 2003. Role of snow cover in the warming of arctic permafrost. Geophysical Resources Letters 30(13): 541-544.

Stone RS, Dutton EG, Harris JM, Longnecker D. 2002. Earlier spring snowmelt in northern Alaska as an indicator of climate change. Journal Geophysical Resources 107: D10. Available from: doi: 10,1029/2000JD000286.

Sturm M, Benson CS. 2004. Scales of spatial heterogeneity for perennial and seasonal snow layers. Annals of Glaciology 38: 253-260.

Sturm M, Holmgren J, Liston G. 1995. A seasonal snow cover classification system for local to global applications. Journal of Climate 8(5): 1261-1283.

Sturm M, Holmgren J, König M, Morris K. 1997. The thermal conductivity of seasonal snow. Journal of Glaciology 43: 26-41.

Sugiura K, Yang D, Ohata T. 2003. Systematic error aspects of gauge-measured solid precipitation in Arctic, Barrow, Alaska. Geophysical Research Letters 30(4): 1192. Available from: doi: 10.1029/2002GL015547.

Sugiura K, Ohata T, Yang D. 2006. Catch characteristics of precipitation gauges in high-latitude regions with high winds. Journal of Hydrometeorology 7: 984-994.

Sugiura K, Ohata T, Yang D, Sato T, Sato A. 2009. Application of a snow particle counter to solid precipitation measurements under Arctic conditions. Cold Regions Science and Technology 58: 77-83.

Thorpe AD, Mason BJ. 1966. The evaporation of ice spheres and ice crystals. Journal of Applied Physics 17 (4): 541-548.

Vel'tishchev N, Zhupanov V, Pavlyukov Y. 2011. Short-range forecast of heavy precipitation and strong wind using the convection-allowing WRF models. Russian Meteorology and Hydrology 36(1): 1-10.

Walker DA. 1999. An integrated vegetation mapping approach for northern Alaska (1:4 M scale). International Journal Remote Sensing 20: 2895-2920.

Warren SG, Rigor IG, Untersteiner N, Radinov VF, Bryazgin NN, Aleksandrov YI, Colony R. 1999. Snow Depth on Arctic sea ice. Journal of Climate 12: 1814-1829.

Weller G, Holmgren B. 1974. The microclimates of the Arctic tundra. Journal of Applied Meteorology 13: 854-862.

Wendler G. 1978. Snow blowing and snow fall on the North Slope, Alaska. University of Alaska Fairbanks. Geophysical Institute Report: UAG R-259.

Wendler G, Kelley J. 1988. On the albedo of snow in Antarctica: A contribution to IAGO. Journal of Glaciology 34: 19-25.

Wendler G, Ishikawa N, Streten N. 1974. The climate of the McCall Glacier, Brooks Range, Alaska, in relation to its geographical setting. Arctic and Alpine Research 6: 307-318.

Wielgolaski FE. 1972. Vegetation types and plant biomass in tundra. Arctic and Alpine Research 4(4): 291-305.

WMO. 1994. Guide to hydrological practices, data acquisition and processing, analysis forecasting and other applications, Fifth edition. 168.

WMO/Commission on Instruments and Methods of Observation, International Organizing Committee for the WMO Solid Precipitation Measurement Intercomparison, final report of the first session. 1985. Geneva: WMO report No.: 31.

Woo MK. 1982. Upward flux of vapor from frozen materials in the High Arctic. Cold Regions Science Technology 5: 269-274.

Yang D, Ohata T. 2001. A bias-corrected Siberian regional precipitation climatology. Journal of Hydrometeorology 2: 122-139.

Yang D, Goodison BE, Ishida S. 1998. Adjustment of daily precipitation data at 10 climate stations in Alaska: Application of World Meteorological Organization intercomparison results. Water Resources Research 34(2): 241-256.

Yosida Z. 1955. Physical studies on deposited snow. In: 1. Thermal properties, vol. A(7). Hokkaido University, Sapporo, Japan: Contributions Institute of Low Temperature Science. p. 10-74.

Zepka G, Pinto O Jr. 2010. A method to identify the better WRF parameterizations set to describe lightning occurrence. Presented at the 21st International Lightning Detection Conference; Orlando, FL.

Zhang T. 2005. Influence of the Seasonal Snow Cover on the Ground Thermal Regime: An Overview. Reviews of Geophysics 43: RG4002.

Zhang T, Stamnes K, Bowling SA. 1996. Impact of clouds on surface radiative fluxes and snowmelt in the Arctic and Subarctic. Journal of Climate 9: 2110-2123.

Zhang T, Osterkamp TE, Stamnes K. 1997. Effect of Climate on the Active Layer and Permafrost on the North Slope of Alaska, USA. Permafrost and Periglacial Processes 8: 45-67.